DEVELOPMENT OF MUCOADHESIVE POLYMERIC NANOPARTICLES FOR INTRANASAL DELIVERY OF FAVIPIRAVIR IN TREATING SARS-CoV-2 INFECTION

Mr. Khent Alcantara

จุฬาลงกรณ์มหาวิทยาลัย
CHULALONGKORN UNIVERSITY

A Dissertation Submitted in Partial Fulfillment of the Requirements
for the Degree of Doctor of Philosophy in Pharmaceutical Sciences and Technology
Common Course
FACULTY OF PHARMACEUTICAL SCIENCES
Chulalongkorn University
Academic Year 2021

Copyright of Chulalongkorn University

การพัฒนาอนุภาคนาโนพอลิเมอร์ชนิดยึดติดเยื่อเมือกเพื่อการนำส่งฟาวิพิราเวียร์ทางจมูกสำหรับรักษาการติดเชื้อไวรัสซาร์ส-โควี-2

นายเคนท์ อัลคันทารา

จุฬาลงกรณ์มหาวิทยาลัย
CHULALONGKORN UNIVERSITY

วิทยานิพนธ์นี้เป็นส่วนหนึ่งของการศึกษาตามหลักสูตรปริญญาวิทยาศาสตรดุษฎีบัณฑิต
สาขาวิชาเภสัชศาสตร์และเทคโนโลยี ไม่สังกัดภาควิชา/เทียบเท่า
คณะเภสัชศาสตร์ จุฬาลงกรณ์มหาวิทยาลัย
ปีการศึกษา 2564
ลิขสิทธิ์ของจุฬาลงกรณ์มหาวิทยาลัย

Thesis Title	DEVELOPMENT OF MUCOADHESIVE POLYMERIC NANOPARTICLES FOR INTRANASAL DELIVERY OF FAVIPIRAVIR IN TREATING SARS-CoV-2 INFECTION
By	Mr. Khent Alcantara
Field of Study	Pharmaceutical Sciences and Technology
Thesis Advisor	Associate Professor PORNCHAI ROJSITTHISAK, Ph.D.
Thesis Co Advisor	Professor OPA VAJRAGUPTA, Ph.D.
	Associate Professor Pranee Rojsitthisak, Ph.D.

Accepted by the FACULTY OF PHARMACEUTICAL SCIENCES, Chulalongkorn University in Partial Fulfillment of the Requirement for the Doctor of Philosophy

..... Dean of the FACULTY OF PHARMACEUTICAL SCIENCES

(Professor PORNANONG ARAMWIT, Ph.D.)

DISSERTATION COMMITTEE

..... Chairman

(Professor Praneet Opanasopit, Ph.D.)

..... Thesis Advisor

(Associate Professor PORNCHAI ROJSITTHISAK, Ph.D.)

..... Thesis Co-Advisor

(Professor OPA VAJRAGUPTA, Ph.D.)

..... Thesis Co-Advisor

(Associate Professor Pranee Rojsitthisak, Ph.D.)

..... Examiner

(Associate Professor SUPAKARN CHAMNI, Ph.D.)

..... Examiner

(Assistant Professor CHATCHAI CHAOTHAM, Ph.D.)

..... Examiner

(Assistant Professor JITTIMA CHATCHAWALSAISIN, Ph.D.)

จุฬาลงกรณ์มหาวิทยาลัย
Chulalongkorn University

เคนท์ อัลคันทารา : การพัฒนาอนุภาคนาโนพอลิเมอร์ชนิดยึดติดเยื่อเมือกเพื่อการนำส่งฟาวิพิราเวียร์ทางจมูกสำหรับรักษาการติดเชื้อไวรัสซาร์ส-โควี-2. (DEVELOPMENT OF MUCOADHESIVE POLYMERIC NANOPARTICLES FOR INTRANASAL DELIVERY OF FAVIPIRAVIR IN TREATING SARS-CoV-2 INFECTION) อ.ที่ปรึกษาหลัก : รศ. ภก. ดร.พรชัย โรจน์สิทธิศักดิ์, อ.ที่ปรึกษาร่วม : ศ. ภญ. ดร.โอภา วัชระคุปต์,รศ. ดร.ปราณี โรจน์สิทธิศักดิ์

อนุภาคนาโน (NPs) เป็นตัวนำส่งที่มีประสิทธิภาพสำหรับการนำส่งยาผ่านเยื่อเมือก โดยเพิ่มระยะเวลาการยึดเกาะและการสะสมบนเยื่อเมือก รวมถึงการเพิ่มความสามารถในการซึมผ่านเยื่อเมือก งานวิจัยนี้ มุ่งออกแบบตัวนำส่งอนุภาคนาโนโดยใช้คุณสมบัติการยึดเกาะเยื่อเมือก (M) ร่วมกันของไคโตซาน (CS) และอัลจิเนต (ALG) สำหรับนำส่งฟาวิพิราเวียร์ (FVR) ทางจมูกเพื่อรักษาการติดเชื้อของไวรัสซาร์ส-โควี-2 ผลการศึกษาพบว่าอนุภาคนาโนอัลจิเนตเคลือบด้วยไคโตซานที่บรรจุฟาวิพิราเวียร์ (FVR-MCS-ALG-NPs) ที่เหมาะสมสำหรับการนำส่งผ่านเยื่อเมือกมีขนาดอนุภาค 233.5 นาโนเมตร ค่าศักย์ซีต้า -21.6 มิลลิโวลต์ ความสามารถในการบรรจุ 26.0% และประสิทธิภาพการกักเก็บ 84.6% โดยพบว่า FVR-MCS-ALG-NPs มีคุณสมบัติการยึดเกาะเยื่อเมือกที่ดี มีความสามารถในการซึมผ่านและการสะสมที่เยื่อบุจมูกของสุกรสูงกว่าอนุภาคนาโนที่ไม่เคลือบด้วยไคโตซาน (FVR-MCS-ALG-NPs) 3 เท่า และสูงกว่าฟาวิพิราเวียร์ 6 เท่า นอกจากนี้ อนุภาคนาโนที่ประกอบไปด้วยพอลิเมอร์ทั้งสองชนิดมีความเข้ากันได้ทางชีวภาพต่อเซลล์เยื่อบุผิวจมูกชนิด RPMI 2650 และต่อเยื่อบุจมูกของสุกร สำหรับประสิทธิภาพในการยับยั้งการติดเชื้อของโคโรนาไวรัสของ FVR-MCS-ALG-NPs เมื่อเทียบกับฟาวิพิราเวียร์ พบว่าแตกต่างกันอย่างมีนัยสำคัญ โดยมีค่า EC_{50} เท่ากับ 6.63 และ >230 ไมโครกรัม/มิลลิลิตร ตามลำดับ บ่งชี้ถึงศักยภาพของตัวนำส่งนี้ในการเพิ่มฤทธิ์ต้านไวรัสและการสะสมในเยื่อบุจมูกของฟาวิพิราเวียร์

จุฬาลงกรณ์มหาวิทยาลัย
Chulalongkorn University

สาขาวิชา	เภสัชศาสตร์และเทคโนโลยี	ลายมือชื่อนิสิต .....
ปีการศึกษา	2564	ลายมือชื่อ อ.ที่ปรึกษาหลัก .....
		ลายมือชื่อ อ.ที่ปรึกษาร่วม .....
		ลายมือชื่อ อ.ที่ปรึกษาร่วม .....

6271001933 : MAJOR PHARMACEUTICAL SCIENCES AND TECHNOLOGY

KEYWORD: Box-Behnken design, chitosan, alginate, SARS-CoV-2, antiviral, polymeric nanoparticles

Khent Alcantara : DEVELOPMENT OF MUCOADHESIVE POLYMERIC NANOPARTICLES FOR INTRANASAL DELIVERY OF FAVIPIRAVIR IN TREATING SARS-CoV-2 INFECTION. Advisor: Assoc. Prof. PORNCHAI ROJSITTHISAK, Ph.D. Co-advisor: Prof. OPA VAJRAGUPTA, Ph.D.,Assoc. Prof. Pranee Rojsitthisak, Ph.D.

Nanoparticles (NPs) have been used as an effective carrier for transmucosal delivery of drugs through their prolonged residence time and deposition, or the enhanced permeation through the mucosa. In this study, we aimed to design a nanocarrier using the combined mucoadhesive (M) properties of chitosan (CS) and alginate (ALG) polymers for the intranasal delivery of favipiravir (FVR) in treating SARS-CoV-2 infection. The optimized FVR-loaded mucoadhesive CS-coated ALG-NPs (FVR-MCS-ALG-NPs) rendered suitable size (233.5 nm), zeta potential (-21.6 mV), loading capacity (26.0%), and encapsulation efficiency (84.6%) for transmucosal delivery. Superior mucoadhesiveness and higher permeation and deposition in the porcine nasal mucosa of the FVR-MCS-ALG-NPs over uncoated-NPs (3-fold) and free FVR (6-fold) were observed. Both NP formulations rendered good biocompatibility in RPMI 2650 nasal epithelial cell and porcine nasal mucosa. Significant inhibition of coronavirus replication was also observed in the FVR-MCS-ALG-NPs vs free FVR (EC_{50} 6.63 vs >230 μg/mL, respectively) suggesting a promising carrier for FVR to enhance its antiviral activity and deposition in the nasal mucosa.

จุฬาลงกรณ์มหาวิทยาลัย
Chulalongkorn University

Field of Study:	Pharmaceutical Sciences and Technology	Student's Signature .....
Academic Year:	2021	Advisor's Signature .....
		Co-advisor's Signature .....
		Co-advisor's Signature .....

ACKNOWLEDGEMENTS

First and foremost, I am forever grateful to God Almighty for granting me his grace of strength, knowledge, and patience to finish this study.

My sincerest thanks and outpouring of respect to my advisers, Assoc. Prof. Dr. Pornchai Rojsitthisak, Prof. Dr. Opa Vajragupta, and Assoc. Prof. Dr. Pranee Rojsitthisak for their brilliance and generosity of teaching, insightful comments, and encouragement. Your mentorship inspires me truly as an academician.

Special thanks to Dr. Nonthaneth Nalinratana of the Faculty of Pharmaceutical Sciences, Chulalongkorn University, Assoc. Prof. Dr. Wijit Banlunara of the Faculty of Veterinary Science, Chulalongkorn University, and Dr. Nopporn Chutiwitoonchai of the National Center for Genetic Engineering and Biotechnology (BIOTEC), Thailand for sharing their insights and expertise.

To my defense committee, for their valuable contribution and support throughout my journey. Your distinguished skills and experience in your fields are seen in your way of correcting and giving your valuable ideas.

I would like to thank and acknowledge the Office of Academic Affairs, Chulalongkorn University for granting me my graduate scholarship to pursue this study. Also, I thank all the non-teaching staff of the Faculty of Pharmaceutical Sciences, Chulalongkorn University, my laboratory mates, and my classmates for their friendship and support whenever I needed it.

Lastly, to my family and friends, for their encouragement. understanding, and unconditional support. Your prayers for me were what sustained me this far.

Khent Alcantara

จุฬาลงกรณ์มหาวิทยาลัย
Chulalongkorn University

TABLE OF CONTENTS

Page

..... iii

ABSTRACT (THAI) iii

..... iv

ABSTRACT (ENGLISH) iv

ACKNOWLEDGEMENTS v

TABLE OF CONTENTS vi

LIST OF TABLES x

LIST OF FIGURES xi

CHAPTER 1 INTRODUCTION 14

1.1 Background of the study 14

1.2 Rationale and significance 16

1.3 Objectives of the study 17

1.4 Hypothesis 17

CHAPTER 2 REVIEW OF RELATED LITERATURES 18

2.1 Pathogenesis of SARS-CoV-2 18

2.2 Current treatment strategies for nCOVID-19 21

2.2.1 RdRp inhibitors as repurposed antiviral therapeutics against nCOVID-19. 22

2.2.2 Favipiravir 22

2.3 Nanotechnology approaches for the treatment of nCOVID-19 25

2.4 Intranasal delivery of anti-viral 36

2.4.1 Factors affecting drug absorption 37

จุฬาลงกรณ์มหาวิทยาลัย
Chulalongkorn University

2.4.2 Factors affecting the passage across the epithelium 37
2.4.3 Pharmacokinetics of intranasal delivery of drugs 39
2.4.4 Nanotechnology-mediated strategy for intranasal delivery of antivirals .. 41
2.5 Mucoadhesive polymers in intra-nasal drug delivery 43
2.5.1 Mechanisms of mucoadhesion 43
2.5.2 Alginate 52
2.5.3 Chitosan 58
2.5.4 Poloxamer 63
CHAPTER 3 METHODOLOGY 69
3.1. Fabrication of favipiravir-loaded mucoadhesive chitosan-alginate nanoparticles (FVR-MCS-ALG-NPs) 69
3.2. Experimental design for optimization by Box-Behnken Design (BBD) and Response Surface Methodology (RSM) 70
3.3. Physicochemical characterization 71
3.3.1. Particle size, polydispersity index, and ζ potential 71
3.3.2. Morphological characterization 71
3.3.3. Loading capacity and encapsulation efficiency 72
3.3.4. Thermal analysis 73
3.4. *In vitro* favipiravir release 73
3.5. Mucoadhesion studies 75
3.5.1. Effects of mucin on size and surface charge of FVR-MPNPs 75
3.5.2. *In vitro* mucin adsorption studies and adsorption isotherms 76
3.6. *Ex vivo* transmucosal studies 77
3.6.1. Collection and preparation of porcine nasal mucosa 77

จุฬาลงกรณ์มหาวิทยาลัย
Chulalongkorn University

3.6.2. *Ex vivo* transmucosal permeability study through porcine nasal mucosa 77

3.6.3. Histopathological examination of porcine nasal mucosa for preliminary toxicity assessment 79

3.7. *In vitro* biocompatibility and cellular uptake studies in human nasal epithelial cell (RPMI 2650) 79

3.7.1 Cytocompatibility study 79

3.7.2 Cellular uptake 80

3.8. *In vitro* antiviral assay using PEDV model 81

3.8.1. Cell and virus preparation 81

3.8.2. Determination of non-cytotoxic concentration 82

3.8.3. Antiviral assay 82

3.9. Storage stability studies 83

3.10. Statistical analysis 83

CHAPTER 4 RESULTS AND DISCUSSION 85

4.2. Analysis of the fitted model 88

4.2.1 The effect of independent variables on particle size 90

4.2.2 The effect of independent variables on ζ potential 94

4.2.3 The effect of independent variables on LC 95

4.2.4 The effect of independent variables on EE 97

4.3. Determining the optimal conditions 98

4.4. Characterization of optimal FVR-MCS-ALG-NP formulation 99

4.4.1. Physicochemical characterization 99

4.4.2. Effects of mucin on the size and surface charge of FVR-NPs 105

4.4.3. *In vitro* release study of FVR from the NP formulations 106

4.5. Nasal mucosa permeation and retention studies 110
4.6. Storage stability studies 113
4.7. Biocompatibility studies 115
4.8. Cellular uptake of FVR-MCS-ALG-NPs 118
4.9. Antiviral activity of FVR against PEDV 120
CHAPTER 5 SUMMARY, CONCLUSION, AND RECOMMENDATION 127
REFERENCES 134
APPENDIX A. Calibration curve of standard FVR 158
APPENDIX B. Calibration curve of standard mucin 159
APPENDIX C. Release kinetics of free FVR solution 160
APPENDIX D. Release kinetic of FVR from MCS-ALG-NPs 161
APPENDIX E. Release kinetic of FVR from ALG-NPs 162
APPENDIX F. Quantitative data of the antiviral effect of FVR (formulated and unformulated) from 3 independent experiments 163
APPENDIX G. Antiviral effect of FVR (formulated and unformulated) from trial 2 164
APPENDIX H. Antiviral effect of FVR (formulated and unformulated) from trial 3 165
APPENDIX I. Antiviral effect of free FVR at high concentrations 166
VITA 167

จุฬาลงกรณ์มหาวิทยาลัย
Chulalongkorn University

LIST OF TABLES

Page

Table 1 Polymeric NP-based delivery of antiviral agents 32

Table 2 Summary of studies for the investigation of various antiviral agents delivered via the intranasal route 45

Table 3 Application of Alginate as a mucoadhesive polymer for drug delivery..... 55

Table 4 Application of Chitosan as a mucoadhesive polymer for drug delivery 60

Table 5 Application of Poloxamer as a mucoadhesive polymer for drug delivery..... 65

Table 6 Different levels of variables in Box-Behnken Design..... 71

Table 7. Formulation design for FVR-MCS-ALG-NPs using BBD with its actual and predicted responses of all dependent variables 86

Table 8. Fit summary and the selected mathematical model of the responses..... 88

Table 9. Statistical analysis of the mathematical model 91

Table 10. The compositions and values of optimal conditions and their predicted and observed responses 99

Table 11. Comparison of the physical characteristics of the NP formulations 101

Table 12. Comparison of the permeation profiles of FVR-MCS-ALG-NPs, FVR-ALG-NPs, and free FVR through PNM 113

จุฬาลงกรณ์มหาวิทยาลัย
Chulalongkorn University

LIST OF FIGURES

Page

Fig. 1 The SARS-CoV-2 structure and the in-depth look into the structure of its spike glycoprotein (Created with BioRender.com). 19

Fig. 2 SARS-CoV-2 replication in humans (Created with BioRender.com) 20

Fig. 3 (A) Conversion of FVR to its active form (FVR-RTP) via ribosylation and phosphorylation. (B) Mechanism of action of FVR-RTP against nCOVID-19 26

Fig. 4 Advantages of NP-mediated antiviral delivery for nCOVID-19 [90] 29

Fig. 5 Anatomy of the human nasal cavity and the olfactory epithelium 39

Fig. 6 Transport mechanisms in the nasal epithelium 40

Fig. 7 Process of the interaction of MPNPs with the mucosa (mucoadhesion) 49

Fig. 8 Chemical structure of Alginic acid 54

Fig. 9 Chemical structure of Chitosan (CS) 59

Fig. 10 Chemical structure of Poloxamer 64

Fig. 11 Three-dimensional surface model plots showing the interaction between the independent factors to (a-c) size, (d-f) ζ potential, (g-i) LC, and (j-l) EE. 93

Fig. 12 SEM (at 50,000× (a and c) and 100,000× (b and d) magnification) and TEM images (100,000× (e and g) and 50,000× (f and h) magnifications) of the optimal formulations; size distribution and ζ-potential of the optimal FVR-MCS-ALG NPs 103

Fig. 13 (a) TGA and (b) DTG thermal curves of FVR, blank-NPs, and FVR-MCS-ALG- NPs; (c) XRD pattern of CS, ALG, FVR, blank- NPs, and FVR-MCS-ALG-NPs. 104

Fig. 14 (A) ζ-potential and (B) size of (a) CS-coated FVR-MCS-ALG-NPs (b) uncoated FVR-ALG-NPs, and (c) the free FVR control before and after 1 h incubation with mucin; (C) mucin binding efficiency of the FVR-MCS-ALG-NPs and FVR-ALG-NPs as a function of time, n = 9. (* p = 0.017, ** p = 0.0036, ns = no significance). 108

จุฬาลงกรณ์มหาวิทยาลัย
Chulalongkorn University

Fig. 15 In vitro FVR released from NPs at (a) physiological pH and (b) SNF (n=3); permeability study of FVR through SnakeSkin™ synthetic membrane: (c) cumulative FVR permeated, and (d) approximate amount of FVR deposited in the PNM after 1 h; **** p< 0.0001; (n=9)..... 110

Fig. 16 Storage stability of FVR-MCS-ALG-NPs (A and B) and FVR-ALG-NPs (C and D) at 4 ºC and ambient room temperature (ART) for 6 months. The values are expressed as mean ± SD of 3 individual batches of each formulations. *p value <0.005 compared to 0 month..... 115

Fig. 17 Cytocompatibility of the (A) H_2O and blank NPs as a diluent and (B) free and FVR-MCS-ALG-NPs in RPMI 2650 nasal epithelia (passage number: 5-9) after 24 h of exposure to treatment. The line signifies the lower limit for safety assessment (>70% viability) based on the ISO 10993-5 criteria [275]. The values are expressed as mean ± SD of 3 independent experiments. *p value < 0.001 (compared to the control), ns = no significance..... 116

Fig. 18 Histopathological examination of porcine nasal mucosa after 1h exposure to NP formulations (FVR-ALG-NPs and FVR-MCS-ALG-NPs) and free FVR. The sections were stained with HE and examined by light microscopy..... 118

Fig. 19 Fluorescence microscope observation of the cellular uptake of free 5-aminofluorescein (5-AF) and 5-AF loaded MCS-ALG-NPs through RPMI 2650 cell line (passage number: 10-12) after 4 and 24 h of exposure..... 120

Fig. 20 Vero cell viability: (a) diluents and (b) FVR (formulated and unformulated) after 18 h. The line signifies the lower limit for safety assessment (>70% viability) based on the ISO 10993-5 criteria [275]; Anti-coronavirus effect: (c) Average quantitative mCherry fluorescence intensity data of infected cells from 3 independent experiments, (d) Quantitative data of mCherry fluorescence intensity of the infected cells treated with high concentrations of FVR. Data are mean ± SD, n = 3; ($^{\#}p < 0.05$ and *<0.0001 compared to the control)..... 122

Fig. 21 Cytotoxicity of the FVR-MCS-ALGP-NPs. eGFP-Vero cells were treated with H_2O or NPs at the indicated concentrations for 18 h. Control cells were the cells cultured

จุฬาลงกรณ์มหาวิทยาลัย
Chulalongkorn University

in medium only. Cell viability was visualized by fluorescent microscopy and measured with a CCK-8 kit at an absorbance of 450 nm using a spectrophotometer. 123

จุฬาลงกรณ์มหาวิทยาลัย
Chulalongkorn University

CHAPTER 1
INTRODUCTION

1.1 Background of the study

The novel coronavirus disease 2019 (COVID-19) caused by severe acute respiratory syndrome-corona virus 2 (SARS-CoV-2) has developed a major pandemic, which causes a surge in mortality and morbidity worldwide [1]. In 2019, the World Health Organization (WHO) has declared SARS-CoV-2 as a global public health concern, which is also expected to greatly affect global economies. Due to transmission dynamics and polyphasic characteristics of the infection, COVID-19 has placed an enormous burden on the healthcare system. To curtail the impact of subsequent local waves of COVID-19, treatment strategies based on potent antiviral medicines against SARS-CoV-2 are required.

Clinical investigations on repurposed antivirals that were initially used for other coronaviruses such as SARS and Middle East Respiratory Syndrome (MERS) CoV and other RNA virus infections have shown to shorten the course of the disease by targeting key enzymes of the virus, hence interfering with the viral cycle and reducing viral load and shedding [2]. While the use of repurposed antivirals seems to be promising to some patients, major hindrances still exist concerning its therapeutic dosage, safety, and delivery. For instance, FVR a broad -spectrum antiviral drug that is being repurposed for SARS-CoV-2 faces major challenges in their physicochemical properties that limits its pharmacologic potential. Recent reports found that pharmacokinetic/pharmacodynamic (PK/PD) indices of FVR fail to achieve sufficient concentrations when half maximal effective concentration (EC_{50}) values are compared with the plasma PK, which partially explains limited clinical success [3]. Problems on solubility, permeability (biopharmaceutics classification system class IV,

BCS IV) and rapid metabolism were the main causes for FVR's poor PK, bioavailability, and efficacy [4, 5].

High doses (3600 mg/day) are required for FVR to achieve effective concentration against SARS-CoV-2 and to compensate for the loss in drug concentration during delivery [6]. Combination therapy of FVR with steroids and other antiviral agents and monoclonal antibodies (mAbs) have been explored to enhance its efficacy. However, the significantly high dose requirement and multiple medications can trigger problems in antiviral resistance, drug interaction, detrimental side effects, and toxicity risk to patients, especially geriatrics and those with underlying diseases. [7-9]. To achieve successful drug repurposing, it is imperative to explore the best way possible to maximize drug efficacy with the new target disease or infection. Several pharmaceutical technological approach *via* co-crystallization, ionic-liquid based formulations, and lipid-based nanoparticle have been done to address the abovementioned limitations of FVR. However, the disadvantage of drug polymerization and the risks of instability and lipid degradation of these formulations were reported.

In addition, a suitable strategy that would require less time and resources is to adopt a different route of administration from its initial mode of delivery. The modification of route of delivery has been investigated for various drugs that resulted in their improved bioavailability and high drug concertation at the new site of action [10-13]. The intranasal delivery route has gained a lot of attention in the delivery of various drugs and treatments due to their simplicity, non-invasiveness, ease of administration, fast onset of action, less adverse effects, and circumvent first-pass metabolism [14-16]. In contrast to conventional oral and parenteral administration of antivirals, intranasal delivery provides a superior advantage as an alternative route since the nasal mucosa is the common initial site of infection and the primary location for viral replication [17]. The application of nanocarriers can also be

จุฬาลงกรณ์มหาวิทยาลัย
Chulalongkorn University

advantageous in intranasal delivery owing to their small size and high surface area that can be beneficial for the absorption in nasal epithelia. Nanoparticles (NPs) have also been known in nasal and lung delivery as drug carriers that could overcome mucociliary clearance and phagocytosis by alveolar macrophages, enhancing absorption through the epithelium and the respiratory system [18]. Studies have also shown that macrophages are less efficient in engulfing ultrafine particles than larger particles [19]. However, recent studies provide evidence that conventional NPs are receptive to entrapment and rapid clearance in the mucus [20]. Therefore, this study aims to fabricate a mucoadhesive polymeric based-NPs to enhance the physicochemical properties of FVR and to successfully deliver and deposit this drug through the nasal cavity in treating SARS-CoV-2.

1.2 Rationale and significance

Intranasal administration provides a promising alternative route in delivering antivirals for SARS-CoV-2 treatment because it closely matches the normal route of infection. However, its poor drug permeability, mucociliary clearance, low drug retention time are common limitations for a successful intranasal drug delivery [21, 22]. The utilization of NPs has been shown to enhance drug absorption owing to their unique characteristics, small size, and large surface area.

จุฬาลงกรณ์มหาวิทยาลัย
CHULALONGKORN UNIVERSITY

To optimize intranasal administration, we aim to fabricate mucoadhesive and -penetrating nanoparticles by combining the different bioadhesive mechanisms of various polymers and their roles in promoting intranasal absorption. Cationic chitosan (CS) and anionic alginate (ALG) polymers were chosen as the materials to construct NPs due to their different mucoadhesion mechanisms by electrostatic interaction and hydrogen bonding to mucin, respectively. A non-ionic mucoadhesive poloxamer was also chosen to stabilize the system due to its absorption-enhancing effects in nasal epithelia [23]. In addition, CS/ALG-based NPs have also shown great advantages as carriers in encapsulating hydrophobic molecules and demonstrated

high tolerance *in vitro* and *in vivo* [24, 25]. Furthermore, the combined advantage of NPs as drug carriers and the nasal administration as an alternative route of delivery aims to improve the efficacy, bioavailability, and pharmacokinetics of repurposed antiviral drugs for SARS-CoV-2.

1.3 Objectives of the study

The overall objective of this study is to fabricate a mucoadhesive CS-coated ALG NPs (FVR-MCS-ALG-NPs) to successfully deliver and deposit FVR in the nasal mucosa for the treatment of SARS-CoV-2 infection. To achieve this, the following are the specific objectives formulated:

1. To fabricate, optimize, and characterize FVR-MCS-ALG-NPs.
2. To evaluate the biocompatibility and cellular uptake of the FVR-MCS-ALG-NPs *in vitro* in human nasal epithelial cells (RPMI 2650) and its mucoadhesive properties *in vitro*.
3. To evaluate the efficacy of the optimized FVR-MCS-ALG-NPs as an antiviral agent against SARS-CoV-2 in the PEDV model.

1.4 Hypothesis

The optimized mucoadhesive FVR-MCS-ALG-NPs can improve the nasal mucosal absorption, permeation, and deposition of FVR, while subsequently enhancing its anti-coronavirus effect for the treatment of SARS-CoV-2 infection.

จุฬาลงกรณ์มหาวิทยาลัย
CHULALONGKORN UNIVERSITY

CHAPTER 2
REVIEW OF RELATED LITERATURES

2.1 Pathogenesis of SARS-CoV-2

Up to this day, the pathogenesis and treatment strategies underlying nCOVID-19 are still developing and barely understood. The virus can be transmitted from person-to-person via the respiratory droplets and aerosolization that are "shed" when the infected person coughs, sneezes, breathes, or speaks. The inhaled microparticles from an infected person are deposited in the airways depending on the size, breathing dynamics, and others [26]. Once deposited, the viral particles will land on the airways covered with an aqueous layer and mucus. The thick and sticky mucus layer in the airway will immobilize the viral particle where it will propel to the epithelium or be washed off by the mucociliary clearance down to the nasopharynx and the lungs [26].

Coronaviruses consist of four structural proteins: (1) nucleocapsid proteins (N) that is bound to the RNA genome and facilitates RNA synthesis, (2) spike proteins (S) that are critical for binding to host cell receptors and to facilitate its entry, (3) envelope protein (E) that facilitates assembly, envelop formation, and budding, and (4) membrane protein (M) for viral integration (Fig. 1) [1]. The S forms a large protrusion on the viral surface; hence it is named "corona" (Latin word for crown). The S-protein is composed of three sections: (1) large ectodomain, (2) transmembrane domain, and (3) intracellular tail. The ectodomain comprises of receptor-binding subunit (S1) and membrane-fusion subunit (S2) [27]. Electron microscopic analysis of the S-protein showed a clove-shaped trimer S1 head and a trimeric S2 stalk. When the viral particle reaches the epithelium, the S-protein binds to the angiotensin-converting enzyme -2 (ACE-2) receptor of the ciliated secretory

จุฬาลงกรณ์มหาวิทยาลัย
Chulalongkorn University

cells of the nasal epithelium. During the viral entry, the S1 binds to the receptor, and the S2 fuses the host and viral membranes and mediates clathrin-endocytosis [28].

The virus then invades the host cell by releasing its viral content and undergoes replication (Fig. 2). The viral genomic-RNA (+) undergoes polypeptide translation and encode nonstructural proteins (NSPs) that are crucial for the assembly of the structural proteins needed for the new virion. The NSPs 1a and 1ab are translated and cleaved to form functional NSPs including helicase or RNA-dependent RNA polymerase (RdRp) complex. The RdRp is responsible for the structural proteins (SPs) RNA. The SPs S1, S2, envelop (E) and membrane (M) are translated by ribosome-bound in the endoplasmic reticulum (ER) and presented onto its surface to initiate virion assembly. And finally, the new virions are released from the infected host cell through exocytosis [29, 30].

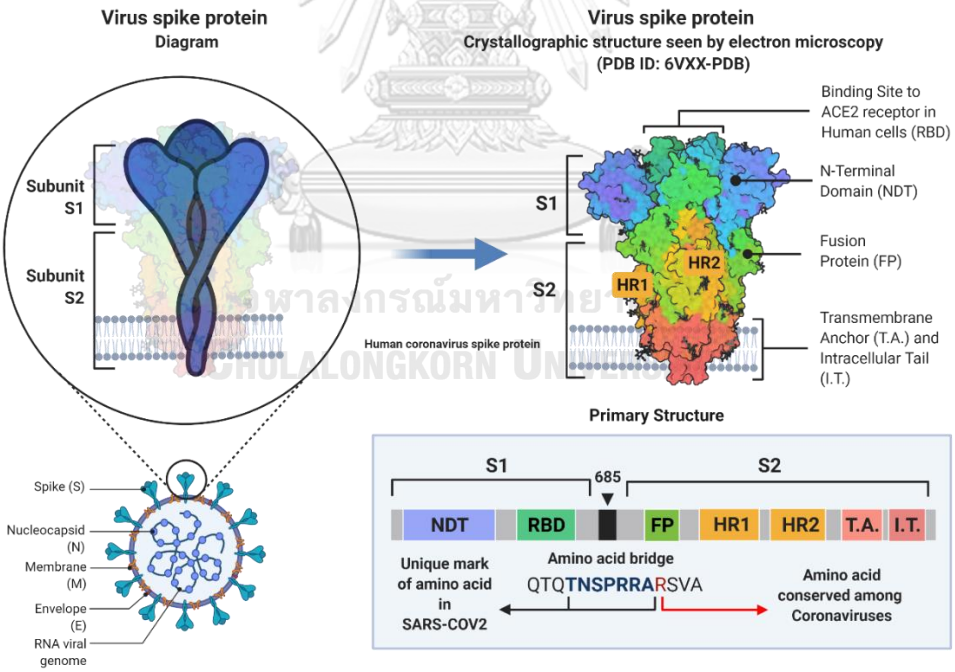

Fig. 1 *The SARS-CoV-2 structure and the in-depth look into the structure of its spike glycoprotein (Created with BioRender.com).*

SARS-CoV-2 infection results in all-encompassing immune and inflammatory responses in the host that leads to tissue damage. Acute respiratory distress syndrome (ARDS) is the most common immunopathological complication of SARS-CoV-2 infection [31]. ARDS is a complex complication that is difficult to control due to the cytokine storm associated with the uncontrollable release of pro-inflammatory cytokines including interferons (IFN)-α and γ, interleukin (IL)-1 β, 1, 3, 6, 10, 12, and 18, and -1RA, tumor necrosis factor (TNF)- α, transforming factor (TGF) beta and other chemokines such as CCL2, CCL3, CXCL8, CXCL9, and CXCL10 [32]. The cytokine storm and low lymphocytes are also observed in other severe corona infections including SARS and MERS CoV that are associated with their disease progression and severity [33, 34]. Current data showed that the mortality rate of SARS-CoV-2 is significantly higher in patients aged 60 and above and patients with underlying diseases such as diabetes and cardiovascular diseases [35].

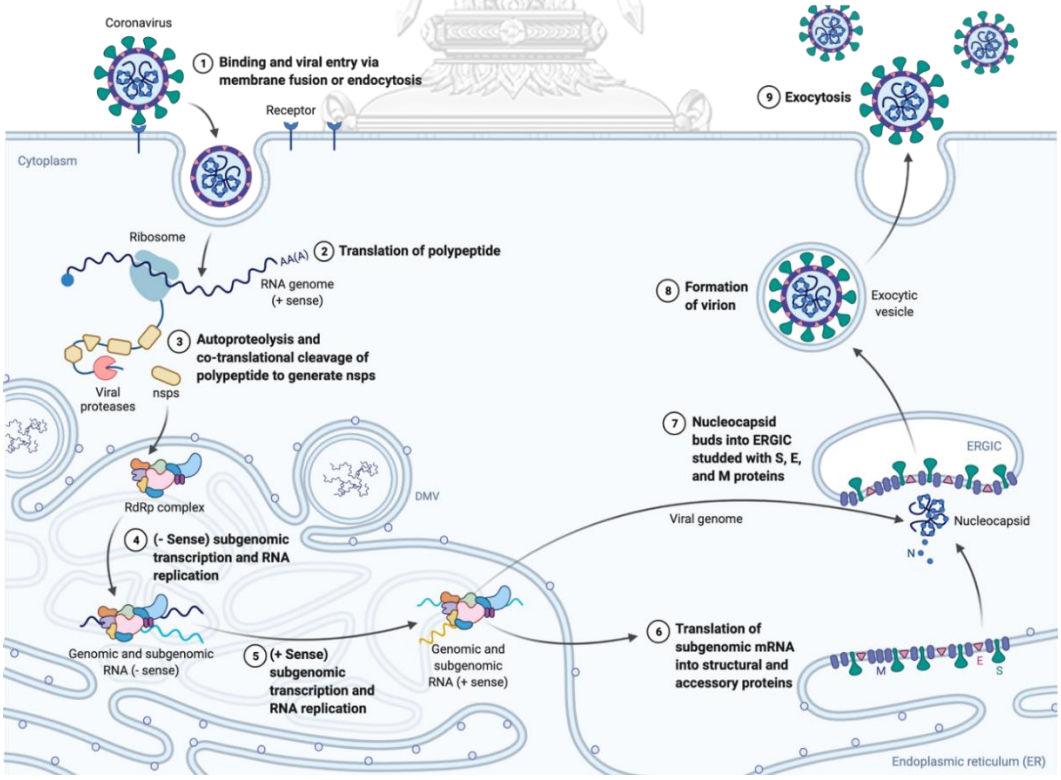

Fig. 2 *SARS-CoV-2 replication in humans (Created with BioRender.com)*

2.2 Current treatment strategies for nCOVID-19

As the effective treatment against SARS-CoV-2 is still ongoing, some medications have demonstrated a beneficial effect in patients for immediate response to the infection. Some of these are off-label use drugs for malaria such as chloroquine and hydroxychloroquine, natural products and Chinese herbal medicines, and patient-derived plasma therapy.

The chloroquine and hydroxychloroquine have been proven before as an effective treatment for SARS and MERS *in vitro* and *in vivo* [36]. These drugs were initially approved medication as immunomodulatory drugs for malaria. Both drugs were investigated for antiviral effects through their competitive binding to ACE2 receptors on host cells and their anti-inflammatory effects. In recent studies, chloroquine resulted to a more potent antiviral effect than hydrochloroquine [37]. Its superior effect against SARS-CoV-2 was proven through the detection of viral RNA and the N protein expression in Vero E6 cells, which resulted in the inhibition RNA replication of SARS-CoV-2 [38]. In a clinical study in China, which involved over 20 participants, chloroquine showed a slightly higher recovery rate than in the lopinavir/ritonavir group at 7-, 10- and 14-days of treatment [39].

จุฬาลงกรณ์มหาวิทยาลัย
CHULALONGKORN UNIVERSITY

In addition, natural compounds and Chinese herbal medicines seem to contribute a potential treatment option in SARS-CoV-2 infection. Chinese herbal medicines such as Weijing decoction and others have been shown to have decreased mortality and alleviate symptoms of nCOVID-19 with maximum safety and lesser toxicity [40, 41]. Some components of Chinese herbal medicines including emodin from the genus *Rheumand polygonum*, baicalin from *Scutellaria baicalensis*, scutellarin from *Erigeron breviscapus*, tetra-O-galloyl-β-D-glucose from *Galla chinensis*, and luteolin from *Veronicalina riifolia,* shown to inhibit the ACE2 receptor interaction of SARS-CoV-2 in the host cells [42, 43].

2.2.1 RdRp inhibitors as repurposed antiviral therapeutics against nCOVID-19

Drug repurposing or repositioning is a basic strategy of using approved or investigational drugs beyond their scope during emergencies. These drugs proven to be safe in humans can skip phase 1 and 2 clinical trials, hence shortening the clinical investigation. Although the mechanism of infection for SARS-CoV-2 is still not clear, the basis of using repurposed antiviral drugs is those that are genetically like SARS-CoV-2 and other coronaviruses [44]. As per the recent development on studying SARS-CoV-2, the replication of the virus depends directly on the RNA-dependent RNA polymerase (RdRp) enzyme. The RdRp is a conserved enzyme encoded by RNA viruses that represent a unique class of processive nucleic acid polymerases, carrying out DNA-independent replication/transcription processes. Interestingly, the RdRp protein of SARS-CoV-2 showed an identical binding site with the same amino acid residue having 96% structural similarity with SARS-CoV and other coronaviruses [45]. Hence, antivirals that act and target protease and polymerase enzymes can be promising for the treatment of SARS-CoV-2. Several RdRp inhibitors against SARS-CoV-2 are being used including ribavirin, remdesivir, galidesivir. In this study, we focused on favipiravir (FVR) and in overcoming its physicochemical limitations as antiviral agent for coronavirus.

จุฬาลงกรณ์มหาวิทยาลัย
Chulalongkorn University

2.2.2 Favipiravir

Favipiravir (FVR) (MW: 157.104 g/mol) or 6-fluoro-3-hydroxyl-2-pyrazine carboxamide is a prodrug that is converted to its active form, FVR-ribofuranosyl-5B-triphosphate (FVR-RTP) intracellularly by ribosylation and phosphorylation (Fig. 3A-B) [3]. FVR is a broad-spectrum oral antiviral agent from a member of the class of pyrazines that is pyrazine substituted by aminocarbonyl, hydroxy, and fluoro groups at positions 2, 3, and 6, respectively. FVR appears as a white to yellow crystalline powder. This compound with a pKa of 5.1 and Log P <1.63 of soluble in acetonitrile

and methanol (>30 mg/mL) but is almost insoluble in water (<1 mg/mL) and ethanol (<10 mg/mL).

It is originally designed to selectively inhibit RNA-dependent RNA polymerase (RdRp) in various serotypes and strains of influenza A, B, and C in Japan [46]. Moreover, FVR was also investigated to be a broad-spectrum antiviral agent against other negative-sense RNA viruses including RSV (*Pneumoviridae*, EC_{90} = 36 µM), CCHFV (*Nairoviridae*, EC_{50} = 6.37 µM), LSAV (*Arenaviridae*, EC_{50} = 29.3 µM), JUNV (*Arenaviridae*, EC_{50} = 0.79 µM), Rabies virus (*Rhabdoviridae*, EC_{50} = 32.4 µM), and EBOV (*Filoviridae*, EC_{50} = 67 µM). It was also found to inhibit positive sense RNA viruses such as *Flaviviridae* ZIKA (EC_{50} = 22 µM), WNV (EC_{50} = 53 µM), YFV (EC_{50} = 180 µM), and enterovirus EV71 (*Picornaviridae*, EC_{50} = 68.74 µM).

In recent studies, FVR was reported to efficiently reduce SARS-CoV-2 infection with an EC_{50} of 61.88 µM, half-cytotoxic concentration (CC_{50}) of >400 µM, and selectivity index of >6.46 [38, 47]. This wide gap of CC_{50} and EC_{50} give a wide margin of safety for the required high doses of FVR to achieve its effective concentration of 40-80 µg/mL in treating nCOVID-19 [48]. In some parts of Asia, particularly in Thailand, FVR is given to nCOVID-19 patients at 1600 mg dose on the first day, a sudden decrease to 400 mg twice a day from day 2 to 6, followed by 400 mg doses once a day on the 7^{th} day, which has an estimated AUC of 1453.73 µg h/mL and 1324.09 µg h/mL on the 1^{st} and 7^{th} day, respectively [48]. The maximum plasma concentration can be reached after 2 hours following oral administration and rapidly decreased with a short half-life of 2-5.5 h [49]. FVR is also high protein bound in human plasma (54%) having 65% and 6.5% bound percentages in the albumin and α1-acid glycoprotein, respectively [46, 50]. The FVR is primarily metabolized by hepatic enzyme aldehyde oxidase and partially by xanthine oxidase to its inactive oxidative metabolite (T-705M1), which are excreted to its hydroxylated form by the kidneys [49]. Because of its high protein binding, short half-life, and fast hepatic

metabolism and excretion, FVR can boost its plasma concentration by dose- and time-dependent self-inhibition of the inactivation of metabolism of the FVR while subsequently increasing the FVR/T-705M1 metabolite ratio after chronic dosing [49]. This increase in circulating FVR/T-705M1 ratio is supposed to mediate cellular uptake and the trapping of active FVR-RTP in the tissue by increasing the extracellular-intracellular concentration gradient [51]. This phenomenon can explain the accelerated circulating clearance of FVR after chronic and repeated administration. However, constant monitoring of the tissue distribution of FVR-RTP is still necessary to prevent toxicity [48, 51].

The SARS-CoV-2-RdRp complex was more active by at least 10-folds than any other RdRp viruses known [52]. Currently, anti-viral drugs that act on RpRd like FVR are being used as promising candidates for the treatment of nCOVID-19. Over the past few years, clinical investigations on the efficacy of FVR in the management of nCOVID-19 have been done worldwide. In China, Chen, Zhang [53] conducted prospective open-labeled multicentric clinical trials to compare FVR and Umifenovir (UFR) to manage nCOVID-19 patients within the 12-day maximum duration of symptoms onset. Results showed no significant difference in the recovery rate of the two groups with 61.21% and 51.67% recovery for FVR and UFR, respectively, after the 7th day of treatment. Further analysis confirmed that patients who received FVR had significant clinical improvement among patients with moderate symptoms (71.43% vs. 55.86%) after 7 days. In Japan, FVR was given to patients at a dose of 1800 mg for day 1 followed by 800 mg twice a day on subsequent days. It was found out that a significant clinical improvement was shown at 7th to 14th-day treatment in different cases with a rate of 73.8% and 87.8%, 66.6% and 84.5%, and 40.1% and 60.3% for mild, moderate, and severe disease, respectively [54].

2.3 Nanotechnology approaches for the treatment of nCOVID-19

NPs (NPs) are being used in various fields of medicine because of their remarkable characteristics. According to the Food and Drug Administration (FDA), nanotechnology presents unique physicochemical and biological properties that cannot be seen in macro and micro materials. The NPs' size, surface charge, and tunable surface; their exceptional release kinetics, and targeted delivery are some of its highlighted characteristics that paved the way for developing safer and more efficacious therapeutics for many diseases and infections primarily viral infection including hepatitis, HIV, and influenza [55, 56]. Several published studies have reported the consideration of nano-based antivirals as a promising treatment strategy against SARS-CoV-2 [57-59]. Lipid-based nanocarriers have been utilized in delivering mRNA vaccines against this virus that are currently rolling out worldwide. In addition, as we currently see the potential of nanotechnology-based vaccines in producing effective immunization and providing safe alternatives, scientists are now looking at the benefits of this platform in delivering antiviral medications. In recent publications, NPs are being exploited to enable efficient antiviral transport by overcoming biological barriers like mucus in ARDS. Patel, Patel [60] demonstrated the increased oral bioavailability of lipophilic efavirenz-nanosuspension due to its enhanced solubility, permeability, and absorption in rabbits. Also, NPs can improve the physicochemical properties of antivirals, but they can also reduce the dose frequency while subsequently limiting adverse drug effects (ADR). Sneha, Vedha Hari [61] improved this through lamivudine-polymeric NPs loaded buccal films for HIV therapy in pediatrics. The results showed an excellent sustained release of lamivudine for 8 h, hence reducing the dose and unwanted toxicity in pediatrics.

จุฬาลงกรณ์มหาวิทยาลัย
CHULALONGKORN UNIVERSITY

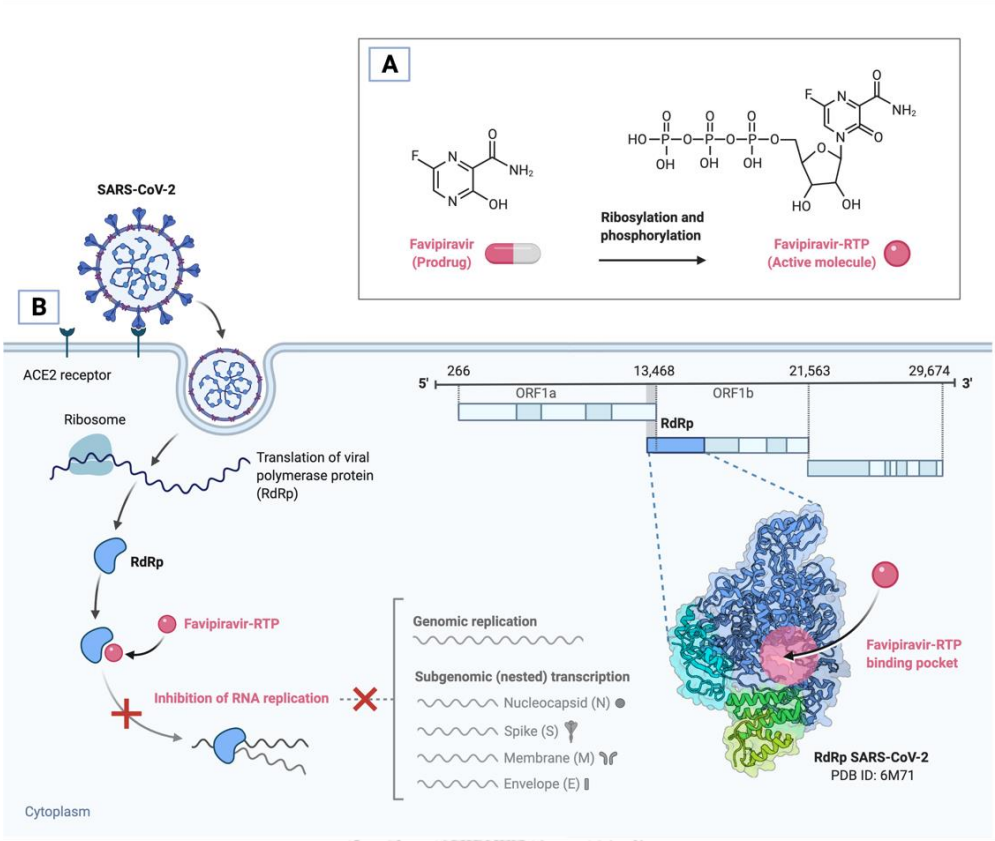

Fig. 3 (A) *Conversion of FVR to its active form (FVR-RTP) via ribosylation and phosphorylation.* ***(B)*** *Mechanism of action of FVR-RTP against nCOVID-19*

Furthermore, buccal administration of lamivudine-polymeric NPs had high tolerability and acceptance to pediatric patients with HIV due to its convenience. The advantage of NPs has also been evaluated against respiratory viral infections such as H1N1 in combating multidrug resistance. Selenium surface decorated NPs loaded with amantadine [62] and oseltamivir [63] showed efficient antiviral activity *in vitro*. In addition, Hu, Chen [64] proved the enhanced antiviral activity and sustained drug release of polyethylene glycol/poly (lactic-co-glycolic acid) (PEG-PLGA) NPs loaded with diphyllin and bafilomycin against influenza. The Food and Drug Administration (FDA) has approved some NP-based antivirals for hepatitis and HIV such as peginterferon alfa-2a (Pegasys®) for the treatment of hepatitis virus B and C [65], and

VivaGel® a dendrimer-loaded SPL7013 used as a microbicide against human immunodeficiency virus (HIV) and herpes simplex virus (HSV) [66].

The utilization of NP-based delivery systems for antivirals follows the emergence of NPs antiviral therapeutics for nCOVID-19. In the diagnosis of nCOVID-19, many nanomaterials have been employed for their biosensing capabilities and other properties such as chemical stability, electrical conductivity, and localized surface plasmon resonance (LSPR) effect [67, 68]. Nano-platforms such as gold (Au) and silver (Ag) NPs, graphene-based NPs, and magnetic NPs have been integrated with various analytical devices to increase the sensitivity and specificity of nCOVID-19 diagnosis [69]. Au NPs are one of the most explored inorganic-based NPs as a material for diagnosis and biosensing, particularly colorimetric, electrochemical, and plasmonic-based detections. Recently, Karakus, Erdemir [70] developed a probe Au-NP biosensors that exhibits dual sensing capability to detect SARS-CoV-2 spike antigen through saliva samples. The developed Au-NP-mAb biosensor allows simple and rapid analysis for both colorimetric and electrochemical assay with a detection limit of 48 ng/mL and 1 pg/mL, respectively. Furthermore, the integration of colloidal Au-NP with lateral-flow (Au-NP LF) assay was investigated by Huang, Wen [71] for rapid detection of IgM antibody against SARS-CoV-2 via indirect immunochromatography method. The accuracy and sensitivity of the Au-NP LF were tested in serum samples of both healthy and nCOVID-19 patients compared to their real-time polymerase chain reaction (RT-PCR) results. Au-NP LF showed a remarkable sensitivity and specificity of 100 and 93.3%, respectively in detecting IgM in SARS-CoV-2 positive patients without any interference from other viral infections.

NP-based platforms have recently been used as coatings or material in face masks designed for nCOVID-19 like polymer-based nanofibers [72, 73], copper [74, 75] and silver [74] NPs, and silver/silica composites [76] to render more efficient physical barrier with antiviral and antimicrobial properties. In recent years, the polymeric and

จุฬาลงกรณ์มหาวิทยาลัย
CHULALONGKORN UNIVERSITY

lipid-based NPs have been utilized in the development of vaccines for other coronaviruses like MERS-Cov and SARS-CoV both in avian and murine models [77-80]. The adaptive and ideal characteristics of NPs have also been utilized in developing highly promising platforms for nCOVID-19 vaccine development, especially in delivering new generations of vaccines, e.g., mRNA-based vaccines. As of 2021, there are at least 26 NP-based vaccine candidates against nCOVID-19 undergoing clinical trials. Two of the nCOVID-19 vaccines we use nowadays which were granted emergency used authorization (EAU) by the US-FDA in 2020 utilized lipid-based NPs as their delivery platform. The Moderna vaccine (mRNA-1273) is a mRNA vaccine loaded in cationic lipid NPs. This lipid-based mRNA vaccine high antibody response in clinical trials without any safety issues identified [81]. Further clinical studies on this vaccine also suggest that the mRNA-1273 showed 94.1% efficacy in preventing nCOVID-19 in over 30,000 volunteers enrolled in the study [82]. On the other hand, the BNT162b2 or the Pfizer-BioNTech vaccine also utilized ionizable cationic lipid-based NP as its delivery vehicle. The first phase clinical trial of BNT162b2 showed promising safety and immunogenicity in young adults [83]. Furthermore, the safety and efficacy clinical studies in over 40,000 volunteer participants showed 95% protection in persons 16-year-old and above against nCOVID-19 with negligible adverse reactions such as muscle pain, fatigue, and headache [84]. These successes in the use of lipid NPs made a lasting impact in revolutionizing mRNA vaccine delivery. The engineered lipid-based NPs not only enable safe and efficient mRNA vaccine delivery but also maintain their stability [85]. Through these milestones, it opened the way for utilizing other NP platforms for various clinic applications [85].

With this, researchers have looked upon the future possibilities of using NPs platforms in finding cures against nCOVID-19. For instance, the development of novel inhalable liposome [86] and magnetic [87] delivery of hydroxychloroquine has been investigated, resulting in the amplification pharmacodynamics and pharmacokinetic

จุฬาลงกรณ์มหาวิทยาลัย
CHULALONGKORN UNIVERSITY

profile of the drug as a treatment for nCOVID-19 in an animal model. Surnar, Kamran [88] also showed the potential use of polymeric NPs to enhance oral delivery of ivermectin (IVM) for the treatment of nCOVID-19. The IVM-polymeric NPs demonstrated potent antiviral activity by inhibiting viral spike protein and ACE-2 receptors. In addition, Sanna, Satta [89] reported a promising approach in constructing remdesivir-loaded ACE-2 targeted NPs against SARS-CoV-2. The poly/(epsilon-caprolactone)/poly(*D,L*-lactic-*co*-glycolic acid)-*block*-poly(ethylene glycol) (PCL/PLGA-PEG) polymeric NPs were conjugated with various ACE-2 targeting ligands which showed an improved antiviral effect against SARS-CoV-2. Moreover, the enhanced antiviral property of the targeted NPs was associated with its increased cellular uptake and its competitive binding mechanism in ACE-2 expressing cells. Ranjbar, Fatahi [90] summarized the probable advantages of NP platforms in drug delivery for nCOVID-19 (**Fig. 4**).

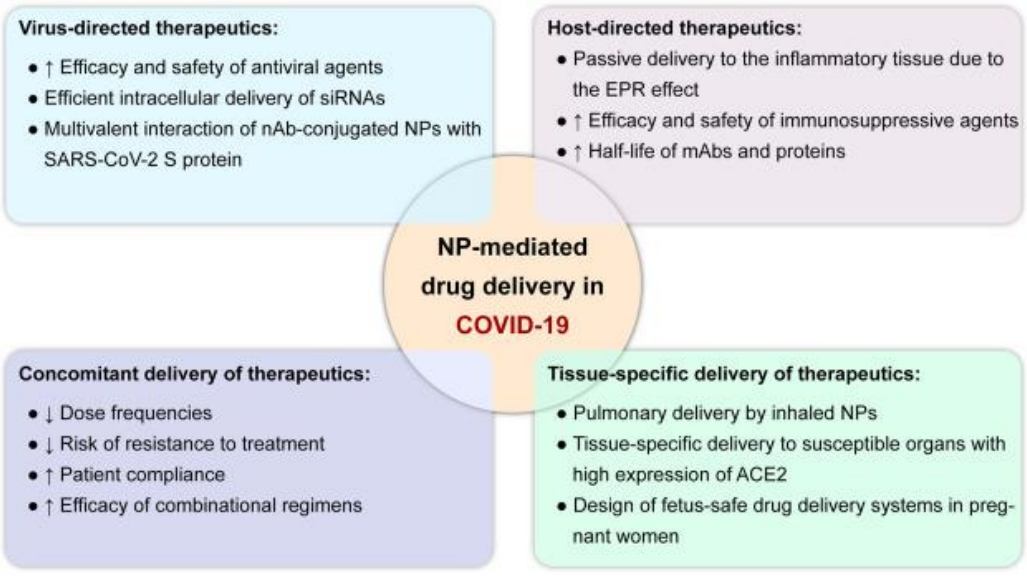

Fig. 4 *Advantages of NP-mediated antiviral delivery for nCOVID-19 [90]*

Although NPs seem to be an excellent platform to enhance viral inhibition and pharmacokinetics of antiviral agents, their scalability and production costs are the common challenges that affect their further development [91, 92]. Moreover, the

toxicity of NPs that is associated with their distribution and high permeability through most cells, tissues, and organs also limit their utilization as drug carriers [93]. Hence, for the nano-based antiviral delivery to work, scientists need to consider these issues to maximize the capacity of nanotherapeutics in fighting nCOVID-19.

To have a successful antiviral mechanism, NPs must target the crucial steps in the infection process including viral attachment, penetration, replication, and release [94]. Chen and Liang [95] reviewed various possible antiviral mechanisms of NPs which can be either direct or indirect viral inactivation through the inhibition of attachment or penetration depending on the nanomaterial used. Typically, these mechanisms can be associated with altering the capsid protein of the viral surface through physical or chemical means, while subsequently reducing its virulence and eventually decreasing viral load [94, 95]. Generally, viral replication starts with its attachment to the host cell by targeting specific receptors. If the NPs stop this attachment, the host cells can be free from infections. The entry of the virus into the host cells can be complex, which involves stable and multiple interactions with different cell surface receptors. Dey, Bergmann [96] synthesized multivalent flexible nanogels that could block the viral entry into the host cell. The development of multivalent NPs that could target heparan sulfate proteoglycans on the cell surface was designed using dendritic polyglycerol sulfate (DPS) to mimic cellular heparan sulfate. The interaction of the DPS with the host cell can block the virus from its interaction with cell surface receptors. In addition, the research also concluded that the DPS nanogels render nontoxicity and multivalent interaction with viral glycoproteins, thus forming a shielded virus that would prevent its interaction with the host cell. Seemingly, viral suppression can be possible by blocking penetration and entry of the virus into the host cell through the alteration of the cell surface membrane and its protein structures [95]. Recently, Halder, Das [97] proved the use of highly monodispersed Au NPs to efficiently inhibit herpes simplex virus (HSV)

จุฬาลงกรณ์มหาวิทยาลัย
CHULALONGKORN UNIVERSITY

infections. The authors reported that the Au NPs render no toxicity to normal cells and showed dose-dependent antiviral activity with an EC_{50} of 32.3 μM and 38.6 μM in HSV-1 and 2, respectively. Further analysis revealed that the enhanced antiviral activity of Au NPs was associated with its capability in interrupting the viral penetration stage. The authors also noted the possible invasion of Au NPs into infected Vero cells during its entry stage and could interfere the viral proliferation.

จุฬาลงกรณ์มหาวิทยาลัย
CHULALONGKORN UNIVERSITY

Table 1 *Polymeric NP-based delivery of antiviral agents*

NPs platform	Synthesis	Antiviral agent	Antiviral activity	Benefits of nanocarrier for drug delivery
CS/TPP NPs [98]	Electrostatic cross-linking via ionotropic gelation	α interferon (α-INF)	↑ antiviral response in vitro and in vivo in α-INF-CS/TPP NPs treated group compared to the control as observed in the significant ↑ in the OAS2 and PKR antiviral markers.	Sustained release and antiviral response in α-INF-CS/TPP NPs were observed *in vivo* and *in vitro*. ↑ cellular uptake by human cell line.
Peptide functionalized PLGA-based NPs Dhoke [99]	Interfacial Activity Assisted Surface Functionalization (IAASF) and Double emulsion solvent evaporation method	Lamivudine	None reported.	2.17- and 3.84 – fold ↑ in cellular uptake and retention in HepG2 cells. ↑ AUC and efficient targeted strategy to mice liver was observed in pharmacokinetics and biodistribution studies.

NPs platform	Synthesis	Antiviral agent	Antiviral activity	Benefits of nanocarrier for drug delivery
CS/TPP NPs [100]	Electrostatic cross-linking via ionotropic gelation	Saquinavir (SQR)	Significantly ↓ viral proliferation for both HIV strains (NL4-4 and Indie-C1) in SQR-CS NPs treated cells compared to SQR suspension.	↑ SQR encapsulation (75%), cell targeting efficiency (92%), and uptake, hence superior antiviral activity.
Thiolated CS Nanofibers (NFs) [101]	Electrostatic cross-linking and Coaxial electron-spinning	Tenofovir (TFV)	None reported	↑ drug loading (13 - 25 % w/w), sustained-release, and enhanced mucoadhesive properties were exhibited by TFV nanofibers. Nontoxic *in vivo* and *in vitro*.

จุฬาลงกรณ์มหาวิทยาลัย CHULALONGKORN UNIVERSITY

NPs platform	Synthesis	Antiviral agent	Antiviral activity	Benefits of nanocarrier for drug delivery
Lipid-coated PLGA NPs [102]	Emulsion solvent evaporation	Latency-reversing agents (LRAs)	LRA-NPs are rendered equal to ↓ cytotoxicity compared to free LRDs; thus, LRA-NPs could potentially deliver ↑ LRAs required for efficiency. LRA combinations in NPs exhibited synergistic latency reversal with low cytotoxicity in the HIV cell model and $CD4^+$ T cells.	↑ accumulation, longer retention, and sustained release were observed in LRA-NPs

จุฬาลงกรณ์มหาวิทยาลัย
Chulalongkorn University

NPs platform	Synthesis	Antiviral agent	Antiviral activity	Benefits of nanocarrier for drug delivery
CMC/Compritol-PEG Hybrid NPs [103]	Double emulsion solvent evaporation	Zidovudine (ZVD)	None reported	ZVD-NPs had modest drug loading and slower release than free ZVD. Efficient cellular uptake in glioma cells and no cytotoxicity in both glioma and neuro2a brain cells were exhibited by ZVD-NPs compared to the controls.
Poly (vinyl pyrrolidone) PVP/Lipid-based NPs [104]	Double emulsion solvent evaporation	Zidovudine (ZVD)	None reported	Significant improvement in the cellular transport through murine neuro2a and HeLa cells by ZVD-PVP/Lipid NPs compared to free ZVD.

Chulalongkorn University

2.4 Intranasal delivery of anti-viral

Intranasal drug delivery has been recognized as an alternative route for parenteral administration since the richly vascularized nasal mucosa provides an effective route for drug absorption [105, 106]. The human nasal cavity is divided in the midline by the septum, creating two physiologically distinct nasal passages with the external nares or nostrils in the anterior and the *choana* in the posterior end [107]. The nostrils can be subdivided into three turbinates or conchae as superior, middle, and inferior conchae [107]. The anterior part of the nasal passage contains numerous hairs that act as filters of large, inhaled particles. To safeguard high drug deposition of nasal sprays in the nasal cavities, the droplets require at least 30 – 120 μm. The larger particles tend to deposit in the anterior part of the nasal cavity while finer particles can penetrate further with high chances of deposition in the lungs [108, 109].

Aerosol inhalation has been studied and utilized for so long in delivering drugs through the nose. The nasal cavity has a complex design, with specific anatomical regions targeted by drug delivery for nasal deposition. It has a large air-filled surface area of 160 cm^2 and a volume capacity of 15 mL [108]. The three turbinates in the nasal cavity serve as the primary target for local [110] and systemic [111] drug delivery. In addition, the olfactory region that sits above the superior turbinate with a surface area of about 5 cm^2 is being targeted for nose-to-brain drug delivery [112]. The respiratory region along the inferior turbinate is the main site for systemic absorption of drugs due to its large surface area (120 – 150 cm^2) and highly vascularized and permeable chorion. Other regions contain glands that produce nasal mucus serving as another layer of protection for the entire nasal cavity. The nasal epithelium constitutes basal cells, ciliated cells, and mucus-secreting goblet cells held together by intercellular tight junctions [14] (Fig. 5). The main blood supply

จุฬาลงกรณ์มหาวิทยาลัย
CHULALONGKORN UNIVERSITY

of the nose comes from the external carotid system via sphenopalatine and facial arteries and the internal carotid system through the ophthalmic artery [14].

2.4.1 Factors affecting drug absorption

One of the most important factors to consider in intranasal delivery is the site and surface area of drug absorption. The relatively small surface area of the nasal cavity limits the high volume of drugs to be administered to avoid drug loss through anterior or posterior run-off. Newman, Steed [113] reported that the intranasal administration of insulin of about 80 to 160 µL showed 100% retention in the nasal cavity with no passage to the lungs. The unit volume administered was also found significant since the administrate ion of single 100 µL volume results in more retention the over large surface area than administering two 50 μL volumes [113, 114]. Furthermore, viscosity of the formulation is another factor due to retention and absorption issues. Kundoor and Dalby [114] reported that the increase in the viscosity of the formulation causes the decrease in the retention of drug in the nasal cavities which can also be associated with an increase in the droplet size. To maximize the delivery and retention of drugs, Foo, Cheng [115] studied the importance of spray administration angle on intranasal deposition. The combination of administration and plume angle of 30° led to the retention of the drug in the anterior region of the nose, with an approximately 90% deposition efficiency [115].

จุฬาลงกรณ์มหาวิทยาลัย
Chulalongkorn University

2.4.2 Factors affecting the passage across the epithelium

After being retained in the nasal mucosa, the drug must cross the nasal epithelium for intracellular metabolism for prodrug activation and systemic absorption. The mucus covering the entire epithelial surface has become a rate-limiting step in drug permeation. The mucin, which is formed from the mucus, is a protein that can bind to the drug and thus affect its diffusion through the epithelium [116]. The drug absorption in the nasal epithelium has been challenging because of

the constant elimination of deposited drug particles by mucociliary clearance during its diffusion through the mucus layer. Mucociliary clearance is one of the major limitations for nasal delivery. It is an innate defense mechanism in removing inhaled insoluble particles such as biologicals, chemicals, and physical nature (e.g., dust) from the respiratory tracts [117, 118]. The inhaled particles are trapped in a blanket of mucus that sits on the ciliated epithelial cells and transported to the pharynx down to the esophagus via the rhythmic beating of the cilia [117, 118]. The deposited inhaled particles that are trapped in the mucus are eliminated by this mechanism within 30 minutes [105].

During the deposition, the particles may penetrate through the epithelium by either transcellular (across the cell membrane) or paracellular route (between cells) [119] (Fig. 6). Generally, lipophilic drugs are transported via transcellular mechanism either passive diffusion or through receptor-, carrier-, and vesicle-facilitated transport [120-122]. On the other hand, the paracellular transport mechanism is mostly for polar molecules that can cross through the gaps between the epithelium, except molecules with a molecular weight (MW) of >1,000 Daltons (Da) such as peptides and other proteins [121, 123].

จุฬาลงกรณ์มหาวิทยาลัย
CHULALONGKORN UNIVERSITY

Three basic physicochemical characteristics have a significant impact on the transepithelial passage of a molecule: (1) molecular weight (MW), (2) polarity, and (3) degree of ionization. As previously discussed, non-polar molecules take the transcellular route, while polar molecules can either take transcellular or paracellular routes depending on their MW. As a general knowledge, higher MW limits the paracellular entry through the tight epithelial junctions. Rapid nasal absorption was observed in drug molecules below 300 Da, while drug molecules above 1 kDa had slower absorption, which resulted in low bioavailability (0.5-5%) [120, 124-126]. Although the degree of ionization has minimal effect in the intranasal absorption, this

is still considered as one of the criteria in drug diffusion since only the non-ionizable fractions of the drug molecules diffuse, hence faster absorption [126].

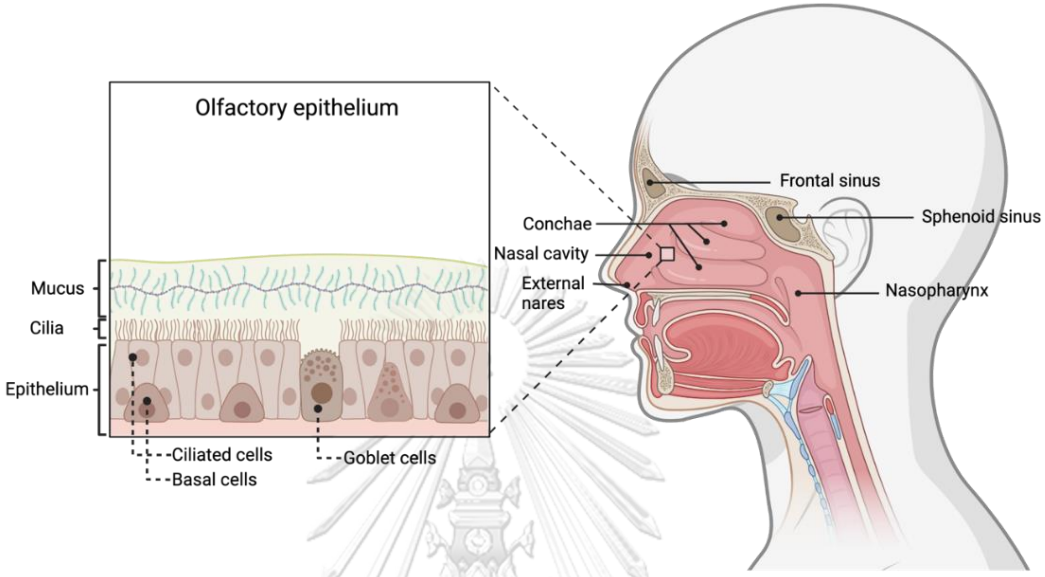

Fig. 5 *Anatomy of the human nasal cavity and the olfactory epithelium*

2.4.3 Pharmacokinetics of intranasal delivery of drugs

The drug's physicochemical characteristics serve as the fundamental determinant of its efficient absorption in the nasal mucosa and adequate bioavailability in achieving desired pharmacologic effect either locally or systemically. However, it is still imperative to study the pharmacokinetics of drugs administered through this route to have a deeper understanding of its benefits compared to other conventional delivery routes. Cass, Efthymiopoulos [127], studied the pharmacokinetics of zanamivir (ZMR) (MW:332 Da, Log *P*: -3.2), an antiviral drug for influenza A and B virus after IV, oral, and intranasal administration in healthy volunteers. In their study, the ZMR was administered randomly as single or multiple doses via different routes. Serum and urine samples were used to quantify the absorbed and excreted ZMR for the analysis of its pharmacokinetics. In addition, nasal washes and throat gargles were also used to recover drug concentration in the

จุฬาลงกรณ์มหาวิทยาลัย
Chulalongkorn University

nose and throat, respectively. As a result, ZMR was well tolerated in all doses and routes, without any adverse effects observed throughout the study. The IV route resulted in linear kinetics after a single administration of up to 600 mg without any alteration in the kinetics after repeated administration of ZMR.

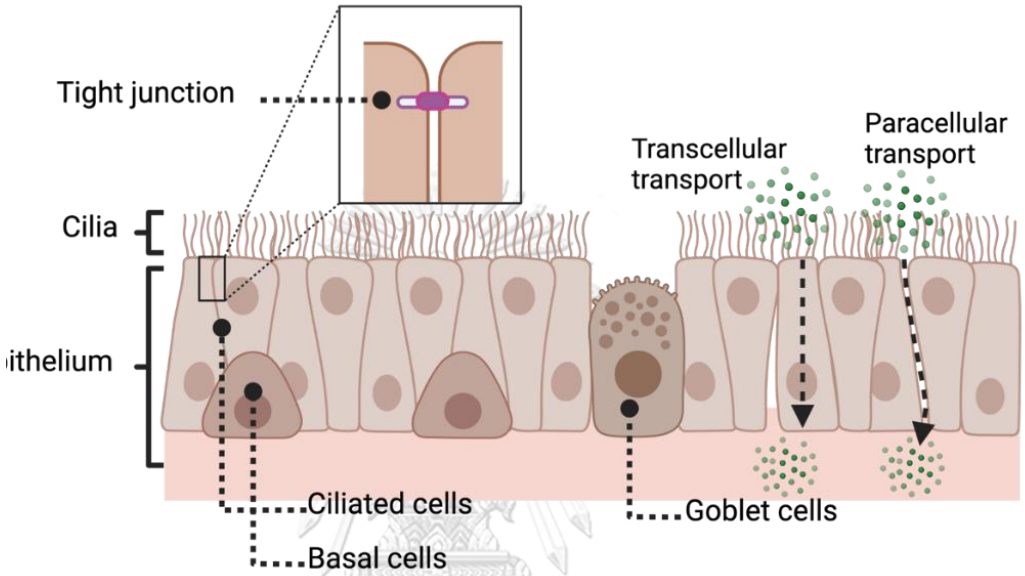

Fig. 6 *Transport mechanisms in the nasal epithelium*

Also, the oral route had a very low bioavailability of 2%, while intranasal administration rendered a median serum concentration of 10-20%, with maximum serum concentration reached within 1-2 h. Further analysis also confirmed that the median serum $t^{1/2}$ of ZMR after intranasal administration was within 2.5-5.05 h which is indicative that the elimination rate is greatly affected by its absorption in the nasal cavity. Sumatriptan (MW:295 Da, Log P: 0.9), a vasoconstrictor for migraine which is more lipophilic than ZMR but almost has similar MW also showed modest bioavailability of 16% after intranasal administration in comparison with SQ route (~100%) [128]. However, it is also worth mentioning that the T_{max} of intranasal administration is 1.5 h compared to 0.17 h of the SQ route, which also reflects that the low bioavailability of intranasal administration is associated with its slower

จุฬาลงกรณ์มหาวิทยาลัย
Chulalongkorn University

absorption in the nasal mucosa. To further prove the effect of drug absorption in the bioavailability of the intranasal route, Haschke, Suter [129], studied the intranasal pharmacokinetics of midazolam (MW:326 Da, Log *P*: 2.5), a benzodiazepine that is even more lipophilic than sumatriptan. The mean bioavailability of midazolam after intranasal administration ranged from 79-92 % with a mean C_{max} of 28-30% and T_{max} of 9.4-11.3 min, which mainly attributed to its rapid absorption due to its high lipophilicity. Furthermore, midazolam was also co-administered with CS as an absorption and retention enhancer which significantly increased the C_{max} (80%) and reduced the T_{max} (7.2 min) in the high-dose formulation.

In summary, the pharmacokinetics of the intranasal route relies mainly on its absorbance and retention on the nasal cavity brought by the physicochemical characteristics of the molecule. This can be achieved through several approaches including the co-administration of absorption promoters that could open the tight junctions and increase the paracellular transport [130, 131], utilization of bioadhesive formulations to increase the contact time and slow down the mucociliary drainage [120, 126], and the use of nanotechnology for better drug transport [14].

2.4.4 Nanotechnology-mediated strategy for intranasal delivery of antivirals

Nanotechnology has proven its advantage as an efficient strategy in improving nasal drug delivery. For the drug to be efficiently delivered through the nasal mucosa, several barriers like the improvement of nasal residence time or drug deposition, mucociliary clearance, and mucosal absorption are the three essential processes that must be addressed. From a general point of view, it is expected that the smallest particles must penetrate to any membrane. In transmucosal permeation smallest nanosized particles permeate through the paracellular route since the normal diameter of the tight junctions of the epithelial cells is < 8.4 Å [132]. On the other hand, larger particles use the transmucosal route through either endocytosis or carrier-/receptor-mediated transport [133]. However, it is still imperative to know and

understand how the particles are taken up by the cells in the nasal cavity. Behrens, Pena [134] reported a comparative analysis of the uptake of bioadhesive and non-bioadhesive NPs in MTX-E12 (mucus-producing) and Caco-2 (non-mucus producing) cell lines using fluorescent markers and confocal microscopy. As a result, the bioadhesive NPs had a significant increase in mucus binding and cellular transport than non-bioadhesive NPs. However, it was also found out that the hydrophobic non-bioadhesive NPs had slightly higher uptake in Caco-2 followed closely by bioadhesive NPs. Through this comparison, the researchers hypothesized that the presence of mucus plays a vital role in the cellular uptake of NPs. To prove this concept, the mucus secreted by the MTX-E12 was removed before incubation with both NPs. Interestingly, the cellular uptake of the two NPs showed no significant difference proving that the presence of mucus significantly affects the permeation of the NPs through the cells.

Another interesting mechanism to note for the cellular uptake is the effect of the NP materials on the transepithelial electrical resistance (TEER). Artursson, Lindmark [135] first investigated the significant effect of cationic CS on a dose-dependent decrease in the TEER of Caco-2 cell monolayer. Smith, Wood [136] also investigated the effect of CS on the tight junction complex at the molecular level through immunofluorescence and Western blot analysis. It was found that the significant reduction in the TEER of Caco-2 monolayer to up to 83% is caused by the translocation of tight junction proteins from the membrane to the cytoskeleton, hence the disruption and opening of the tight junction.

Nanotechnology has also been used as a drug carrier to overcome mucociliary clearance and evade phagocytosis by alveolar macrophages to increase drug absorption in the respiratory system [18]. It was also found that the alveolar macrophages are less efficient in engulfing ultrafine particles than larger particles [19]. Despite the capabilities of NPs in overcoming the permeation and mucociliary

จุฬาลงกรณ์มหาวิทยาลัย
CHULALONGKORN UNIVERSITY

clearance, the improvement of particle residence in the nasal cavity seems to be impossible for all NP platforms. In addition, the final form of the formulation either a liquid or dry powder matters longer retention. For instance, insulin/CS powder formulation was found to have greater absorption and bioavailability of 3.6% than insulin/CS solution, which can be attributed to the much higher deposition of powders in the nasal cavity [133]. There has been an apparent disparity between the nasal delivery of NPs in either powder or solution forms. NPs in solutions have been reported to overcome mucociliary clearance and improve mucosal absorption; however, the NP solution also compromises drug deposition in the cavity. To meet this gap, NPs for intranasal administration have been developed using mucoadhesive materials to increase the retention and deposition of drugs regardless of the final dosage form.

2.5 Mucoadhesive polymers in intra-nasal drug delivery

The nasal cavity is a promising administration route for anti-viral drugs, as it serves as the first point of contact for inhaled respiratory viruses. Intranasal delivery can be challenging due to the rapid clearance and disposition of inhaled materials from the nasal cavity. For these reasons, the utilization of mucoadhesive polymers was developed to enable longer retention and higher drug disposition in the nasal mucosa.

2.5.1 Mechanisms of mucoadhesion

Bioadhesion is a phenomenon when two biological surfaces adhere to each other by interfacial forces. The bond between the mucoadhesive material and the mucus which we referred to as “mucoadhesion” can be achieved through a series of steps and mechanisms. Mucoadhesion has gained a lot of interest in the pharmaceutical sciences due to the increasing demand for drug localization in the mucosa to render non-invasive therapy to patients, especially for drug molecules like

proteins and oligonucleotides that are difficult to deliver systemically. Several research has been published on the promising potentials of mucoadhesive drug delivery in drug localization at the site of action including the GI tract or even systemic absorption via the nasal cavity.

Mucous membranes or mucosa are moist surfaces on various body cavities composed of epithelial membranes containing mucosal cells that secrete mucus. Mucus is present in all body mucosa such as the oral cavity, gastrointestinal region, reproductive tract, eyes, and respiratory tracts [137, 138]. It is a highly hydrated gel that is composed of 95% water, 5% mucin glycoprotein, and some electrolytes [139]. Mucin is the primary and the most important constituent of mucus, which is composed of a protein core and carbohydrate-made side chains that are covalently bound with the protein core via *O*-glycosidic linkage [140, 141].

Mucoadhesive materials are composed of hydrophilic macromolecules which consist of several hydrogen bonds forming groups. Due to the cysteine-rich subdomains of mucin glycoproteins, it allows the formation of intra-/inter-molecular disulfide bonds with these macromolecules facilitating mucoadhesion [142].

จุฬาลงกรณ์มหาวิทยาลัย
Chulalongkorn University

Table 2 *Summary of studies for the investigation of various antiviral agents delivered via the intranasal route*

Antiviral agent	Delivery system	Target virus	Benefit/s of delivery route
Zanamivir (ZMR) [127]	Powder	Influenza A and B	↓ systemic absorption of ZMR following intranasal administration to healthy volunteers, thus enabling local effect in the respiratory tract.
Ribavirin (RBV) [143]	Microparticulate powder for insufflation	-	↑ permeation through nasal mucosa and ↑ accumulation of RBV in the brain *in vivo*.
Acyclovir (ACR) [144]	Liposome	-	significantly ↑ plasma concentration and enhanced bioavailability and permeation of liposomal ACR than the free drug.
Acyclovir (ACR) [145]	Suspension	-	Nasal uptake of acyclovir suspension was moderately improved through the rat nasal cavity.

จุฬาลงกรณ์มหาวิทยาลัย Chulalongkorn University

Antiviral agent	Delivery system	Target virus	Benefit/s of delivery route
Saquinavir (SQR) [146]	Nanoemulsion	Neuro-AIDS	↑ permeation rate through the nasal mucosa and ↑ drug concentration in the brain *in vivo* compared to a free drug suspension.
Zidovudine (ZDV) [147]	Thermoreversible gel	-	53% increase in nasal permeation and ↑ drug concentration in the plasma and various regions in the brain *in vivo*. Total drug concentration in the CSF and brain in intranasal delivery of ZDV were 4.7-56 times ↑ than IV administration.

จุฬาลงกรณ์มหาวิทยาลัย
Chulalongkorn University

Antiviral agent	Delivery system	Target virus	Benefit/s of delivery route
Ribavirin (RBV) [148]	Solution and Powder	Viral encephalitis	No significant difference in the RBV concentration in the olfactory bulb between IV and intranasal administration. However, ↓ drug concentration was measured in different brain compartments following intranasal administration than IV. RBV powder had significantly ↑ concentration in the olfactory bulb and all brain compartments than both IV and intranasal solutions due to stronger and longer contact of the powder with the mucosa.

Chulalongkorn University จุฬาลงกรณ์มหาวิทยาลัย

Mucoadhesive were initially used as denture fixatives due to the presence of hydroxyl, carboxyl, and/or amine groups on its molecule that promotes adhesion when moistened [149, 150]. Commonly, natural mucoadhesives such as carbomers, CS, sodium ALG, cellulose, and their derivatives are used in dental medicine and pharmaceutical sciences in formulating tablets, patches, pastes, ointments, etc., [149]. Mucoadhesion is a complex process that involves three steps that describe the interaction of the mucoadhesive material and the mucosa by Ponnusamy, Sugumaran [151] (Fig. 7). The first phase is called the (1) contract stage wherein the mucoadhesive material touches the mucous membrane to form intimate contact. It can be brought mechanically by holding and pressing the material onto the mucosa which can be further enhanced contact by wetting and/or spreading the material to increase its surface area. The second stage is called the (2) inter-penetration stage, wherein the mucoadhesive material diffuses into the mucus layer. Lastly is the (3) consolidation stage, wherein it strengthens the mucoadhesive via mechanical or chemical interaction or the combination of both for more prolonged adhesion. Mechanical bonds refer to the physical interaction of the mucoadhesive with the mucosa, while chemical bonds happen through strong primary or weak secondary bonds, depending on the mucoadhesive functionalities [151].

จุฬาลงกรณ์มหาวิทยาลัย
CHULALONGKORN UNIVERSITY

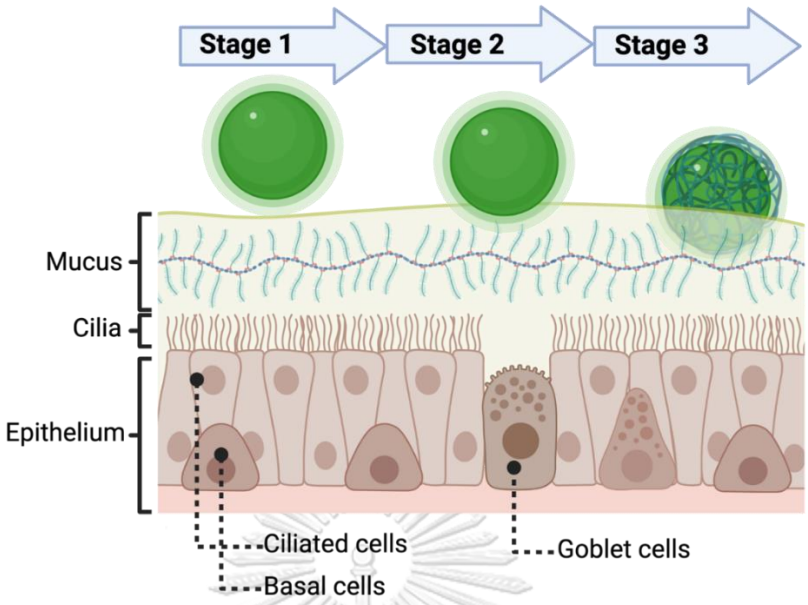

Fig. 7 *Process of the interaction of MPNPs with the mucosa (mucoadhesion)*

Numerous theories have been proposed by various research explaining deeply how this phenomenon work. Although no standalone theory could explain these interactions, various theories were combined to define the process [152-154]. Below are the five widely accepted theories that involve mucoadhesion:

- ***Mechanical theory***

The mechanical interlocking theory of mucoadhesion refers to the interaction and locking mechanism of the mucoadhesive material onto the irregularities of the mucosal surface. The rough surface not only provides a lock-and-key mechanism in promoting adhesiveness but also increases the surface area of the mucoadhesive while improving its wetting characteristics. Seemingly, the increase in the surface area also amplifies the viscoelastic and plastic dissipation of the energy at the interface during the joint failure [155].

- ***Electronic theory***

The electronic theory relies on the transfer of electrons upon the contact of the mucoadhesive and the mucosa by the differences in their electronic structures.

Through this, the electrical double layer of the interface will be formed and eventually triggers adhesion due to the attractive forces of the electrons [156].

- ***Diffusion theory***

Diffusion theory, also interpenetration theory, relies on the concentration gradient and its relation with the available molecular chain lengths and their mobilities [157]. This theory was first proposed by Voyutskii [158] in his discussion on the autohesion of rubbery polymers. He explained that when two polymers come in contact, the polymer chains in the rubbery state have sufficient mobility to diffuse across the initial interface [158]. The interpenetration depth of polymer across an adhesive interface also depends on its molecular weight, diffusion coefficient, and contact time [157].

- ***Wetting theory***

The wetting theory refers to the extemporaneous spread of the mucoadhesive polymeric material onto the mucosal surfaces and its immediate interaction with the mucus. The wetting theory applies to liquid systems and their surface and interfacial energies to develop adhesion. The affinity of the liquid onto the surface can be analyzed using contact angle goniometry to determine the contact angle of the liquid on the surface. As a general rule, low contact angle would mean a greater affinity of the liquid onto the surface [149].

- ***Adsorption theory***

This theory refers to the attachment of the mucoadhesive material considering their hydrogen bonding, hydrophobic interactions, and van der Waals' forces with the mucosa [156]. After the initial contact of the two surfaces, the material interacts with mucosa due to the surface forces acting between the atoms of the two surfaces. This interaction can be either (1) a primary chemical bond of covalent nature or a (2) secondary chemical bond that is brought by different forces

of attraction such as their surface charge, hydrophobicity, and functional groups [156]. Below are the thorough discussions concerning these chemical interactions that play a crucial role in mucoadhesion:

❖ *Hydrogen bond*

Hydrogen bond are formed, when the hydrogen atoms themselves or as a functional group of hydrophilic nature such as amino, hydroxyls, carboxyls, and sulfate groups are covalently linked to a highly electronegative like oxygen, nitrogen, and fluorine atoms and another electronegative atom bearing a lone pair of electrons. Qaqish and Amiji [159] explained that in addition to electrostatic interactions between the D-glucosamine residue of CS and the sialic acid residue of mucin, the attractive forces through hydrogen bonding and/or hydrophobic interaction are also involved in CS-mucin binding mechanism. Dinu, Yakubov [160] also reported the mucin immobilization in calcium-ALG by hydrogen bonding.

❖ *Van der Waals' interaction*

This interaction is a relatively weak force which includes attraction and repulsion between atoms, molecules, and surfaces, as well as other intermolecular forces caused by the correlations in the fluctuating polarizations of nearby particles [161]. For example, TM, Lau [162] explained that the sialic acid and ester sulfates in the mucus layer render a negative charge that would create electrostatic interaction with positively charged polymers like CS. Also, negatively charged polymers can form electrostatic interaction through their interaction with the positively charged amino acid terminals of the mucin backbone [163]. Although electrostatic interaction is the weakest form of interaction that arises from the dipole-dipole and dipole-induced dipole interaction amongst chemical bonds involved in mucoadhesion, this is still the most widely accepted theory of all.

จุฬาลงกรณ์มหาวิทยาลัย
CHULALONGKORN UNIVERSITY

❖ *Hydrophobic bond*

Also described as the “hydrophobic effect”, refers to the interaction of the indirect bonds that occur when a lipophilic group is present in the aqueous solution. The non-polar molecule adjacent to the water molecule can form a hydrogen bond that could lower the system entropy. The hydrophobic interaction is vital in the tail-to-tail aggregation of mucins. This can form when the hydrophobic naked protein core of the mucin or its lipid components interact with the diffusion compound (drug/polymer) [163]. The intensity of the hydrophobic interaction relies on the high energy and low sensitivity of the environment. For instance, the gastric environment where the pH is low could have greater hydrophobic interaction than physical interaction due to the suppression of electrostatic phenomenon [164].

The selection of the polymers used in this study is merely due to their highly tunable properties, biocompatibility, and mucoadhesive properties that benefit the intended transmucosal delivery. CS and ALG were two established polymers that efficiently encapsulate hydrophobic molecules with excellent stability. In addition, the CS coating on the polymeric ALG NPs could be an advantage in the pH-dependent release in the nasal epithelia. Most importantly, the CS, ALG, and Poloxamer were preferred in constructing the nanoparticulate carrier owing to their different mucoadhesive properties. Below is detailed information on CS, ALG, and Poloxamer in various pharmaceutical preparations. The summary of mucoadhesive studies on these polymers is presented in Tables 3-4.

จุฬาลงกรณ์มหาวิทยาลัย
CHULALONGKORN UNIVERSITY

2.5.2 Alginate

Alginate (ALG) is a water-soluble linear anionic polysaccharide primarily isolated from several brown algae worldwide such as *Ascophyllum nodosum,*

Laminaria hyperborean, and Macrocystis pyrifera [165]. ALG is extracted from algae by mixing with the mineral acid to remove the counterions, such as calcium, magnesium, sodium which are naturally incorporated with ALG in seawater, and then produce alginic acid which is neutralized by alkalies such as sodium carbonate or sodium hydroxide to produce sodium ALG [166, 167]. Although ALG can be extracted from bacteria like *Pseudomonas* and *Azotobacter* species, these sources are still unavailable for commercial applications [168]. Currently, most ALG is commercially above 30,000 metric tons synthesized from farmed brown seaweeds annually [169]. The chemical structure of ALG is composed of β-D-mannuronic acid (M) and α-L-glucuronic acid (G) residues which are covalently linked by 1,4- glycosidic linkage in different sequences or blocks [170]. The block patterns can be consecutive G blocks (G residue) which exhibit rigid and folded structural conformation, consecutive M blocks (M residue) providing flexible and linear conformation, or an alternating G and M block (GM block) (Fig. 8) [170, 171]. Not only compositions but also block sequences may vary depending on the sources of algae [172]. ALG has several remarkable properties such as its good biocompatibility, biodegradability, chemical versatility, mucoadhesiveness, pH sensitivity, cross capability, low toxicity, prolonged circulation time, and gelling properties [173, 174]. In addition, it can be modified chemically to alter these properties [167]. ALG has been explored as an ideal biomaterial especially in chemotherapeutic agent delivery [174]. The drug encapsulation occurs through the gelation of ALG by ionic crosslinking of the carboxylate components of the guluronate moieties on the ALG's backbone with different divalent cations (e.g., Ba2+, Mg2+, Ca2+) to obtain the NPs [175]. However, these nanocarriers are not stable at room temperature [176] and can easily cause leakage of the active moieties loaded in the core of the NPs [177]. Reports showed that these limitations could be overcome by coating the ALG NPs with cationic biopolymer in the form of CS. It was also reported that the 2-step process of forming

CS-ALG-NPs by ionotropic gelation of ALG with Ca^{2+} followed by electrostatic interaction by CS could increase the drug loading and stability and create a more rigid structure of the NPs [178].

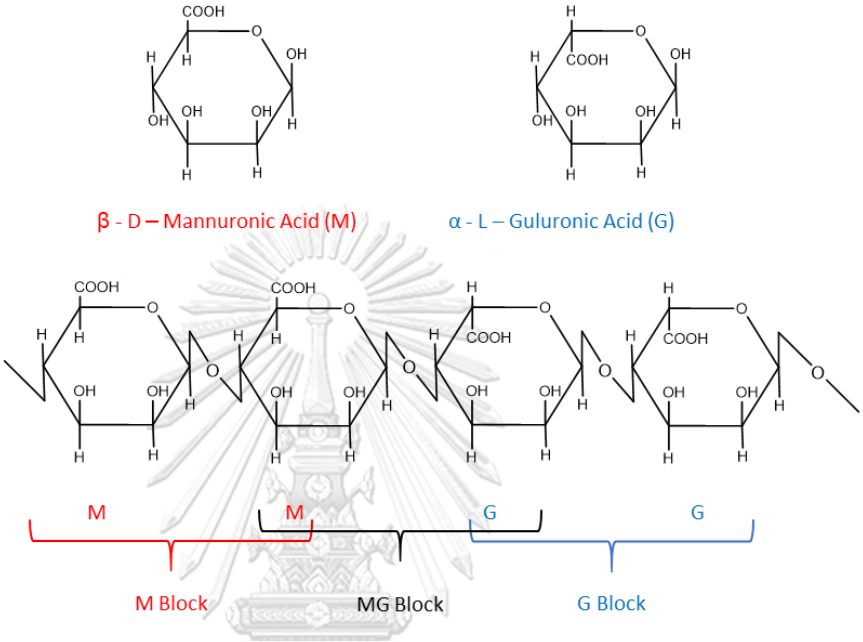

Fig. 8 *Chemical structure of Alginic acid*

ALG has poor mucoadhesive properties making it the least favorable material in nasal drug delivery [179]. To improve its mucoadhesive property, Bernkop-Schnurch, Kast [180] covalently linked cysteine to the polymer backbone through carbodiimide chemistry. Results showed that the thiolated ALG demonstrated an increase in viscosity by about 50% when mixed with mucus at neutral pH compared to mucus/ALG mixture indicating an enhanced interaction with mucus. Further analysis also confirmed that the thiolated-ALG was able to form inter-/intra-molecular disulfide bonds with great stability and prolonged residence time when used as excipient. Below are some of the notable studies on ALG as a mucoadhesive material in delivering various types of drug molecules (Table 3).

Table 3 *Application of Alginate as a mucoadhesive polymer for drug delivery*

Drug	Polymeric platform	Dosage form	Application	Therapeutic goal
Captopril [181]	ALG/Calcium chloride beads	Beads	Oral	↑ retention and controlled release of captopril in the stomach.
Gatifloxacin [182]	ALG/Carboxymethyl cellulose	Gel	Ophthalmic	Enhance bioadhesion property and prolong retention on the external ocular surface.
Doxorubicin (DOX) [183]	ALG/Liposome	Paste	Oral mucosa	Sustain release formulation of doxorubicin for oral cancer treatment that is stable in the physiological conditions of the oral cavity.
Carvedilol [184]	Microspheres	Liquid spray	Nasal mucosa	Avoid first-pass metabolism and improve the efficacy of carvedilol in treating angina and hypertension (HTN).

Chulalongkorn University จุฬาลงกรณ์มหาวิทยาลัย

Drug	Polymeric platform	Dosage form	Application	Therapeutic goal
Metoprolol [185]	Microspheres	Liquid spray	Nasal mucosa	Provide alternative therapy to injection and enhance the pharmacokinetics and therapeutic efficacy of metoprolol.
Dexamethasone (DEX) [186]	Lipid/ALG NPs	Gel	Nasal mucosa	Prolong residence time and release of corticosteroid.
Pilocarpine [187]	ALG/Poloxamer	Solution	Ophthalmic	↑ ocular bioavailability of pilocarpine using combined *in situ* gelling polymers with different phase transition mechanisms.
DEX-moxifloxacin (MOX) [188]	Liposome Collagen/Gelatin/ ALG (CGA) hydrogel	Hydrogel	Ophthalmic	Sustain release of DEX-MOX while ↓ microorganism growth and improving corneal wound healing.

Chulalongkorn University จุฬาลงกรณ์มหาวิทยาลัย

Drug	Polymeric platform	Dosage form	Application	Therapeutic goal
Ropinirole HCl (RH) [189]	ALG microparticles	Microparticulate powder spray	Nasal mucosa	Enhance bioavailability of RH by delivering the drug from nose-to-brain for the treatment of Parkinson's disease.
Dopamine (DOP) [190]	Oxidized-ALG/DOP conjugate	Solution	Nasal mucosa	Nose-to-brain delivery of DOP by surpassing blood-brain-barrier through its conjugation with oxidized-ALG.

จุฬาลงกรณ์มหาวิทยาลัย
Chulalongkorn University

2.5.3 Chitosan

Chitosan (CS) is an FDA-approved cationic natural polymer from partial deacetylation of chitin (β-(1→4)-linked *N*-acetyl-D-glucosamine unit) (Fig. 10) [162]. It comprised of β-(1→4)-2-acetamido-2-deoxy-b-D-glucan (*N-acetyl* D-glucosamine unit/acetylated monomer) and β-(1→4)-2-amino-2-deoxy-b-D-glucan (D-glucosamine/deacetylated monomer) linked *via* β-,4 glycosidic bonds with less molecular weight and crystallinity than chitin. CS is the second most abundant biopolymer with ideal properties for biomedical research such as bioactivity, biocompatibility, biodegradability, non-toxicity, and its broad-spectrum antibacterial activity [139]. Furthermore, CS is used to construct NPs as a drug delivery system due to its excellent mucoadhesive properties and modifiable characteristics. The mucoadhesive property of the positively charged CS can be explained by its interaction with the negatively charged mucin [191]. Sogias and Williams [191] also demonstrated the role of the primary amino group (protonated) of CS concerning the electrostatic interaction, hydrogen bonding, and hydrophobic effects on gastric mucin aggregation. Results suggest that the reduction in the number of amino groups of CS via partial deacetylation also reduces its interaction with mucin as shown in the reduction of mucin aggregation. In addition, due to the formation of hydrogen bonding, the deprotonated amino group of CS interacts with the nonionic hydroxyl groups alongside the mucin molecules [139]. CS has been used in nasal delivery of polar drug molecules across the epithelial membrane due to its strong mucoadhesive properties and transient opening of the cell-cell tight junctions. Illum, Farraj [192] reported that using cationic CS for nasal administration promotes excellent enhancement in the absorption of insulin across the nasal mucosa of rats and sheep. Furthermore, they also noted that the histological examination confirmed that CS rendered non-toxic and non-irritating to the nasal membrane for up to 30-

mins of exposure. In addition, several research proved the increased absorption of macromolecules and their in vivo bioavailability across nasal epithelial barriers with CS as demonstrated by its plasma concentration and AUCs [133, 193, 194]. CS was also recently investigated for improved nasal mucosa absorption of poorly water-soluble drugs with poor bioavailability. Jin and Zhao [195] used CS in the nasal delivery of poorly water-soluble drug hesperidin for the treatment of inflammatory lung disease. The developed hesperidin-loaded CS NPs showed significant improvement in the cellular uptake in vivo and in vitro compared to the free hesperidin. The hesperidin-CS NPs also showed a remarkable suppression of inflammatory cytokines and vascular permeability in mice, demonstrating an improved drug delivery of hesperidin when loaded in CS NPs. Table 4 shows recent studies on CS as a material for various delivery routes.

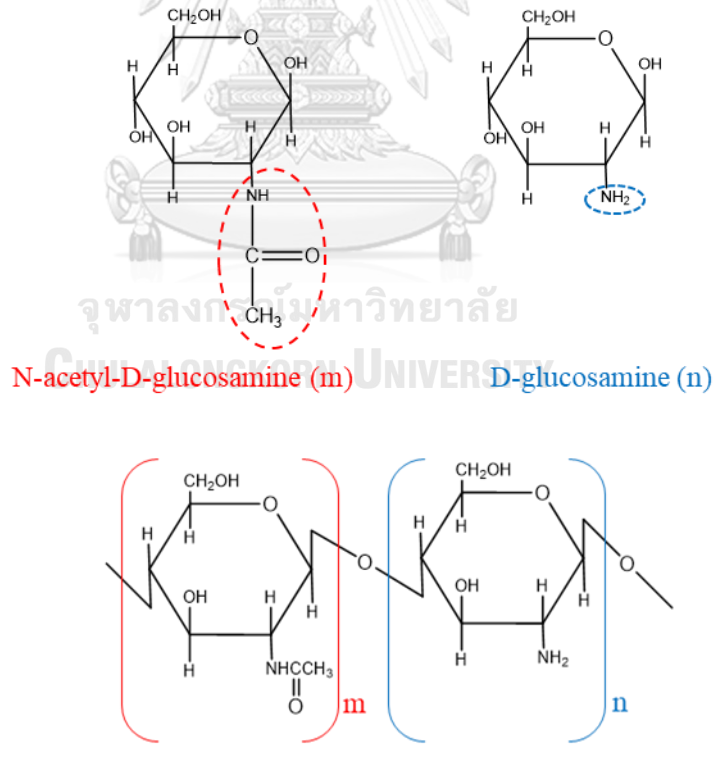

Fig. 9 *Chemical structure of Chitosan (CS)*

Table 4 *Application of Chitosan as a mucoadhesive polymer for drug delivery*

Drug	Polymeric platform	Dosage form	Application	Therapeutic goal
Ibuprofen [196]	Thermosensitive CS hydrogel	Thermosensitive hydrogel	Nasal mucosa	Formulation of non-toxic CS-**β**-glycerophosphate (**β**-GP) thermosensitive hydrogel for nose-to-brain delivery of ibuprofen for neurological disorders.
Rosmaniric acid (RA) [197]	CS-coated nanoemulsion	Emulsion	Nasal mucosa	Enhance permeability, stability, and bioavailability of RA through nasal delivery for neuroprotective therapy.
Ropinirole HCl (RH) [198]	CS-coated PLGA		Nasal mucosa	Enable nose-to-brain delivery of RH to avoid first-pass metabolism and enable passage through BBB for Parkinson's treatment.

Chulalongkorn University

Drug	Polymeric platform	Dosage form	Application	Therapeutic goal
Curcumin (CUR) [199]	Guanidine/CS (GCS)	Thermosensitive hydrogel	Nasal mucosa	Facilitate drug permeation through the nasal mucosa and bypass BBB for better bioavailability of CUR for the treatment of depression.
Astragalus polysaccharide (APS) [200]	Microspheres	Microparticulate powder spray	Nasal mucosa	Enhance residence time and permeation of APS in the nasal cavity for the treatment of allergic rhinitis.
Exenatide (EXD) [201]	CS/hydrogel	Thermosensitive hydrogel	Nasal mucosa	Enhance the release behavior, biodistribution, pharmacokinetics, and pharmacodynamics of exenatide-loaded hydrogels for nasal delivery.

Chulalongkorn University

Drug	Polymeric platform	Dosage form	Application	Therapeutic goal
Levofloxacin (LEV) [202]	CS/Cyclodextrin Nanosphere	Solution	Ophthalmic	↑ antibacterial activity and better ocular bioavailability of LEV by nanoencapsulation and surface property modification.
DEX-LEV [203]	Glycol CS/ Oxidized HA	Hydrogel film	Ophthalmic	Dual delivery of LEV and DOX from glycol CS/oxidized HA hydrogel film for the treatment of postoperative endophthalmitis.
Clotrimazole [204]	CS/Pectin Polyelectrolyte complexes	Multilayer film	Buccal	Controlled delivery of clotrimazole from multilayered CS/Pectin mucoadhesive film for oral fungal infection.
Curcumin (Cur) [205]	CS NPs	Carbohydrate film	Buccal	Enhance physical property and pharmacokinetics of Cur by nanoencapsulation enabling buccal administration.

Chulalongkorn University

2.5.4 Poloxamer

Poloxamer, also Pluronic, belongs to the unique class of synthetic tri-block copolymers comprising central hydrophobic chains of poly (propylene oxide) (PPEO) and two hydrophilic chains of poly (ethylene oxide) (PEO) (Fig. 10) [206]. In this study, poloxamer acts as the surfactant to increase the solubility and dispersion of FVR in the aqueous phase and to facilitate high drug loading into the CS-ALG-NPs. Poloxamer is also a mucoadhesive agent, but its mechanism is still unclear. Some studies linked its mucoadhesion mechanisms to its temperature-dependent self-assembly and gelling properties. Because of its thermo-responsive feature, it attracts significant attention in the biomedical field. One of the most common uses of poloxamer in the biomedical field is the development of hydrogels for drug delivery, wound dressing, biosensors, and implantable devices. Apart from being thermo-responsive, its amphiphilic nature and mucoadhesive properties make it ideal for various biomedical applications [206, 208]. Xu, Xu [209] develop a thermosensitive and mucoadhesive heparin-poloxamer (HP) hydrogel using ε-polylysine (EPL) as a functional excipient for endometrial injury. It was found that the rheological and mucoadhesive properties of the HP hydrogel can be tunable by altering the amount of EPL in the formulation. It was also proven that the addition of EPL provides a significant increase in the drug release *in vitro* compared to the HP hydrogel. Moreover, the mucoadhesiveness and accelerated release of drug from the hydrogel had significantly increased its absorption in the uterus basal layer and endometrial glans after 8 h of administration in the uterus cavity. Below are some of the notable studies on poloxamer as a mucoadhesive material in delivering various types of drug molecules (Table 5).

จุฬาลงกรณ์มหาวิทยาลัย
Chulalongkorn University

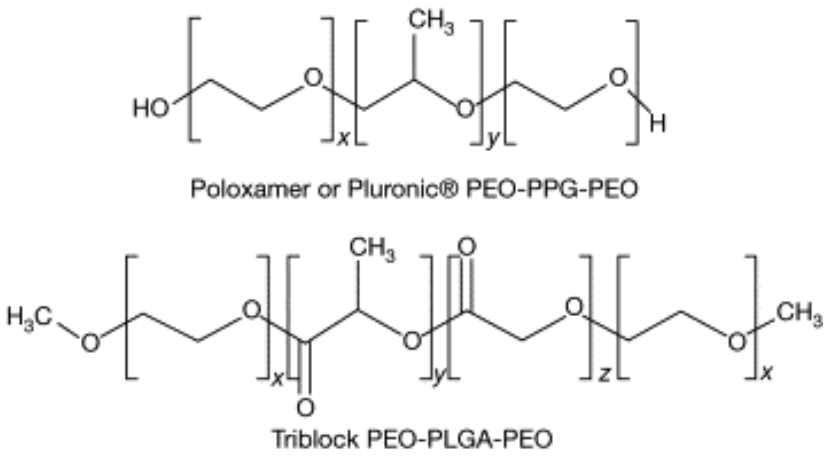

Fig. 10 *Chemical structure of Poloxamer*

จุฬาลงกรณ์มหาวิทยาลัย
CHULALONGKORN UNIVERSITY

Table 5 *Application of Poloxamer as a mucoadhesive polymer for drug delivery*

Drug	Polymeric platform	Dosage form	Application	Therapeutic goal
Ribavirin [210]	Poloxamer microparticles	Microparticulate powder for insufflation	Nasal mucosa	Direct nose-to-brain delivery of ribavirin through its enhanced absorption and drug retention in the nasal cavity.
Tacrolimus [211]	Poloxamer/CS	Thermosensitive gel	Ophthalmic	Enhanced precorneal retention and sustained delivery of tacrolimus from poloxamer/CS thermosensitive gel.
Desloratadine (DES) [212]	Poloxamer 188 and 127 *in situ* gel	Thermosensitive hydrogel	Nasal mucosa	Solubility enhancement of DES in situ gel system to enable better bioavailability *via* the intranasal route.

Chulalongkorn University

Drug	Polymeric platform	Dosage form	Application	Therapeutic goal
Amisulpride [213]	Lipid/Poloxamer/ Gellan gum complexes	Nanoemulgel	Nasal mucosa	Provide noninvasive nose-to-brain delivery of amisulpride *via* intranasal delivery while subsequently reducing exposure to the systemic circulation, thus reducing side effects.
Midazolam [214]	Poloxamer *in situ* gel	Thermosensitive hydrogel	Nasal mucosa	Provide a well-tolerable and alternative route of administration for midazolam with better pharmacokinetics and bioavailability through intranasal administration.
Artemisinin [151]	Polyvinylpyrrolidone/ Poloxamer nanomicelles	Liquid micelles	Ophthalmic	Improve the solubility of artemisinin *via* nanomicelle formulation, allowing better trans corneal permeation and retention.

CHULALONGKORN UNIVERSITY จุฬาลงกรณ์มหาวิทยาลัย

Drug	Polymeric platform	Dosage form	Application	Therapeutic goal
Gentamicin [215]	Poloxamer 407/188 hydrogel	Thermosensitive hydrogel	Cavity wound	Provide a minimally invasive delivery route for gentamicin while enhancing its antibacterial potential for cavity wound treatment.
Royal jelly [216]	Poloxamer *in situ* hydrogel	Hydrogel	Ophthalmic	Enable longer precorneal residence time and bioavailability of royal jelly-in situ gel formulation compared to conventional eye drops.
Dexamethasone [217]	Poloxamer *in situ* hydrogel	Hydrogel spray	Buccal	Local oral cavity delivery of dexamethasone in mucoadhesive hydrogel spray for better absorption and patient compliance in treating lichen planus.

Chulalongkorn University

Drug	Polymeric platform	Dosage form	Application	Therapeutic goal
Hypericin [218]	Poloxamer *in situ* hydrogel liquid crystalline precursor system	Thermosensitive hydrogel	Intravaginal	Enhance the permeability and retention of hypericin in the vaginal mucosa through a poloxamer-based carrier system in treating vaginal candidiasis.

Chulalongkorn University

CHAPTER 3
METHODOLOGY

3.1. Fabrication of favipiravir-loaded mucoadhesive chitosan-alginate nanoparticles (FVR-MCS-ALG-NPs)

FVR-MCS-ALG-NPs was fabricated by oil-in-water emulsification and ionotropic gelation as previously reported by Sorasitthiyanukarn and co-workers [219] with some modifications. Briefly, 1 mL of FVR (anhydrous, >98% purity from Aurore Pharmaceuticals, India) solution in methanol was added dropwise into ALG (medium viscosity: ≥ 2000 cP at 2% in H2O at 25 °C; MW: 490 kg/mol; mannuronate/guluronate ratio, M/G ratio: 1.56 from Sigma-Aldrich, USA) aqueous solution (20 mL, 0.6 mg/mL dissolved in Milli-Q® water; pH was adjusted to 5.5 by 1% acetic acid) containing various concentrations of Poloxamer 407 under continuous magnetic stirring at 1000 rpm for 20 min followed by sonication at a frequency of 45 kHz and sonic power at 80 W for 15 min using an ultrasonication bath (Model CP 230, Crest Ultrasonic Corp., NY, USA). $CaCl_2$ aqueous solution (4 mL, 0.67 mg/mL dissolved in Milli-Q water) was added dropwise using an automatic syringe pump (NE 100, New Era, Pump System Inc., NY, USA) at a rate of 20 mL/h and continuously stirred for 30 min. The resulting suspension was combined with 4 mL of CS (molecular weight, MW: 73 kDa, degree of deacetylation, DD: 91.74% was supplied by Marine Bio-Resources, Thailand) aqueous solution in various ALG: CS mass ratios

จุฬาลงกรณ์มหาวิทยาลัย
Chulalongkorn University

(pH of CS solution was adjusted to pH 5.5 by 10% NaOH solution) and stirred for another 30 min at ambient room temperature (ART). The resulting suspension was equilibrated overnight in a light-proof cabinet at ART. FVR-MCS-ALG-NPs was obtained as a clear dispersion in an aqueous solution. The uncoated-FVR-ALG NPs was prepared in similar manner but without the addition of CS.

3.2. Experimental design for optimization by Box-Behnken Design (BBD) and Response Surface Methodology (RSM)

To optimize the fabrication process and to determine the effect of various factors in the particle size, ζ potential, encapsulation efficiency (EE), and loading capacity (LC) of the FVR-MCS-ALG NPs, a three-factor, two-level Box-Behnken design was used based on the preliminary experimental data gathered considering the ALG: CS mass ratio, FVR concentration, and poloxamer 407 concentration as the independent variables. A total of 15 formulation conditions was generated using Design-Expert® with three replicated center points to limit the error. The detailed summary of independent and dependent variables to achieve the optimum FVR-CS-ALG NPs is shown in Table 6. As described above, the ALG: CS mass ratio (A), FVR (B), and Poloxamer 407 (C), was selected as the main factors, with their corresponding levels. Data were analyzed using the ANOVA test available in the software, and a polynomial model equation for each response was generated.

จุฬาลงกรณ์มหาวิทยาลัย
Chulalongkorn University

Table 6 *Different levels of variables in Box-Behnken Design*

Variables	Levels		
	Low	**Medium**	**High**
Independent			
A = ALG: CS mass ratio	1:0.025	1: 0.50	1: 0.10
B = FVR (mg)	5	10	15
C = Poloxamer 407 ($\%^{w}/_{v}$)	1	1.5	2
Dependent	**Constraints**		
Y_1 = Particle size (nanometer, nm)	Minimize		
Y_2 = ζ potential (millivolts, mV)	± 20		
Y_3 = EE (%)	Maximize		
Y_4 = LC (%)	Maximize		

3.3. Physicochemical characterization

3.3.1. Particle size, polydispersity index, and ζ potential

The hydrodynamic size and dispersity were determined by dynamic light scattering (Zetasizer Nano ZS®, Malvern Panalytical Ltd., UK) at a controlled temperature of 25 ± 2 ºC with a detection angle of 90º. The surface charge was determined using laser doppler electrophoresis of the same instrument. All samples were measured in triplicates.

3.3.2. Morphological characterization

Transmission Electron Microscope (TEM, JEM-1400Flash, JEOL Ltd., Tokyo, Japan) and Field Emission-Scanning Electron Microscope (FE-SEM, JSM-7610F, Oxford

X-Max 20, JEOL Ltd., Tokyo, Japan) was used to observe the morphology of the FVR-NPs. The samples were freshly prepared by diluting the samples 50× with filtered Milli-Q™ water to homogeneously disperse the particles. An aliquot of the MPNP suspension was dropped onto the grid, stained with uranyl acetate, and allowed to dry for 24 h in a desiccator.

3.3.3. Loading capacity and encapsulation efficiency

The LC and EE of the FVR-MCS-ALG NPs was determined using an indirect method as described by Sorasitthiyanukarn [219]. In brief, an aliquot of the suspension was subjected to ultracentrifugation with a speed of 105,000 × *g* at a controlled temperature of 4 °C for 1 h. The supernatant was collected and diluted with an appropriate volume of Milli-Q™ water and vortexed for 5 min. The amount of free FVR from the supernatant was quantified by determining its absorbance at 363 nm using a UV-Vis spectrophotometer (Agilent Cary 60, Agilent Technology Ltd., CA, USA) after appropriate dilution in acetonitrile. The quantitative estimation of FVR from the supernatant was computed against the calibration curve of the FVR in acetonitrile with a concentration range of 0.5-18 µg/mL (Appendix A). The % EE (Eq. 1) and %LC (Eq. 2) of the FVR-MPNPs were calculated as follows:

จุฬาลงกรณ์มหาวิทยาลัย
CHULALONGKORN UNIVERSITY

Eq. 1

% EE = [(Wt – Ws)/Wt] x 100

Eq. 2

% LC = [(Wt – Ws)/Wnp] x 100

Whereas *Wt* is the total amount of FVR used in FVR-MPNPs, *Ws* is the amount of FVR in the supernatant after ultracentrifugation and *Wnp* is the weight of the FVR-MPNPs obtained after lyophilization.

3.3.4. Thermal analysis

Differential thermal analysis (DTA) and thermogravimetric analysis (TGA) were done on the thermogravimetric analyzer (TG 209 F3 Tarsus®, Netzsch, Germany) from 30 to 500 ºC in the nitrogen atmosphere at a constant heating rate of 20 ºC min^{-1}. Moreover, the x-ray diffraction (XRD) pattern of the same samples were obtained on a wide-angle x-ray diffractometer (PANalytical X'Pert Pro model, Germany) operated at 30 mA and 40 kV, and a scanning speed of 0.2º, 2 Θ/step at room temperature.

จุฬาลงกรณ์มหาวิทยาลัย
CHULALONGKORN UNIVERSITY

3.4. *In vitro* favipiravir release

The release of FVR from the NPs was determined *via* the dialysis diffusion method by Clementino, Pellegrini [220] with some modifications. A ready-to-use SnakeSkin™ dialysis tubing (10kDa MWCO, 35 mm dry; Thermo Scientific, Illinois, USA) was used as the membrane for the study. 20 mL of the suspension and free FVR

solution at the same concentration were separately placed in the tube and sealed with dialysis clips on both ends. The sealed samples was submerged in 500 mL simulated nasal fluid (SNF: sodium chloride 8.77 mg/mL, 2.98 mg/mL potassium chloride and 0.59 mg/mL calcium chloride in deionized water with 5% mucin and 0.5% w/v bovine serum albumin; pH 5.5) and physiological fluid (PBS: potassium dihydrogen phosphate 1 mg/mL, dipotassium hydrogen phosphate 2 mg/mL, and sodium chloride 8.5 mg/mL in deionized water, pH 7.4) to mimic nasal and physiological pH of human body fluids, respectively. The medium was maintained at 37 °C and magnetically stirred at 100 rpm. At pre-determined time points, 5 mL of the media was withdrawn and replaced with an equal volume of fresh media. The collected samples were centrifuged at 4000 rpm for 20 min to separate the FVR. The supernatant was diluted in acetonitrile and analyzed and quantified by UV-Vis spectrophotometer at 363 nm. The % cumulative FVR released was computed using Eq 3. The *in vitro* release study for all samples was done in triplicates.

จุฬาลงกรณ์มหาวิทยาลัย
CHULALONGKORN UNIVERSITY

Eq. 3

$$CR\ (\%) = \frac{V_e \sum_{i=1}^{n-1} C_{n-1} + V_o C_n}{\mathrm{m}} \times 100$$

Whereas *CR* (%) is the cumulative FVR released from the medium, V_e is the volume which was taken out from the medium (mL), V_o is the volume of the release medium (mL), C_n is the concentration of the time point (mg/mL), and *m* is the total

amount of FVR (mg) in the dialysis bag. The release kinetic models, i.e., zero-order, first-order, Higuchi, Korsmeyer-Peppas, Hixson-Crowell, and Weibull were calculated using the DDsolver software, Microsoft Excel plugin program (Version 2010, Microsoft Corporation, Redmond, WA). The best-fitted model was selected based on the highest computed R^2 *adjusted* and MSC values and the lowest AIC [219].

3.5. Mucoadhesion studies

3.5.1. Effects of mucin on size and surface charge of FVR-MPNPs

The hydrodynamic size and the ζ-potential of the FVR-NPs were used to observe its interaction with the commercially available porcine mucin [221]. Porcine mucin-type III was utilized for this study owing to its reproducibility and consistency of results [222]. Briefly, mucin solution (0.4 mg/mL) was prepared in simulated nasal fluid (SNF) at pH 5.5. An equal amount of mucin solution and FVR-MPNPs suspension was transferred to a 50 mL volumetric flask and subjected to an orbital incubator shaker at a speed of 150 rpm and a temperature of 37 ºC to mimic normal physiological temperature. An aliquot of the incubated mucin: FVR-MPNPs mixture was collected at 0.5, 1, 2, 3, 4, and 5 h and was ultracentrifuged at 105,000 × *g* at a controlled temperature of 4 ºC for 1 h. The precipitate was washed twice with Milli-Q™ water to remove unabsorbed mucin and resuspended in the same solvent. The resuspended FVR-MPNPs was analyzed for the change in hydrodynamic size and surface charge.

จุฬาลงกรณ์มหาวิทยาลัย
Chulalongkorn University

3.5.2. *In vitro* mucin adsorption studies and adsorption isotherms

The adsorption and interaction of FVR-NPs and mucin was evaluated based on the published method [223]. In brief, an equal volume of mucin solution (0.4 mg/mL in SNF) and the NP formulations (FVR-MCS-ALG or FVR-ALG NPs) (5 mg/mL) was transferred to a 50 mL volumetric flask and subjected to orbital incubator shaking at a speed of 150 rpm at 37 ºC. An aliquot of the incubated mucin: NP mixture was collected at 0.5, 1, 2, 3, 4, and 5 h and was ultracentrifuged at 105,000 × g at a controlled temperature of 4 ºC for 1 h. The precipitate was washed twice with Milli-Q™ water to remove unadsorbed mucin and resuspended in the same solvent. Moreover, the unbound or unabsorbed mucin from the supernatant was quantified by bicinchoninic acid (BCA) protein analysis. An equal volume of BCA working reagent (50:1, Reagent A: B) and the supernatant was incubated at 37 ºC for 2 h for color development. Afterward, the absorbance of the mixture was measured at 562 nm and quantified against the calibration curve of mucin (Appendix B). The % mucin binding efficiency was computed as follows:

จุฬาลงกรณ์มหาวิทยาลัย
CHULALONGKORN UNIVERSITY

Eq. 4

Mucin binding efficiency (%) = $[(mucin_{total} - mucin_{unbound})/ mucin_{total}] \times 100$

3.6. *Ex vivo* transmucosal studies

3.6.1. Collection and preparation of porcine nasal mucosa

The porcine nasal mucosa (PNM) was excised from the noses of freshly slaughtered pigs in the local slaughterhouse and stored in ice during transportation to the pathology laboratory. The harvested porcine noses were cross sectioned using a pathology saw (Exakt 302, Exakt Technologies, Oklahoma, USA) through each nostril to expose the tissue. The nasal mucosa was precisely and carefully excised by surgical blade and forceps to separate the underlying cartilage of the nasal septum. The harvested PNM was washed several times with a normal saline solution to remove unwanted debris. The cleaned PNM was placed on ice and submerged in Hanks' balanced salt solution in a sterile plate to maintain tissue integrity.

3.6.2. *Ex vivo* transmucosal permeability study through porcine nasal mucosa

The freshly harvested PNM was mounted onto the Franz cell with a permeation area of 1.77 cm^2. SNF (pH 5.5) was used as the medium to mimic nasal physiological conditions. The PNM was pre-saturated with SNF by placing 500 µL of the medium onto the donor compartment and equilibrate for 15 min. Afterwards, the surface of the PNM was treated with 1 mL of freshly prepared FVR NP formulations (FVR-MCS-ALG or FVR-ALG NPs) or free FVR solution (at equivalent to amounts of FVR) onto the donor compartment. The receptor chamber was filled with 12 ml of the SNF, maintained at 37 ± 0.5 ºC and stirred at 150 rpm. The study

จุฬาลงกรณ์มหาวิทยาลัย
Chulalongkorn University

was conducted for 1h. At pre-determined time points, 500 µL of the medium was withdrawn from the receptor chamber. The same volume of fresh SNF maintained at the same temperature was replaced in the receptor after every sampling to keep the volume and temperature constant during the study. The collected samples were filtered before quantification of permeated FVR using a UV/Vis spectrophotometer at 363 nm. The cumulative amount of FVR permeated per unit area (µg/cm^2) was plotted as a function of time (min). After finishing the experiment, the FVR retained in the donor compartment was quantified by washing the apical side of the membrane several times to collect the adsorbed FVR on the surface. The flux (*J*, µg/cm^2/min), permeability coefficient (*P; cm^2/min*), and the enhancement ratio (*ER*) were estimated as per **Eq. 5,6**, and **7**, respectively.

The cumulative amount of FVR permeated per unit area (µg/cm^2) was plotted as a function of time (min). After finishing the experiment, the FVR retained in the donor compartment was quantified. The flux at steady state (*Jss*) and permeability coefficient (K_P) were estimated as per Eqs. 5 and 6, respectively.

จุฬาลงกรณ์มหาวิทยาลัย
Chulalongkorn University

Eq. 5

$$Jss = \Delta Qt / \Delta t \times A$$

Eq. 6

$$K_P = Jss/C_0$$

Where ΔQt (*µg*), difference in the permeated drug amount between the time points; Δt (*h*), diffusion area (*cm^2*); C_0 (*µg*), initial drug concentration in the donor

compartment. To determine the effect on the permeability compared to the free FVR solution, the enhancement ratio of the flux (ER_{flux}) was computed as (Eq. 7):

Eq. 7

$$ER_{flux} = Jss_{FVR-NPs} / Jss_{free\ FVR}$$

3.6.3. Histopathological examination of porcine nasal mucosa for preliminary toxicity assessment

The histopathological examination of the treated and untreated PNM was performed after 1 h of treatment to determine whether the treatments will cause any mucosal damage. PNM treated with the negative (no treatment) and experimental controls (FVR-MCS-ALG, FVR-ALG NPs and FVR solution) were fixed in 10 % buffered formalin immediately after the experiment. The tissues were embedded in paraffin and processed accordingly for sectioning. The sectioned tissues were stained with hematoxylin and eosin and analyzed by a pathologist blinded to the experimental conditions.

จุฬาลงกรณ์มหาวิทยาลัย
Chulalongkorn University

3.7. *In vitro* biocompatibility and cellular uptake studies in human nasal epithelial cell (RPMI 2650)

3.7.1 Cytocompatibility study

RPMI 2650 human nasal epithelial cells (ATCC, USA) was cultivated in MEM media supplemented with 10% (v/v) fetal bovine serum (FBS) at 37 ℃ in a 95% air/5% CO_2 incubator. To study the biocompatibility of the FVR-MCS-ALG NPs to RPMI

2650, the confluent cells in a 96-well plate was treated with the samples diluted in blank-MCS-ALG NPs and water, respectively to achieve various concentrations. The diluents were used as the control to observe the cytotoxic effect of the test samples. After 1 h of incubation with the treatments, the cells were washed and incubated again for 3 h with the addition of 3-(4,5-dimethylthiazol-2-yl)-2,5-diphenyl tetrazolium bromide (MTT) solution (0.5 mg/mL). The amount of formazan crystals formed was dissolved in dimethyl sulfoxide (DMSO) and the optical density at 570 nm (OD_{570}) was measured by a microplate reader (Wallac 1420, Perkin-Elmer, USA).

3.7.2 Cellular uptake

To observe enhanced cellular uptake of the FVR and FVR-MPNP into the cells, a qualitative determination was performed through fluorescence microscopy (Fluorescence microscope, Nikon Eclipse Ts2, Nikon, Japan). Due to the weak fluorescence of FVR, 5-aminofluorescein (5-AF) was used and loaded in the MCS-ALG NPs. The confluent RPMI 2650 was treated with free or unencapsulated 5-AF and 5-AF-MCS-ALG NPs for 4 and 24 h. The cells were washed with PBS 5× to remove the excess and uninternalized samples. To track the internalization of the test samples in RPMI 2650, the cells were stained with 4′,6-diamidino-2-phenylindole (DAPI) for 10 min at room temperature and observed under fluorescence microscope.

จุฬาลงกรณ์มหาวิทยาลัย
Chulalongkorn University

3.8. *In vitro* antiviral assay using PEDV model

3.8.1. Cell and virus preparation

Due to the complexity and hazard brought by the SARS-CoV 2 experiment, the researcher employed another coronavirus. The porcine epidemic diarrhea virus (PEDV, NCBI accession LC053455), a non-zoonotic virus belonging to the alpha-coronavirus genus was served as a surrogate for antiviral assay. In this study, the researcher selected the PEDV model to test the potential of the test samples in enhancing the antiviral activity of FVR in SARS-CoV 2 inhibition due to its low health risks and minimal laboratory requirement.

Specifically, PEDV carrying mCherry fluorescent reporter gene (mCherry-PEDV) in its genome and Vero cells stably expressing eGFP (eGFP-Vero) as the host cell were used for the assay. The viral genome was constructed by reverse genetics and the infectious viral particles were prepared as previously described by Jengarn and co-workers [224]. eGFP-Vero was constructed through the transfection of the pEGFP-N1 (Clontech) plasmid into Vero cells (ATCC: CCL-81) and the selection of the eGFP positive cells using 0.8 mg/ml of G418 antibiotic (Sigma-Aldrich). The cells were maintained in Opti-MEM (Gibgo) supplemented with 10% (v/v) fetal bovine serum and antibiotics.

จุฬาลงกรณ์มหาวิทยาลัย
CHULALONGKORN UNIVERSITY

3.8.2. Determination of non-cytotoxic concentration

eGFP-Vero cells were seeded overnight at 2.5×10^4 cells in a 96-well tissue culture microplate at 37 °C in a 5% CO_2 incubator. The formulations and the free FVR was diluted added to the cells at the various concentrations. The diluents were used as the control to observe the cytotoxic effect of the test samples. After 15 h of treatment, the cytotoxicity was determined by adding Cell Counting Kit-8 reagent into the cells and subjected to incubation for 1 h. The optical density at OD_{450} was measured by a microplate reader and the % cell viability was calculated by normalization with the control.

3.8.3. Antiviral assay

eGFP-Vero cells were seeded overnight at 2.5×10^4 in a 96-well tissue culture microplate at 37 °C in a 5% CO_2 incubator. mCherry-PEDV was added into the cells to allow viral absorption/infection for 1 h. The unattached viruses were then removed through washing with PBS. The formulations and the free FVR was diluted and added to the cells with fresh media supplemented with 1% tryPLE. The diluents (10% v/v) were used as the control to observe the antiviral effect of the test samples. At 15 h post-infection, the fluorescent images of mCherry (at excitation wavelength 561 nm and emission wavelength 570-630 nm) and eGFP (at excitation wavelength 488 nm and emission wavelength 500-550 nm) was obtained by Opera Phenix high-content screening system (PerkinElmer). The area of mCherry

จุฬาลงกรณ์มหาวิทยาลัย
CHULALONGKORN UNIVERSITY

fluorescence represented by its syncytia formation from the infection in each well was specified. The total mCherry fluorescent intensity was quantified by Harmony high-content imaging and analysis software (PerkinElmer). The relative reduction of mCherry intensity (syncytia formation) by the test samples was calculated by comparing it with the control. Dose-respond curves were fitted using the normalized sum of mCherry fluorescent intensity data and the half-maximal effective concentration (EC_{50}) was calculated by GraphPad® Prism software 9.3.0.

3.9. Storage stability studies

The storage stability studies were conducted by transferring the optimal FVR-MPNPs to an amber glass bottle with a tight screw cap. The bottles were stored at ambient room (ART) and refrigerated (4 °C) temperatures away from light exposure. The physicochemical characteristics (size, ζ potential, and EE) were measured every month for 6 months. The stability of the formulations was evaluated by the change of its characteristics over time and the effects of storage temperatures.

จุฬาลงกรณ์มหาวิทยาลัย
Chulalongkorn University

3.10. Statistical analysis

The collected data was expressed as mean ± standard deviation (SD). The polynomial equations for the optimization were generated using multiple linear regression followed by model-fitting with one-way ANOVA using the Design-Expert® software 13.0.5.0 (Stat-Ease, Inc., Minneapolis, MN, USA). The cell viability and other results were analyzed using ANOVA with the recommended post-hoc test by

GraphPad® Prism software 9.3.0 (San Diego, CA, USA). The *p* value of < 0.05 is considered statistically significant.

จุฬาลงกรณ์มหาวิทยาลัย
Chulalongkorn University

CHAPTER 4
RESULTS AND DISCUSSION

4.1. Generation of responses by Design Expert Software

To optimize the fabrication process and determine the effect of various factors on the hydrodynamic size (Y_1), zeta (ζ) potential (Y_2), loading capacity (LC) (Y_3), and encapsulation efficiency (EE) (Y_4) of the FVR-MCS-ALG-NPs, a three-factor BBD was used based on the preliminary experimental data gathered considering the (A) ALG:CS mass ratio, (B) the FVR concentration, and (C) the poloxamer-407 concentration as the independent variables. A total of 15 formulation conditions were generated using Design-Expert® with three replicated center points to limit the error. A detailed summary of the independent and dependent variables to achieve the optimal condition for FVR-MCS-ALG-NPs is shown in Table 6. Fifteen formulations were generated by BBD with three replicated center points (F13–F15), as shown in Table 7. As described above, the ALG:CS mass ratio (A), FVR (B), and Poloxamer-407 (C) were selected as the main factors, with their corresponding levels. Data were analyzed using the ANOVA test available in the Design-Expert® software, and a polynomial model equation was generated for each response.

จุฬาลงกรณ์มหาวิทยาลัย
Chulalongkorn University

Table 7. *Formulation design for FVR-MCS-ALG-NPs using BBD with its actual and predicted responses of all dependent variables*

Code	A	B	C	Y_1: Size(nm)		Y_2: ζ-potential (mV)		Y_3: DL (%)		Y_4: EE (%)	
				Actual	Predicted	Actual	Predicted	Actual	Predicted	Actual	Predicted
F1	1: 0.0250	5	1.5	227 ± 6	229.9	−21.9 ± 0.6	−22.2	5.0 ± 0.9	5.5	33.7 ± 5.6	35.6
F2	1: 0.1000	5	1.5	289 ± 16	278.5	−27.8 ± 0.4	−27.7	7.4 ± 0.5	6.4	60.9 ± 5.0	57.7
F3	1: 0.0250	15	1.5	239 ± 2	238.0	−24.7 ± 0.5	−24.8	12.1 ± 0.9	13.1	34.4 ± 3.5	37.6
F4	1: 0.1000	15	1.5	284 ± 5	286.7	−20.8 ± 0.6	−20.5	24.3 ± 0.3	23.8	84.8 ± 0.7	82.9
F5	1: 0.0250	10	1	243 ± 7	242.8	−21.6 ± 0.9	−21.0	11.4 ± 0.5	10.4	33.6 ± 0.3	29.7
F6	1: 0.1000	10	1	288 ± 5	291.6	−21.3 ± 2.0	−21.7	15.4 ± 0.8	16.2	58.9 ± 0.8	63.4
F7	1: 0.0250	10	2	231 ± 8	225.0	−20.3 ± 0.3	−20.6	7.4 ± 0.6	6.9	37.4 ± 3.8	36.2
F8	1: 0.1000	10	2	274 ± 14	273.7	−21.2 ± 1.1	−21.2	12.0 ± 0.6	12.7	69.4 ± 0.9	69.9
F9	1: 0.0625	5	1	258 ± 16	263.2	−22.5 ± 1.2	−22.7	11.9 ± 0.6	11.5	63.3 ± 0.3	65.9
F10	1: 0.0625	15	1	281 ± 8	271.3	−20.4 ± 0.7	−20.6	23.4 ± 1.1	24.0	82.8 ± 2.9	79.5
F11	1: 0.0625	5	2	245 ± 16	245.3	−22.6 ± 2.3	−22.2	7.3 ± 0.5	8.0	73.7 ± 4.3	72.4
F12	1: 0.0625	15	2	248 ± 12	253.4	−19.9 ± 1.0	−20.0	21.5 ± 1.9	20.5	84.2 ± 3.3	86.0
F13*	1: 0.0625	10	1.5	258 ± 5	258.3	−21.4 ± 0.7	−21.5	22.0 ± 0.8	22.1	90.7 ± 1.0	89.2
F14*	1: 0.0625	10	1.5	260 ± 7	258.3	−22.0 ± 2.8	−21.5	22.6 ± 2.9	22.1	87.1 ± 13.3	89.2
F15*	1: 0.0625	10	1.5	251 ± 14	258.3	−21.2 ± 3.2	−21.5	21.9 ± 0.9	22.1	89.8 ± 0.8	89.2

A: ALG:CS (mass ratio), **B:** FVR (mg/mL), and **C:** Poloxamer-407 (% w/v); (*****) are the three replicated center points of the design

4.1. Selecting the optimum mathematical model

Optimizing the formulation improves system performance to achieve the maximum benefit. The dependent variable data were fit to different mathematical models, including linear, two-factor interaction, and quadratic models to find a suitable model for computing the optimal polynomial model. The optimal model was selected for each response based on the following criteria:

(1) the model must be significant

(2) the lack-of-fit must not be significant

(3) the *adjusted* and *predicted* R^2 must be high and in reasonable agreement, wherein the difference must not be < 0.2.

(4) the selected model must have high adequate precision (>4 is acceptable).

จุฬาลงกรณ์มหาวิทยาลัย
Chulalongkorn University

Adequate precision measures the signal-to-noise ratio, wherein a ratio > 4 is considered desirable; hence, the model can be used to navigate the design space. The fit summary of the responses and the selected model are presented in Table 8.

Table 8. Fit summary and the selected mathematical model of the responses

Model	Sequential *p*-value	Lack of Fit *p*-value	Adjusted R^2	Predicted R^2	Adequate precision	Remarks
Response: Size (Y_1)						
Linear	< 0.0001	0.4312	0.918	0.8729	21.9385	Suggested
2FI	0.143	0.5328	0.9407	0.8653		
Quadratic	0.8048	0.3743	0.9208	0.6516		
Response: ζ-potential (Y_2)						
Linear	0.4431	0.0332	-0.0073	-0.6778		
2FI	0.0726	0.0504	0.394	-0.7722		
Quadratic	0.0006	0.5854	0.9627	0.8681	25.6039	Suggested
Response: Drug loading (Y_3)						
Linear	0.0147	0.0051	0.4922	0.371		
2FI	0.8341	0.0037	0.3695	0.0293		
Quadratic	0.0002	0.0829	0.9775	0.8776	24.8412	Suggested
Response: Encapsulation efficiency (Y_4)						
Linear	0.1088	0.008	0.2499	-0.0122		
2FI	0.947	0.0056	0.0123	-0.9547		
Quadratic	< 0.0001	0.1604	0.9734	0.8621	22.1788	Suggested

จุฬาลงกรณ์มหาวิทยาลัย
Chulalongkorn University

4.2. Analysis of the fitted model

A mathematical model resulting from fitting a data function cannot satisfactorily demonstrate the experimental domain studied [225]. Hence, a more reliable way of analyzing and selecting the quality of a model fit is by using ANOVA to compare the

variation resulting from the change in the combination of variable levels and the variation brought by the random errors in the measurements of the generated responses [225]. The data responses that were fitted to various mathematical models and were statistically analyzed using ANOVA are shown in Table 9. The lack-of-fit test compares the residual error to the pure error from the replicated design points. It is imperative in model selection as it can diagnose how well the regression models (e.g., linear, quadratic, or 2-factor interaction) fit the data. A lack-of-fit error significantly larger than the pure error indicates that something remains in the residuals that can be removed by a more appropriate model. This happens either the model doesn't predict well, or the runs replicate so well that their variance is small, or some combination of the two.

In the optimization using BBD and RSM, we aimed to get data with insignificant lack-of-fit. This would mean that a particular model is well fitted for the data inputs. There could be instances where no appropriate model can be selected among the three. In this study, we carefully checked for the outliers through Box-Cox diagnostic plot generated by the software to get a higher-order model that would fit the data better. Moreover, a polynomial equation was generated from each of the responses (Eqs. 8–11) and was used to analyze the effect of the independent variables as an individual and/or combination of factors on the dependent variables. The coded equations for each response analyzed were used to identify the relative impact of the factors by comparing their factor coefficients. Note that the (+)

จุฬาลงกรณ์มหาวิทยาลัย
CHULALONGKORN UNIVERSITY

coefficients indicate a positive impact or a high-level factor, while (–) coefficients denote otherwise.

4.2.1 The effect of independent variables on particle size

Particle size is one of the critical characteristics to consider in the NPs for nasal transmucosal delivery. It has been reported that particle size <10μM can be deposited in the nasal cavity [52]. However, due to the complexity of the nasal morphology, large particles can be deposited but are not efficient for absorption and internalization by the nasal epithelia [54]. An ideal particle size required for nasal delivery and deposition should be in a range of 300 – 200 nm as smaller particles than this will enter the lungs [64]. Since the particle size we got for the 15 formulations is within the range of an ideal size for transmucosal delivery (ranging from 227-289 nm), we set the goal of minimum possible size to achieve both high deposition and permeation of FVR through the mucosa. As shown in Table 8, a linear model was the optimal model for the particle size with a sequential *p*-value of < *0.0001* and a lack-of-fit *p*-value of 0.4312. The lack-of-fit *F*-value of 1.66 suggests that the lack-of-fit is not significant relative to the pure error. The $R^2_{adjusted}$ and $R^2_{predicted}$ also agreed with a difference of 0.0451. The signal-to-noise ratio of 21.9385 by the computed adequate precision is desirable, indicating that the selected model can be used to navigate the design space.

Eq. 8

$$\boldsymbol{Y_1} = 258.29 + 24.35 \times A + 4.08 \times B - 8.95 \times C$$

Table 9. *Statistical analysis of the mathematical model*

	Y_1	Y_2	Y_3	Y_4
ANOVA for the model				
Sum of squares	5517.47	54.10	660.74	6554.42
Degree of freedom	3	7	7	7
Mean squares	1839.16	7.73	94.39	9.36.35
F-value	53.21	45.22	91.11	69.37
p-value	<0.0001	<0.0001	<0.0001	<0.0001
Inference	significant	significant	significant	significant
Lack-of-fit test				
Sum of squares	335.37	0.8690	6.95	87.52
Degree of freedom	9	5	5	5
Mean squares	37.26	0.1738	1.39	17.50
F-value	1.66	1.06	9.24	5.03
p-value	0.4312	0.5502	0.1005	0.1741
Inference	not significant	not significant	not significant	not significant
Residual				
Sum of squares	380.18	1.20	7.25	94.48
Degree of freedom	11	7	7	7
Mean squares	34.56	0.1790	1.04	13.50

จุฬาลงกรณ์มหาวิทยาลัย
CHULALONGKORN UNIVERSITY

The coded equation showed that the ALG:CS mass ratio (A) and FVR concentration (B) had a positive effect on the hydrodynamic size of the NPs, wherein the ALG:CS mass ratio is the main contributor to its increasing particle size. The hydrodynamic size of the formulation F1-F15 (Table 7) increased with an increasing amount of CS in the polymer ratio, ranging from 227 to 280 nm. This linear relationship of ALG:CS mass ratio to the size of the NPs was attributed to the thicker CS coating on the ALG-NPs (Fig. 11). The formation of FVR-CS-ALG-NPs solely relies on the formation of inter-and intra-molecular interactions between the CS and ALG chains. However, the presence of excess CS molecules causes clumping leading to entanglement of the molecules and larger particle size [226], which is also evident in the formation of highly polydispersed (0.836) particles in increasing CS concentration. In addition, the entanglement of CS in the system could also result in difficulties with ALG to fit inside and be dispersed within the CS [226, 227], which is consistent with previous studies [226-230]. Furthermore, the FVR concentration had a moderate effect on the size due to the increase in the LC. Moreover, the inverse relationship of surfactant concentration to hydrodynamic size was observed, due to the reduction of surface tension and the breakdown of alginate droplets within the system [231].

จุฬาลงกรณ์มหาวิทยาลัย
CHULALONGKORN UNIVERSITY

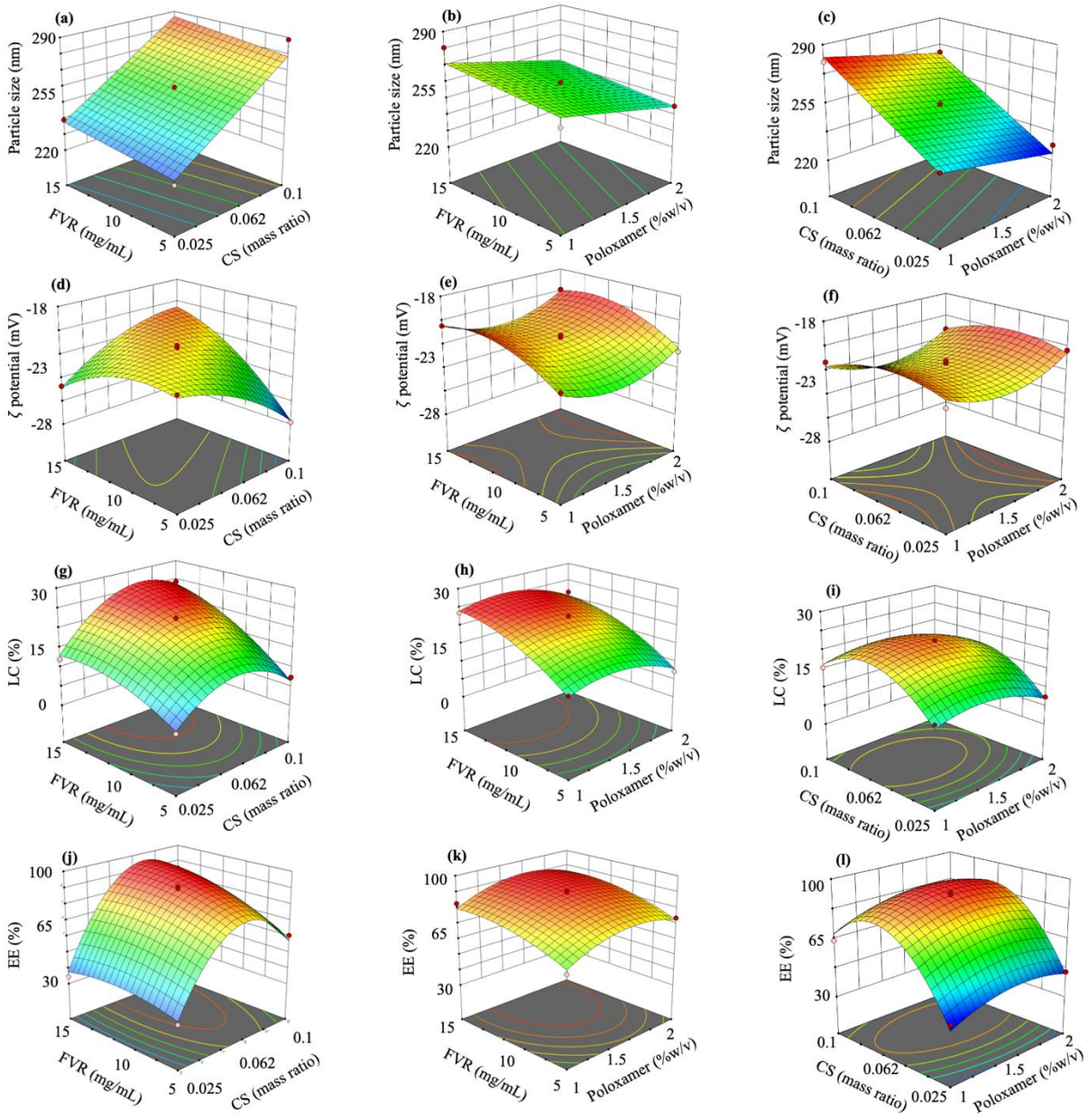

Fig. 11 *Three-dimensional surface model plots showing the interaction between the independent factors to* ***(a-c)*** *size,* ***(d-f)*** *ζ potential,* ***(g-i)*** *LC, and* ***(j-l)*** *EE.*

In contrast, a low surfactant concentration would result in a larger particle size due to the production of unstable droplets within the system and the high propensity of coalescence [232]. It could also result in the formation of irregular

surface tension that is attributed to the incomplete coverage of the particle surface [232]. These results agree with previous studies, wherein an increasing concentration of poloxamer-407 as a stabilizer in the nanoparticulate system in designing a more stable system [233, 234]. A high surfactant concentration also helps emulsify the FVR in water to make it more soluble and well-dispersed in the system. It was also observed that increasing the amount of surfactant resulted in a narrower size distribution (0.2031).

4.2.2 The effect of independent variables on ζ potential

The quadratic model was the selected model for the ζ potential with a sequential *p*-value of 0.0006 and a lack-of-fit *p*-value of 0.5854. The lack-of-fit *F*-value of 1.06 implies that the lack-of-fit is not significant relative to the pure error. The $R^2_{adjusted}$ and $R^2_{predicted}$ also had a reasonable agreement with a difference of 0.0946. The signal-to-noise ratio of 25.6039 was desirable, indicating that the model selected can be used to navigate the design space.

จุฬาลงกรณ์มหาวิทยาลัย
Chulalongkorn University

Eq. 9

$$\boldsymbol{Y_2} = -21.51 - 0.3213 \times A + 1.13 \times B + 0.2362 \times C + 2.46 \times AB - 1.03 \times A^2 - 1.25 \times B^2 + 1.42 \times C^2$$

As shown in Table 7, the surface charge of the FVR-MCS-ALG-NPs was negative ranging from −19.8 to −27.83 mV. The equation showed that the negative surface charge of the FVR-MCS-ALG-NPs was mainly affected by the ALG:CS mass ratio. Notably, they continued to exhibit a (−) surface charge after adding CS to the

system owing to the insufficiency in the CS to neutralize the negatively charged ALG, which is being prevented in the system since the aggregation of polyelectrolyte complexes could occur from charge neutralization after adding a strongly adsorbing species (eg., CS) wherein the net electrical charge in the system becomes almost in equilibrium [235]. Moreover, increasing the FVR concentration contributed to a less negative charge on the particles, owing to the partial positive charge of the FVR amine functional group. Also, the increasing the poloxamer-407 concentration brought a less negative charge of the particle, similar to the result observed by Elgegren et al. in using poloxamer-407 as a stabilizer for polymeric NPs [233]. Skoglund et al. reported that this phenomenon occurs due to charge neutralization of the charged particles by their interaction with increasing concentrations of a non-ionic surfactant [236].

4.2.3 The effect of independent variables on LC

จุฬาลงกรณ์มหาวิทยาลัย
Chulalongkorn University

The quadratic model was the selected model for the LC with a sequential *p*-value of 0.0002 and a lack-of-fit *p*-value of 0.0829. The lack-of-fit *F*-value of 9.24 suggests that the lack-of-fit was not significant relative to the pure error. The $R^2_{adjusted}$ and $R^2_{predicted}$ also had a reasonable agreement with a difference of 0.0999. The signal-to-noise ratio of 24.8421 was desirable, indicating that the selected model can be used to navigate the design space.

Eq. 10

$$\boldsymbol{Y_3} = 22.13 + 2.90 \times A + 6.23 \times B - 1.74 \times C + 2.5 \times AB - 7.19 \times A^2 - 2.76 \times B^2 - 3.37 \times C^2$$

The data showed a relatively high LC ranging from 4.9% to 24.2%. It can be deduced from the equation that the FVR concentration and ALG:CS mass ratio greatly affect the LC of the MCS-ALG-NPs, while poloxamer-407 had an inverse relationship with LC. The highest LC of 24.2% was seen with the highest amount of CS at an ALG:CS ratio of 1:0.1 (F4). The direct relationship between CS and LC was associated with the increasing electrostatic interaction between CS and ALG, thus amplifying the drug loading ability of the MCS-ALG-NPs. Furthermore, the high drug LC was associated with the formation of a more rigid outer matrix of NPs owing to the strong charge interaction between the polymers. A rigorous matrix structure could potentially restrict leakage and premature release of drugs from the polymer matrix. Also, a larger particle size would increase LC, as the amount of FVR in the matrix also increased. These results are consistent with other studies, which confirm the linear effect of the amount of CS and drug concentration in LC of polymeric NPs [227, 232, 237-239]. It can be observed that a particular concentration of surfactant can increase the drug loading due to the enhancement of the solubility of FVR. However, increasing the surfactant concentration antagonized LC, which was attributed to a much higher affinity of FVR to the dispersion medium than to the polymer.

จุฬาลงกรณ์มหาวิทยาลัย
Chulalongkorn University

4.2.4 The effect of independent variables on EE

The quadratic model was the selected model for the EE with a sequential *p*-value < 0.0001 and a lack-of-fit *p*-value of 0.1604. The lack-of-fit *F*-value of 5.03 suggests that the lack-of-fit was not significant relative to the pure error. The $R^2_{adjusted}$ and $R^2_{predicted}$ also had a reasonable agreement with a difference of 0.1113. The signal-to-noise ratio of 22.1788 was desirable, indicating that the selected model can be used to navigate the design space.

Eq. 11

$$\boldsymbol{Y_4} = 89.19 + 16.86 \times A + 6.81 \times B + 3.26 \times C + 5.81 \times AB - 30.96 \times A^2 - 4.80 \times B^2 - 8.42 \times C^2$$

An additional key aspect in NP drug delivery is the EE, which should always be as high as possible. Based on the equation, the ALG:CS mass ratio had the greatest effect on the EE, followed by the FVR and surfactant concentrations. Increasing CS in the ratio, resulted in an increase in EE from 33.6 to a maximum of 90.7%. These results were correlated with those of previous studies where a direct relationship of polymer interaction and the EE was observed [240-242]. This linear relationship between CS and EE is attributed to the increase in amino groups that interact and cross-link with the COOH of ALG. The EE also had a direct relationship with an increase in the FVR concentration from 5 to 15 mg/mL due to the interaction between polymers and the high solubility of FVR in an aqueous solution. Adding poloxamer-407 had a positive effect on the increase in EE due to its interaction with

จุฬาลงกรณ์มหาวิทยาลัย
Chulalongkorn University

ALG. Poloxamer is an amphiphilic copolymer that self-assembles into micelles in an aqueous solution [243]. Poloxamer-407 enhances water solubility, and entraps FVR in the core of its micelles, which has a positive effect on EE during crosslinking of ALG with Ca^{+} ions [244]. Degen and co-workers reported that increasing the surfactant concentration to a level greater than the critical micellar concentration would result in the formation of a multi-layered alginate-surfactant, where the drug molecules would be entrapped between layers [245].

4.3. Determining the optimal conditions

Following the analysis of the relationship between the response data and the independent factors in this study, the optimal conditions for formulation with the desired characteristics were generated by Design-Expert® software. The optimal conditions were computed based on searches for a combination of factor levels that would satisfy the desired goals for each response and independent factor. The constraints or desired goals for each factor and response are shown in Table 6. After computing the values to achieve the desired goals, the values with the highest desirability function were selected and set as the optimized levels for each factor under the optimal conditions [225]. Furthermore, the optimal FVR-MCS-ALG-NP formulation was prepared and re-analyzed based on size, ζ potential, LC, and EE. The observed values for each response must closely agree with the predicted response computed by the models chosen to represent each response to confirm

จุฬาลงกรณ์มหาวิทยาลัย
Chulalongkorn University

the validity of the optimization. The optimal conditions and the predicted and observed responses are reported in Table 10. The percent error for each response was computed and resulted in a reasonable agreement (<10% error) between the experimental observations and the model predictions; thus, we were assured of the validity and robustness of the model selected.

Table 10. *The compositions and values of optimal conditions and their predicted and observed responses*

Optimal conditions	Responses	Predicted responses	Observed responses	% Error
A: 1: 0.057 (ALG:CS mass ratio)	Y_1 (nm)	261.8	233.5 ± 7.7	-10.7
B: 12.871 (mg/mL)	Y_2 (mV)	–21.2	–21.6 ± 0.8	1.8
C: 1.24 (% w/v)	Y_3 (%)	24.0	26.0 ± 0.7	8.5
	Y_4 (%)	84.1	84.6 ± 0.7	0.6

% Error was computed as (observed - predicted/predicted) × 100; (values are expressed as mean ± SD; n = 6)

จุฬาลงกรณ์มหาวิทยาลัย
Chulalongkorn University

4.4. Characterization of optimal FVR-MCS-ALG-NP formulation

4.4.1. Physicochemical characterization

Both the NP formulations (FVR-MCS-ALG and FVR-ALG NPs) resulted to a clear suspension without any precipitate after 24 h of equilibration. The comparison of the physical characteristics of the NPs formulations is presented in Table 6. Particle size is an important factor in nasal delivery to overcome problems with absorption in the

nasal epithelium. Smaller particles have a broader surface area that is advantageous for absorption and transport across the nasal cavity. The SEM images of FVR-MCS-ALG-NPs in Fig. 12.a and 12.b demonstrated well-dispersed particles with minimal aggregation. Interestingly, the SEM images of FVR-ALG-NPs (uncoated) demonstrated an obvious clumping of particles (Fig. 12.c-d). The TEM images of the NPs confirmed the spherical shape of the fabricated NPs with a slightly smaller size (Fig. 12.e-h) compared to the DLS measurements (Table 10) due to dehydration of the particles during preparation for imaging. The physical characteristics of the optimal FVR-MCS-ALG and FVR-ALG NPs were presented in Table 11. To further verify successful coating with CS, the hydrodynamic size and ζ potential of the FVR-ALG-NPs (uncoated) were compared to FVR-MCS-ALG-NPs. The uncoated FVR-ALG-NPs exhibited a relatively smaller size (166.3 ± 7.9 nm) and a highly negative surface charge (−30.3 ± 1.4 mV) than the CS-coated FVR-ALG-NPs (−21.6 ± 0.8 mV) due to the absence of positively charged CS on the surface (Fig. 12.f). A high LC (26.0 ± 0.7 %) and EE (84.6 ± 0.7 %) were achieved in the optimal formulation, which was beneficial for obtaining a high drug concentration in the polymer matrix while subsequently reducing the dosage concentration. Notable, a significant decrease in LC (18.5 ± 2.1 %) and EE (51.1 ± 1.3 %) of FVR-ALG-NPs was observed that is attributed to the formation of a less rigorous matrix structure that could potentially lead to leakage and premature release of FVR from the polymer matrix in the absence of CS.

จุฬาลงกรณ์มหาวิทยาลัย
CHULALONGKORN UNIVERSITY

Table 11. *Comparison of the physical characteristics of the NP formulations*

Sample name	Characteristics			
	Size (nm)	ζ-potential (mV)	DL (%)	EE (%)
FVR-MCS-ALG-NPs	233.5 ± 7.7	−21.6 ± 0.8	26.0 ± 0.7	84.6 ± 0.7
MCS-ALG-NPs (Blank)	203.2 ± 2.1	−13.3 ± 0.9	--	--
FVR-ALG NPs	166.3 ± 7.9	−30.3 ± 1.4	18.5 ± 2.1	51.1 ± 1.3
ALG-NPs (Blank)	143.3 ± 3.2	−26.3 ± 1.5	--	--

Additionally, chemical characterization of the FVR-MCS-ALG NPs was conducted *via* thermal and x-ray diffraction analyses. The thermal behaviors of FVR, FVR-MCS-ALG NPs, and blank-MCS-ALG NPs are shown in Fig. 13.a and 13.b. Thermogravimetric (TGA) measurements were studied in the temperature range of 30–500°C at a constant heating rate of 20°C min^{-1} under a nitrogen atmosphere. As depicted, the pure FVR showed only a single drop at 238.0°C with a corresponding weight loss of 99.4%, which was attributed to decomposition of FVR. Furthermore, three-step weight losses were observed in the TGA/DTG curve of the blank-MCS-ALG NPs. The first stage occurred at 66.9 °C with a 5.9% weight loss, which is typically ascribed to the loss of surface and bound water molecules [246]. The second stage presented a 2.3% weight loss at 222.0 °C, accounting for destruction of the biopolymers and the formation of Na_2CO_3 [246, 247]. And the third stage revealed a −80.3% weight loss at 406.8 °C, which was attributed to the total decomposition of

จุฬาลงกรณ์มหาวิทยาลัย
CHULALONGKORN UNIVERSITY

the polymer chains [248] and carbonized materials [246, 249]. The same thermogram was observed for the FVR-MCS-ALG NPs with an additional 4.3% weight loss at 322.9 °C, which may have been due to degradation of residual FVR.

The diffraction patterns of CS, ALG, FVR, FVR-MCS-ALG NPs, and blank-MCS-ALG NPs are shown in Fig. 13.c. The FVR data suggested high-intensity crystallinity peaks at 12.8, 20.2, 20.6, 23.1, 24.3, 27.6, and 28.3° 2θ. All peaks in the FVR pattern were consistent with previous studies, confirming the crystalline structure and the purity of the compound [250, 251]. Broad crystalline peaks at 19.3° and 23.5° 2θ were observed in both blank-MCS-ALG NPs and FVR-MCS-ALG NPs, was due to the gelation of poloxamer [252] [253]. Furthermore, the absence of the crystalline FVR in the FVR-MCS-ALG-NPs signifies the amorphous dispersion of FVR within the MCS-ALG-NPs. This may also be due to the encapsulation of FVR in the polymer matrix during intermolecular interaction of polymers, thus forming an amorphous complex [254]. Majumdar et al. reported the masking of *β*-carotene crystallinity in polymeric microspheres [255]. Similarly, Hazra et al. and Liang et al. also described an amorphous dispersion of crystalline quercetin and epigallocatechin gallate, respectively after encapsulation in polymeric NPs [254, 256].

จุฬาลงกรณ์มหาวิทยาลัย
CHULALONGKORN UNIVERSITY

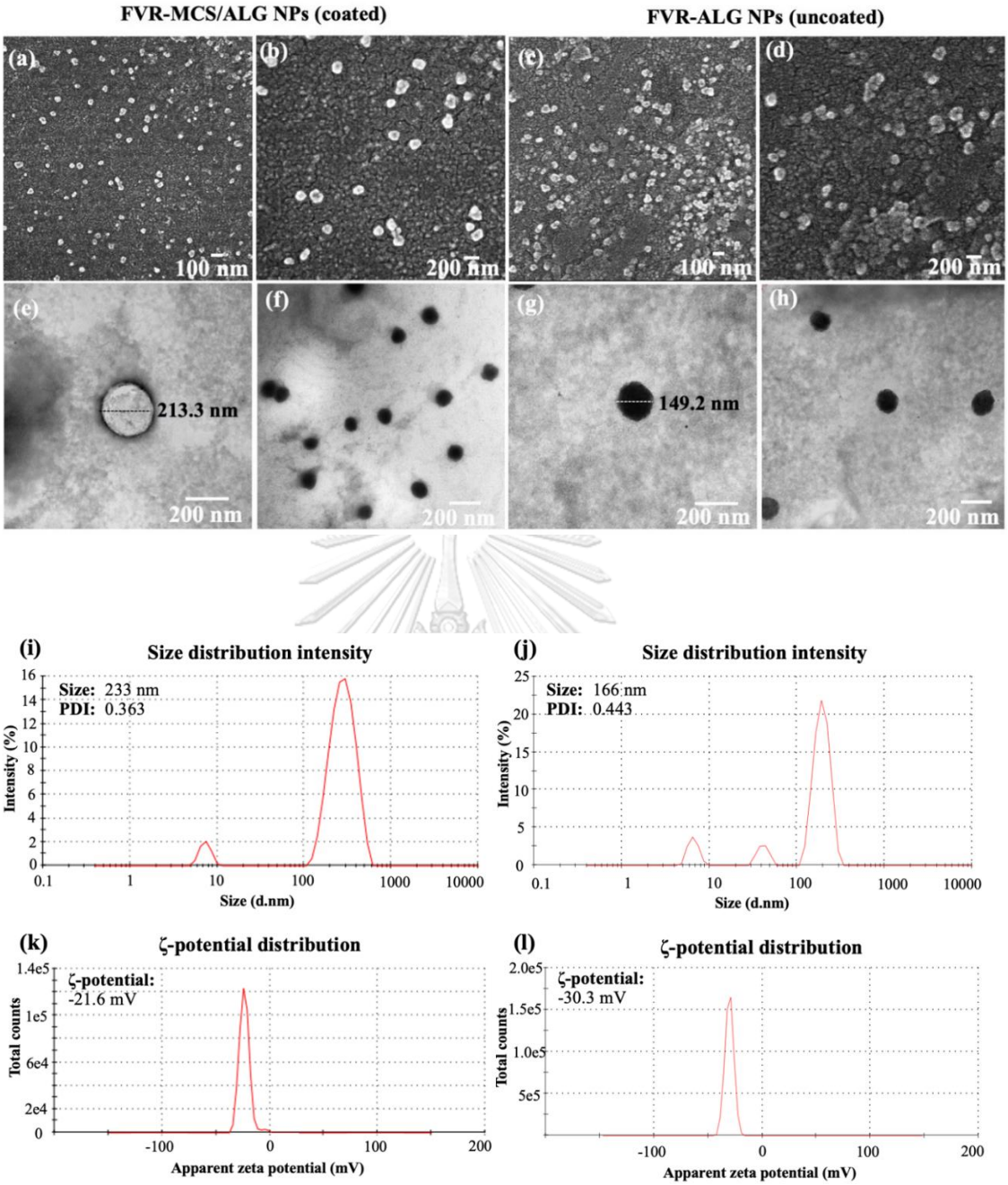

Fig. 12 *SEM (at 50,000× **(a and c)** and 100,000× **(b and d)** magnification) and TEM images (100,000× **(e and g)** and 50,000× **(f and h)** magnifications) of the optimal formulations; size distribution and ζ-potential of the optimal FVR-MCS-ALG NPs **(i and k)** and uncoated FVR-ALG NPs **(j and l)** by DLS.*

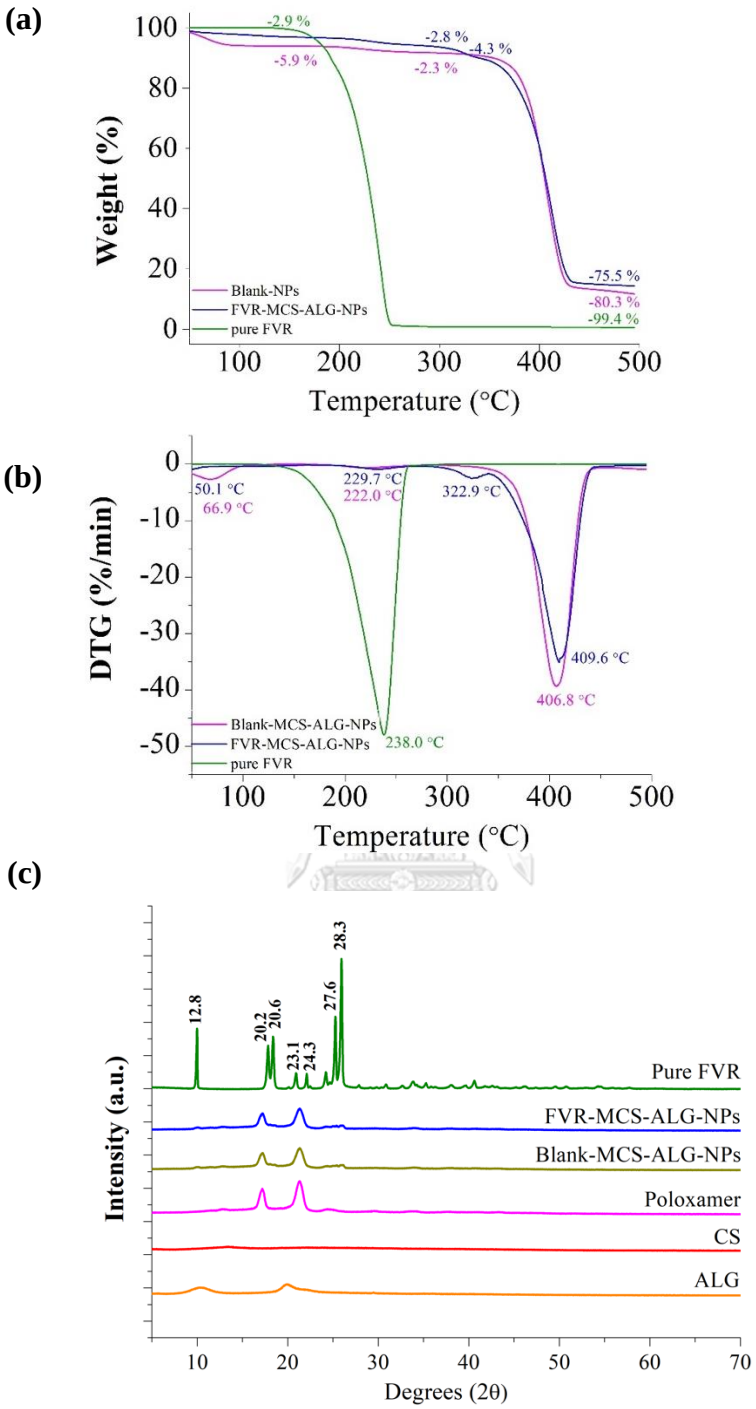

Fig. 13 (a) *TGA and* ***(b)*** *DTG thermal curves of FVR, blank-NPs, and FVR-MCS-ALG-NPs;* ***(c)*** *XRD pattern of CS, ALG, FVR, blank- NPs, and FVR-MCS-ALG-NPs.*

4.4.2. Effects of mucin on the size and surface charge of FVR-NPs

Cationic CS and anionic ALG polymers were chosen as the materials to construct the NPs owing to their different mucoadhesion mechanisms by electrostatic interaction, hydrogen bonding and hydrophobic interactions with mucin. A non-ionic mucoadhesive poloxamer was also chosen to stabilize the system due to its absorption-enhancing effects in the nasal epithelium. We first determined the extent of the interaction between the FVR-MCS-ALG-NPs (CS-coated) and the FVR-ALG-NPs (uncoated) with a fixed concentration of mucin (0.4 mg/mL) by the change in the particle size and ζ potential over time. The electrostatic interaction is one of the most common and expected mechanisms of mucoadhesion. An increase in hydrodynamic size is an indication of mucin binding to the NPs. The FVR-MCS-ALG-NPs changed significantly in size (p = 0.0036) and ζ potential (p = 0.0170) after 1 h incubation with mucin, while the uncoated FVR-ALG-NPs and the free FVR control did not change significantly in (Fig. 14.A and 14.B). Also, a significant decrease in the surface charge of the FVR-MCS-ALG-NPs was observed that is attributed to interactions between the remaining protonated NH_2 of CS and negatively charged sialic acid residues in mucin. Notably, a large gap between FVR-MCS-ALG-NPs and FVR-ALG-NPs was seen, suggesting that the repulsive interactions between charged molecules (CS and sialic acid of mucin) produces a stronger mucoadhesive mechanism than the hydrogen bonding mechanism of ALG.

จุฬาลงกรณ์มหาวิทยาลัย
Chulalongkorn University

The percent mucin binding to the NPs was investigated through a BCA protein analysis to better understand its mucoadhesive properties. The analysis was conducted at different time points to observe the extent of mucin adsorption. As a result, significant mucin binding was observed in the first 10 min of incubation, wherein a greater percentage of mucin was adsorbed onto the FVR-MCS-ALG-NPs (23% ± 6.95%) compared to the FVR-ALG-NPs (10% ± 4.36%) ($p < 0.0001$) (Fig. 14.C). After incubation of both samples, the FVR-MCS-ALG-NPs had a total percentage mucin binding of 46.8% ± 9.13%, which was significantly higher than the FVR-ALG-NPs with only 13% ± 3.12% mucin adsorbed ($p < 0.0001$).

4.4.3. *In vitro* release study of FVR from the NP formulations

The *in vitro* release profile of FVR from the NPs formulations was determined using the SnakeSkin™ artificial membrane (Fig. 15.a and 15.b). Formulations were compared to observe the benefit of a CS coating on the release of FVR from the NPs in a simulated nasal environment. As shown in Fig. 15.a, 60.18% ± 2.49% (CS-coated) and 82.99% ± 2.53% (uncoated) of the FVR were released from the FVR-MCS-ALG-NPs within 24 h at physiological pH (7.4). Total of 83.26% ± 3.84% (CS-coated) and 72.17% ± 6.51% (uncoated) FVR were released from the NPs after 24 h under the SNF condition (pH 5.5).

จุฬาลงกรณ์มหาวิทยาลัย
CHULALONGKORN UNIVERSITY

Furthermore, free FVR had an almost 100% release rate at both pHs, followed by the FVR-ALG-NPs. No significant difference in the release of FVR-MCS-ALG-NPs and FVR-ALG-NPs was observed at pH 5.5 (SNF). Additionally, faster drug

release was observed from FVR-ALG-NPs at pH 7.4 than in an acidic environment due to the repulsion between the H^+ ions of ALG; thus, inhibiting hydrolysis of the polymer [258]. These results confirm that encapsulating FVR in MCS-ALG-NPs sustained the release of FVR at both pHs tested compared to free FVR. Additionally, the CS coating on the ALG-NPs was advantageous in the acidic SNF environment, where faster drug release was observed than with the uncoated ALG-NPs, suggesting its suitability for nasal administration.

Notably, the CS coating greatly affected the release of FVR considering the pH of the environment. The MCS-ALG-NPs had a higher FVR release rate in an acidic environment, while pH 7.4 resulted in a slower release rate. This can be attributed to the pH-responsive drug release mechanism of CS. At acidic pH, the amine groups of CS (pKa = 6.3-6.5) and FVR (pKa = 5.1) contained in the NP are easily protonated and become more soluble leading to swelling and erosion of the CS polymer coating, and the immediate release of the FVR [257]. Likewise, the slower release of FVR from the NPs was due to the deprotonation of FVR and CS in pH > pKa or at pH 7.4 making them almost insoluble to trigger the erosion of polymer coating, where the release of FVR solely relies on the swelling of the polymers. This is beneficial as we expected the FVR to be released in the nasal epithelia with an acidic environment (pH 5.5) than in the mucus layer at physiological pH (7.4).

จุฬาลงกรณ์มหาวิทยาลัย
Chulalongkorn University

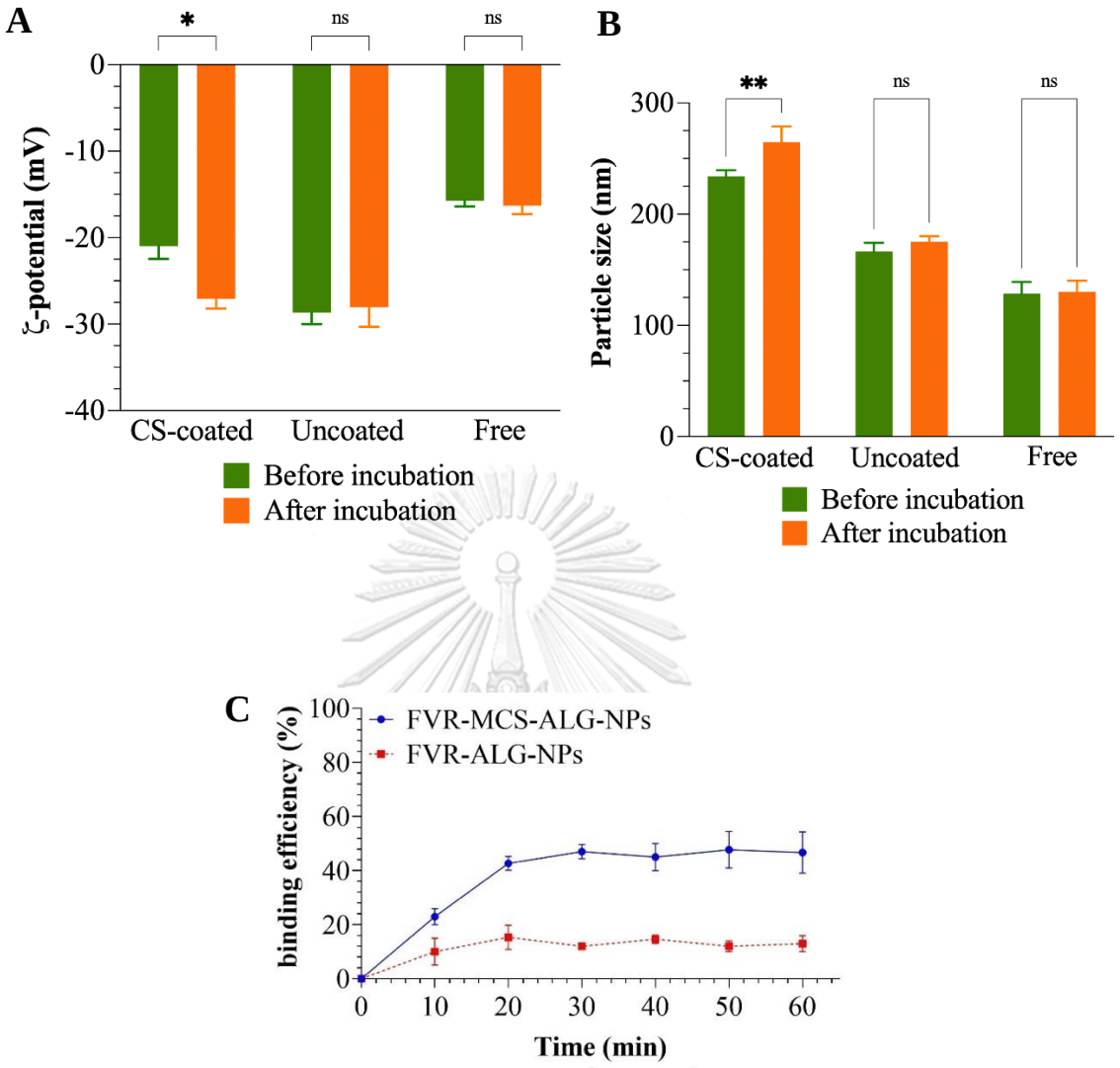

จุฬาลงกรณ์มหาวิทยาลัย
Chulalongkorn University

Fig. 14 (A) *ζ-potential and* ***(B)*** *size of (**a**) CS-coated FVR-MCS-ALG-NPs (**b**) uncoated FVR-ALG-NPs, and (**c**) the free FVR control before and after 1 h incubation with mucin;* ***(C)*** *mucin binding efficiency of the FVR-MCS-ALG-NPs and FVR-ALG-NPs as a function of time, n = 9. (* p = 0.017, ** p = 0.0036, ns = no significance).*

Drug diffusion, matrix swelling, and material erosion are the main solute transport mechanisms for polymeric matrices [259]. The release data were fit to various kinetic models to have a better understanding of the release kinetics of the

NPs. The summary of the release kinetics of the formulations using various mathematical models is shown in Appendix C-E. The best fit model was selected based on the highest $R^2_{adjusted}$, minimum AIC, and maximum MSC. All experimental samples best fit the Weibull model in both media. The computed shape factors (β) for each formulation were used to define the transport mechanism of the drug from the polymer matrix. Kobryn, Papadopoulo and co-workers defined the transport mechanism as $\beta \leq 0.75$, indicating Fickian diffusion (either fractal or Euclidian spaces); β of $0.75 < \beta < 1$ indicates combined transport mechanisms (Fickian diffusion and Case II transport/swelling controlled transport), and $\beta > 1$ indicates a complex release mechanism, wherein the rate of release non-linearly increases up to the inflection point followed by an asymmetrical decrease in drug release [260, 261]. Both formulations in the present study all showed β values ranging from 0.244 to 0.359 in both media indicating a Fickian diffusion mechanism. This mechanism is typical for matrix-type drug carriers, in which diffusion of the drug through the matrix is dependent on the concentration gradient, diffusion distance, and the degree of swelling of the polymers [262, 263]. The same polymeric NPs transport mechanism was reported previously [219, 264].

จุฬาลงกรณ์มหาวิทยาลัย
CHULALONGKORN UNIVERSITY

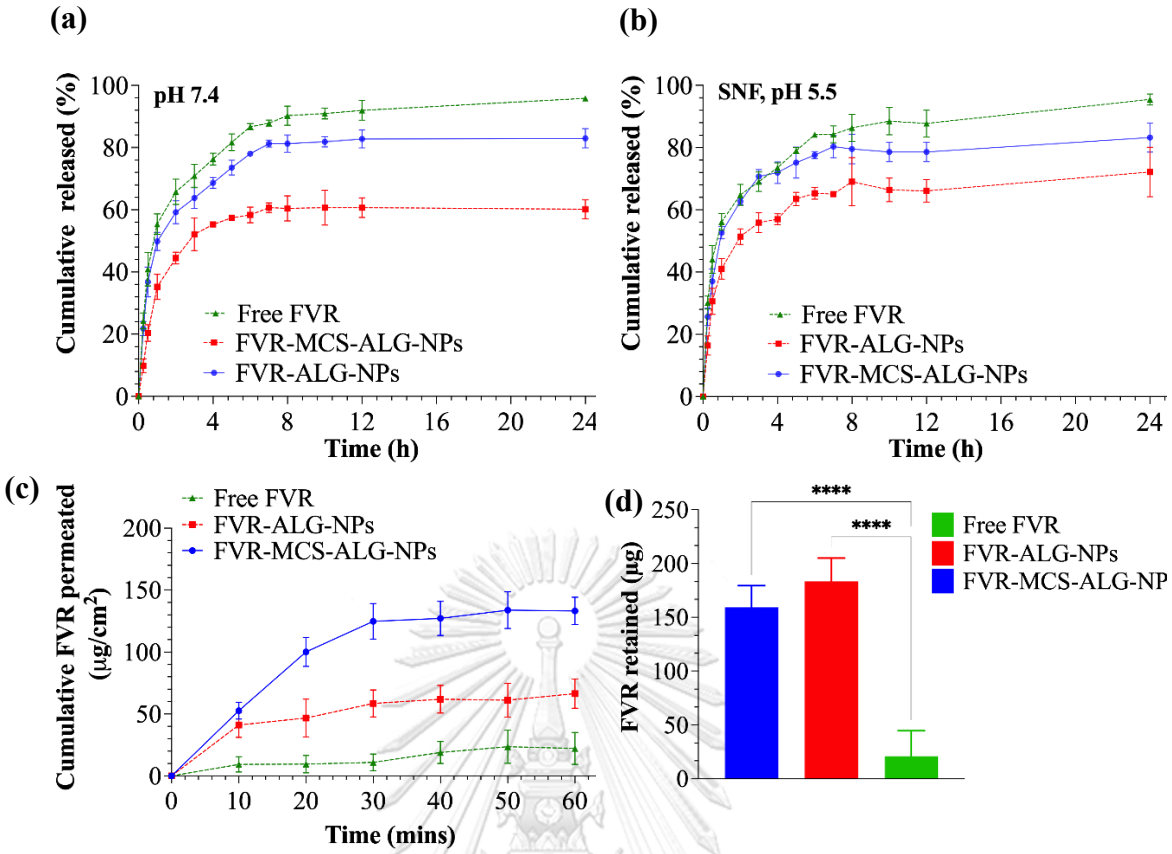

Fig. 15 *In vitro FVR released from NPs at* ***(a)*** *physiological pH and* ***(b)*** *SNF (n=3); permeability study of FVR through SnakeSkin™ synthetic membrane:* ***(c)*** *cumulative FVR permeated, and* ***(d)*** *approximate amount of FVR deposited in the PNM after 1 h; **** p< 0.0001; (n=9)*

จุฬาลงกรณ์มหาวิทยาลัย
Chulalongkorn University

4.5. Nasal mucosa permeation and retention studies

The transport and retention of FVR through PNM were investigated in nine (9) mucosal specimens from each treatment group. PNM was used ascribed to ethical considerations and its morphological similarity and high permeability correlation with human nasal mucosa compared to other animal models including bovines and rabbits. The effect of the CS coating on the permeation and retention of FVR-NPs in the tissue was also studied. As shown in Fig. 15.c, FVR-MCS-ALG-NPs (235.7 ± 19.5 µg) had superior permeation compared to the uncoated FVR-ALG NPs (117.7 ± 20.9 µg)

and free FVR (39.44 ± 22.8 µg). Due to the small size of the NPs and larger surface area, it can be noted that both NP formulations had a significant permeation after 1 h, as compared to the free FVR (p <0.0001). Furthermore, it is evident that the FVR-MCS-ALG-NPs had a significant permeation activity through PNM compared to the FVR-ALG-NPs (p < 0.0001). The enhanced permeation observed through the mucosa after adding the CS coating agreed with previous studies [265-267].

The permeation-enhancing property of positively charged CS was attributed to the interaction between its amino functional groups and negatively charged sialic acid on the cell membranes, hence transient opening of the tight junctions and enhanced permeation through the mucosa [268]. It must be noted, that even though the uncoated FVR-ALG-NPs did not possess any significant mucoadhesive properties from the previous experiments (section 4.4.2.), it can still successfully permeate through the nasal mucosa, attributed to its small size and high surface area.

จุฬาลงกรณ์มหาวิทยาลัย
CHULALONGKORN UNIVERSITY

In addition, the amount of drug retained or deposited was quantified by recovering the FVR in the mucosal tissue after 1 h of treatment. A significant amount of the FVR from the FVR-MCS-ALG-NPs and uncoated FVR-ALG-NPs was deposited in tissues compared to free FVR (p < 0.0001) (Fig. 15.d). Interestingly, the amount of FVR retained (p = 0.0834) was similar between the two FVR-NPs formulations even though the FVR-MCS-ALG-NPs had higher cumulative FVR permeated and faster flux through the nasal mucosa than uncoated FVR-ALG NPs. This can be explained by the slower permeation of the uncoated FVR-ALG-NPs that caused deposition of FVR in the

mucosa. Nonetheless, the computed values for the *Jss* and K_p for the FVR-MCS-ALG-NPs was significantly higher than the uncoated FVR-ALG-NPs and free FVR ($p < 0.0001$) (Table 12). The ER_{flux} values also showed more than a 6-fold and 3-fold enhanced drug flux of the FVR-MCS-ALG-NPs vs. free FVR and uncoated FVR-ALG-NPs, respectively.

However, it must be noted that the pharmacokinetic data on the permeation and retention of FVR-NPs observed in this study may be insufficient due to the absence of mucociliary clearance and some physiological factors (e.g., posture and gravitational pull) [269] that could greatly affect the residence time of FVR on the mucosa. In addition, transport of drugs differs in excised mucosa vs. healthy, intact tissues [270]. Nonetheless, these preliminary data suggest that the use of mucoadhesive polymers for intranasal delivery could potentially increase the permeation, deposition, and residence time of FVR in the nasal cavity. Despite the relatively smaller diameter of FVR-ALG-NPs, the FVR-MCS-ALG-NPs still had superior permeation, which shows the advantage of CS for absorption through the nasal mucosa.

จุฬาลงกรณ์มหาวิทยาลัย
CHULALONGKORN UNIVERSITY

Table 12. *Comparison of the permeation profiles of FVR-MCS-ALG-NPs, FVR-ALG-NPs, and free FVR through PNM*

Parameters	FVR-MCS-ALG-NPs	FVR-ALG-NPS NPs	Free FVR
Cumulative amount of FVR permeated *(μg/cm²)*	133.19 ± 11.0 [a,b]	66.5 ± 11.8 [a,c]	22.28 ± 12.9 [b,c]
Jss *(μg/cm²/h)*	97.0 ± 13.7 [a,b]	30.5 ± 13.5 [a]	15.5 ± 17.1 [b]
K_p *(cm/h)*	0.21 ± 0.03 [a,b]	0.07 ± 0.03 [a,c]	0.03 ± 0.04 [b,c]
ER_{flux}	6.26	1.97	1.00

Values are expressed as mean ± SD; n = 9; The same letter (a,b, and c) within each row indicates a statistical significance at p <0.05.

4.6. Storage stability studies

The storage stability of the NPs was studied by investigating the effects of storage temperature at refrigerated and ambient room temperature for 6 months. The NPs were kept in tightly sealed amber bottles to protect the product from potential photodegradation. At each predetermined time point (1, 2, 3, 4, 5, and 6th months) the particle size, zeta potential, and % DL were evaluated. As shown in Fig. 16.A., it was found that the size of the FVR-MCS-ALG-NPs did not show any substantial change when stored at refrigerated temperatures. However, a major increase in size can be observed in NPs after 4 months of storage at ART. It can also

จุฬาลงกรณ์มหาวิทยาลัย
Chulalongkorn University

be noted that the zeta potential of the FVR-MCS-ALG-NPs stored in both temperatures did not show any significant change up to 6 months (Fig. 16.A.). The EE (%) of the FVR-MCS-ALG NPs had no significant change during the study when stored in refrigerated temperatures, while samples stored at ART had a major loss after 3 months of storage (Fig. 16.B.).

Furthermore, the uncoated FVR-ALG-NPs stored at ambient room and refrigerated temperatures demonstrated a significant increase in the size after 2 and 3 months of storage, respectively (Fig. 16.C.). The change in the size of FVR-ALG-NPs can also be visually observed due to the formation of turbidity and precipitation of the product. Even so, the zeta potential of the FVR-ALG-NPs did not show any substantial shift throughout the study (Fig. 16.C.). Also, a significant decrease in the size of the FVR-ALG-NPs after 2 months of storage in ART, can be attributed to the significant decrease in % EE, while a considerable change in the % EE in samples stored at refrigerated temperature was observed after 4 months of storage (Fig. 16.D.). It is evident in the results that a cooler condition is more favorable for the storage of both formulations, which shows longer stability of the NPs than in ART. This can be because at higher temperature the colloidal dispersion tend to create more kinetic energy that would accelerate the collision of the particles, thus the formation of aggregation, larger particle size, and leakage of loaded drug [271]. Moreover, it is noticeable that the % EE in ALG-NPs was affected by the outer

จุฬาลงกรณ์มหาวิทยาลัย
CHULALONGKORN UNIVERSITY

coating, which can strongly suggest the premature escape of FVR from the crevices of the ALG-NPs in the absence of CS coating.

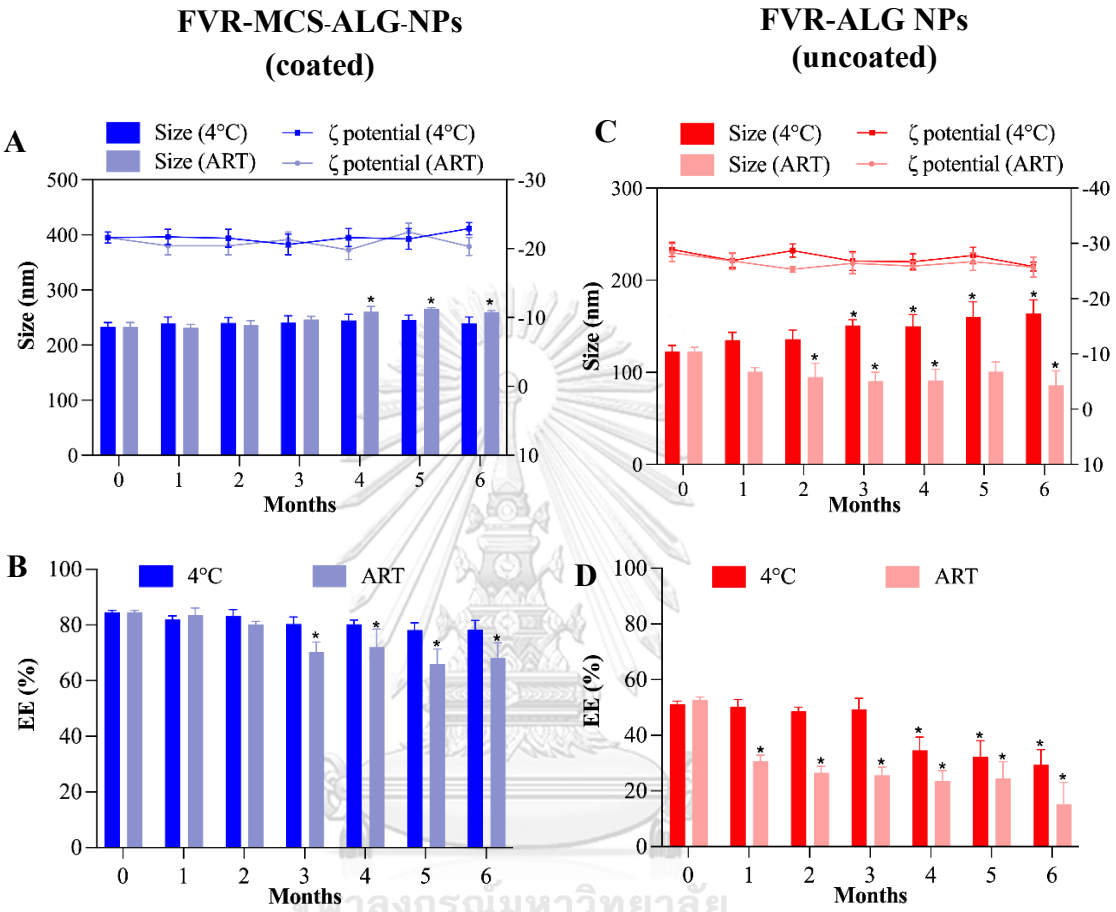

Fig. 16 *Storage stability of FVR-MCS-ALG-NPs (**A** and **B**) and FVR-ALG-NPs (**C** and **D**) at 4 ºC and ambient room temperature (ART) for 6 months. The values are expressed as mean ± SD of 3 individual batches of each formulations. *p value <0.005 compared to 0 month.*

จุฬาลงกรณ์มหาวิทยาลัย
CHULALONGKORN UNIVERSITY

4.7. Biocompatibility studies

Charged polymers like CS and ALG could exert cytotoxicity when they aggregate onto the cell surface and interferes with the intracellular activities, hence, cytocompatibility of the nanocarrier must be established [272]. In this study, we

investigated the cytocompatibility of the NPs formulation towards the RPMI 2650 cell line, which is the only immortalized human nasal epithelial cell that is well-studied for *in-vitro* testing of products that are intended for nasal delivery [273, 274]. The toxicity of the water and blank-NPs as diluent for free FVR and formulated FVR-NPs (FVR-MCS-ALG and FVR-ALG-NPs) were first investigated. Result revealed that the diluents did not cause any significant toxicity to the cell even at its highest concentration, hence 10% v/v of the diluent was normalized as the final concentration for the dilution in succeeding experiments (Fig. 17.A).

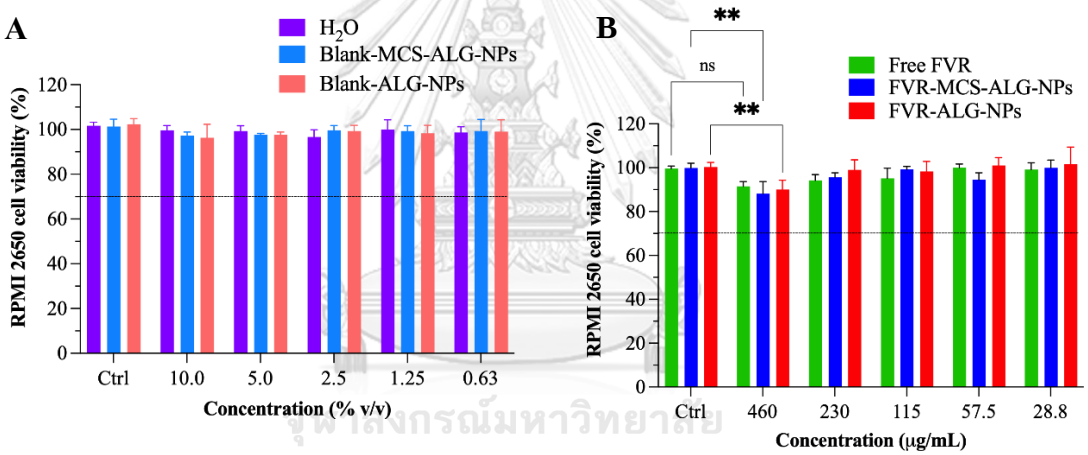

Fig. 17 *Cytocompatibility of the (**A**) H_2O and blank NPs as a diluent and (**B**) free and FVR-MCS-ALG-NPs in RPMI 2650 nasal epithelia (passage number: 5-9) after 24 h of exposure to treatment. The line signifies the lower limit for safety assessment (>70% viability) based on the ISO 10993-5 criteria [275]. The values are expressed as mean ± SD of 3 independent experiments. *p value < 0.001 (compared to the control), ns = no significance.*

Sequentially, the cytotoxicity of the free FVR and FVR-NPs serially diluted in water and blank-NPs, respectively in various concentrations were investigated. As

shown in Fig. 17.B. there was a significant difference in the cell viability of RPMI 2650 when treated with the highest working concentration of 460 µg/mL (> 88% viability) for FVR-NPs as compared to the control cells. It is also evident that the reduction of cell viability is attributed to the drug itself as the control which was treated the diluents used did not have any substantial cytotoxicity observed. Also, the cytotoxicity of FVR-NPs could be from the enhanced cellular uptake of the NPs in the RPMI 2650. Nonetheless, these values still comply with the ISO 10993-5 criteria (Biological evaluation of medical devices Part 5: Test for in vitro cytotoxicity), wherein it says that the reduction of cell viability by >30% is considered cytotoxic [275]. Hence, it can be deduced that the free FVR and FVR-MCS-ALG NPs both have very good compatibility in RPMI 2650.

Moreover, the histopathological changes in the excised nasal mucosa were evaluated after 1 h of exposure to treatment by a licensed veterinary pathologist who is blinded by the treatment (Fig. 18). The nasal pathological templates showed no significant signs of serious apoptosis, necrosis, and inflammation, which are common indication of toxicity in nasal epithelium by NPs. On the basis of the results of cytocompatibility and histopathological studies, a preliminary conclusion could be drawn that the neither the formulated nor free FVR did not show any toxicity rendering it biologically safe. However, a more comprehensive toxicity study using animals must be conducted to further elucidate possible health risks of the formulation.

จุฬาลงกรณ์มหาวิทยาลัย
Chulalongkorn University

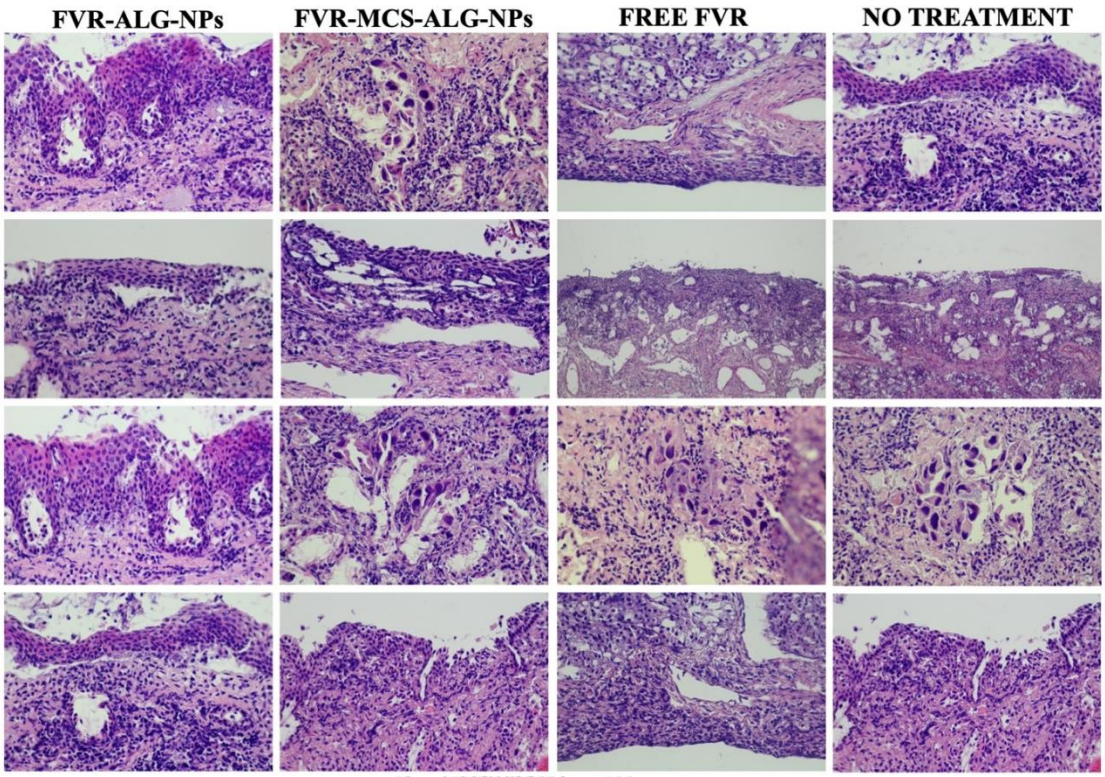

Fig. 18 *Histopathological examination of porcine nasal mucosa after 1h exposure to NP formulations (FVR-ALG-NPs and FVR-MCS-ALG-NPs) and free FVR. The sections were stained with HE and examined by light microscopy.*

จุฬาลงกรณ์มหาวิทยาลัย
Chulalongkorn University

4.8. Cellular uptake of FVR-MCS-ALG-NPs

The enhancement in the cellular internalization of the FVR is important to address its concern about its poor permeability and retention according to its BCS classification. This disadvantage also hinders the transformation of FVR prodrug to its active form, FVR-RTP through its phosphorylation intracellularly. Since, FVR has a poor fluorophore that will suffice microscopic analysis, 5-aminofluorescein (5-AF) was used in replace to FVR and loaded to MCS-ALG-NPs in a manner similar to Section 3.1. DAPI staining was also employed to track the fate of the NPs in the cell. As

shown in the Fig. 19, a significant 5-AF was observed in MCS-ALG NPs than in free 5-AF after 4 h of exposure to the cell. It can also be observed in MCS-ALG NPs treated cells some 5-AF granules that have permeated through the cytoplasm of the cell. Moreover, to observe the time-dependent uptake of the 5-AF-MCS-ALG NPs, 24 h of exposure was also investigated. It can be observed a significant amount of 5-AF-MCS-ALG NPs treated cells throughout the cytoplasm and the perinuclear portion of RPMI 2650 cells than the free 5-AF. There are 2 critical factor which influences the cellular uptake of the NPs: (1) size and (2) surface charge. Recent studies demonstrated that the mechanism of cellular uptake of NPs mainly relies onto the size of the particle. In particular, NPs with the size of >200 nm were taken up by caveolae-medicated endocytosis which involves flask-shaped membrane invaginations called “caveolae that is present in epithelial cells like RPMI-2650 [276]. Another is the surface charge of the NPs, wherein a (+) charged particle could freely interact with the (–) charged cell membrane (CM) [276]. Although the NPs that were developed in this study possesses (–) surface charge, the cationic CS that lies on the outer shell of the NPs could still interact with the CM. In addition the hydrophobicity and mucoadhesiveness of the NPs may also contribute to its adsorption onto the CM [277].

จุฬาลงกรณ์มหาวิทยาลัย
CHULALONGKORN UNIVERSITY

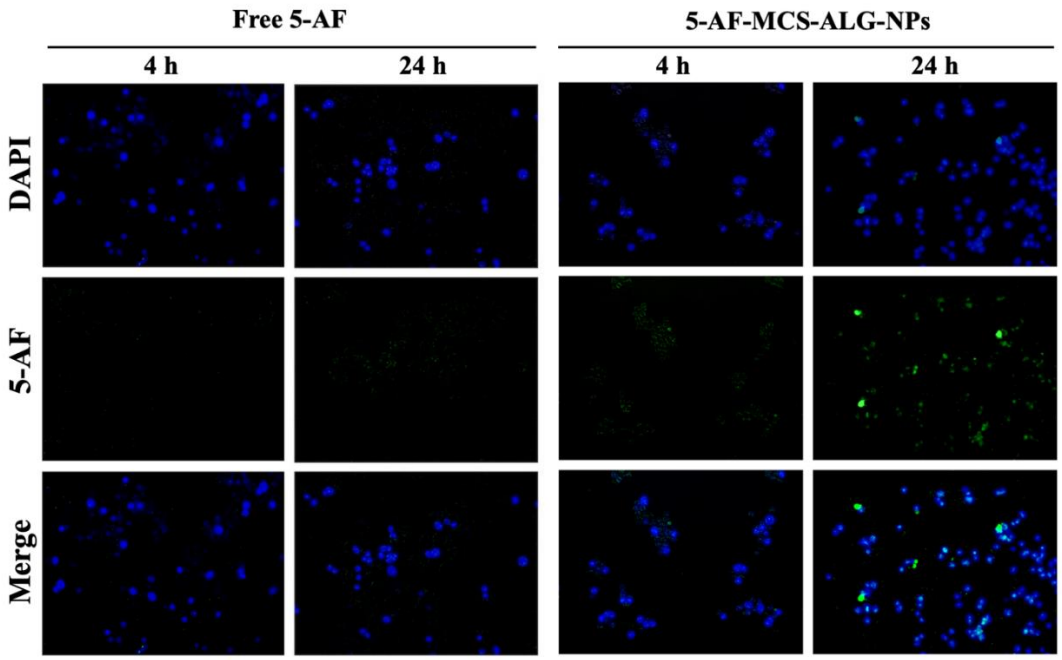

Fig. 19 *Fluorescence microscope observation of the cellular uptake of free 5-aminofluorescein (5-AF) and 5-AF loaded MCS-ALG-NPs through RPMI 2650 cell line (passage number: 10-12) after 4 and 24 h of exposure.*

4.9. Antiviral activity of FVR against PEDV

As SARS-CoV-2 is classified as a risk group 3 pathogen that requires extremely stringent safety precautions and specialized laboratory facilities, we employed the use of non-infectious coronavirus as a surrogate for the antiviral studies. The PEDV, NCBI accession LC053455) is a non-zoonotic virus from the α-coronavirus genus that was selected as a model due to its low health risk and minimal laboratory requirements. It possesses similar biophysical properties and genomic structure as human coronaviruses, such as SARS-CoV-2 [278, 279]. Previous reports on the proof-of-concept on the use of the PEDV corona model have proven it to be a reliable surrogate for SARS-CoV-2 [278, 280, 281].

จุฬาลงกรณ์มหาวิทยาลัย
Chulalongkorn University

Vero cells stably expressing eGFP (eGFP-Vero) were used as host cells for PEDV carrying the mCherry fluorescent reporter gene (mCherry-PEDV). Expression of the mCherry reporter protein would only occur after transcription and replication of the virus in the host cells, wherein the cytopathic effects of the infected eGFP-Vero cells were observed through the formation of syncytia with the mCherry protein [224]. The cytotoxic effect of H_2O and blank-MCS-ALG-NPs was first determined at various concentrations ranging from 0.63% to 10% v/v to determine the possible toxicity of the solvents for dilution in eGFP-Vero cells. As shown in Fig. 20, neither test sample exhibited any relative cytotoxicity to eGFP-Vero cells even at the maximum concentration of 10% v/v. However, some blank NP precipitates were observed in the cell culture at the 10% v/v concentration (Fig. 20.d). This was associated with the formation of NP-protein complexes between the negative surface charge of the blank-NPs and the proteins present in the culture media [282, 283]. Nonetheless, the precipitation of the blank-NPs did not affect the cell viability relative to the H_2O samples; hence, the 10% v/v concentration of the blank-MCS-ALG-NPs and H_2O was fixed and used in diluting the experimental samples (free FVR and FVR-MCS-ALG NPs) for the subsequent experiments.

จุฬาลงกรณ์มหาวิทยาลัย
CHULALONGKORN UNIVERSITY

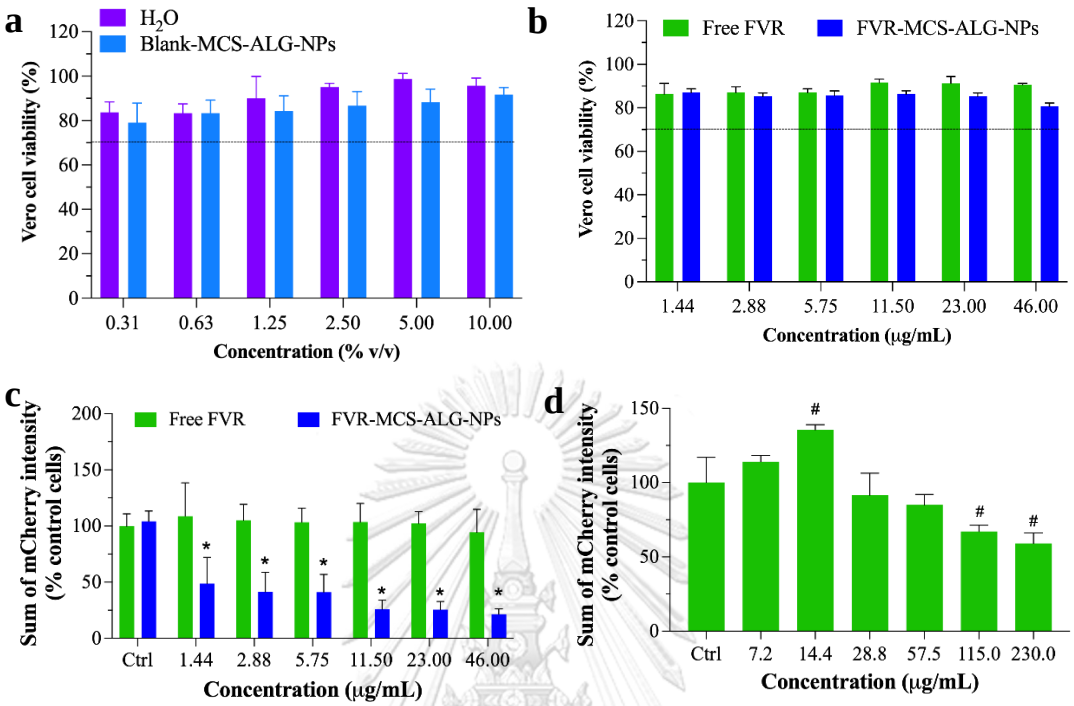

Fig. 20 *Vero cell viability:* ***(a)*** *diluents and* ***(b)*** *FVR (formulated and unformulated) after 18 h. The line signifies the lower limit for safety assessment (>70% viability) based on the ISO 10993-5 criteria [275]; Anti-coronavirus effect:* ***(c)*** *Average quantitative mCherry fluorescence intensity data of infected cells from 3 independent experiments,* ***(d)*** *Quantitative data of mCherry fluorescence intensity of the infected cells treated with high concentrations of FVR. Data are mean ± SD, n = 3; ($^{\#}p < 0.05$ and *<0.0001 compared to the control).*

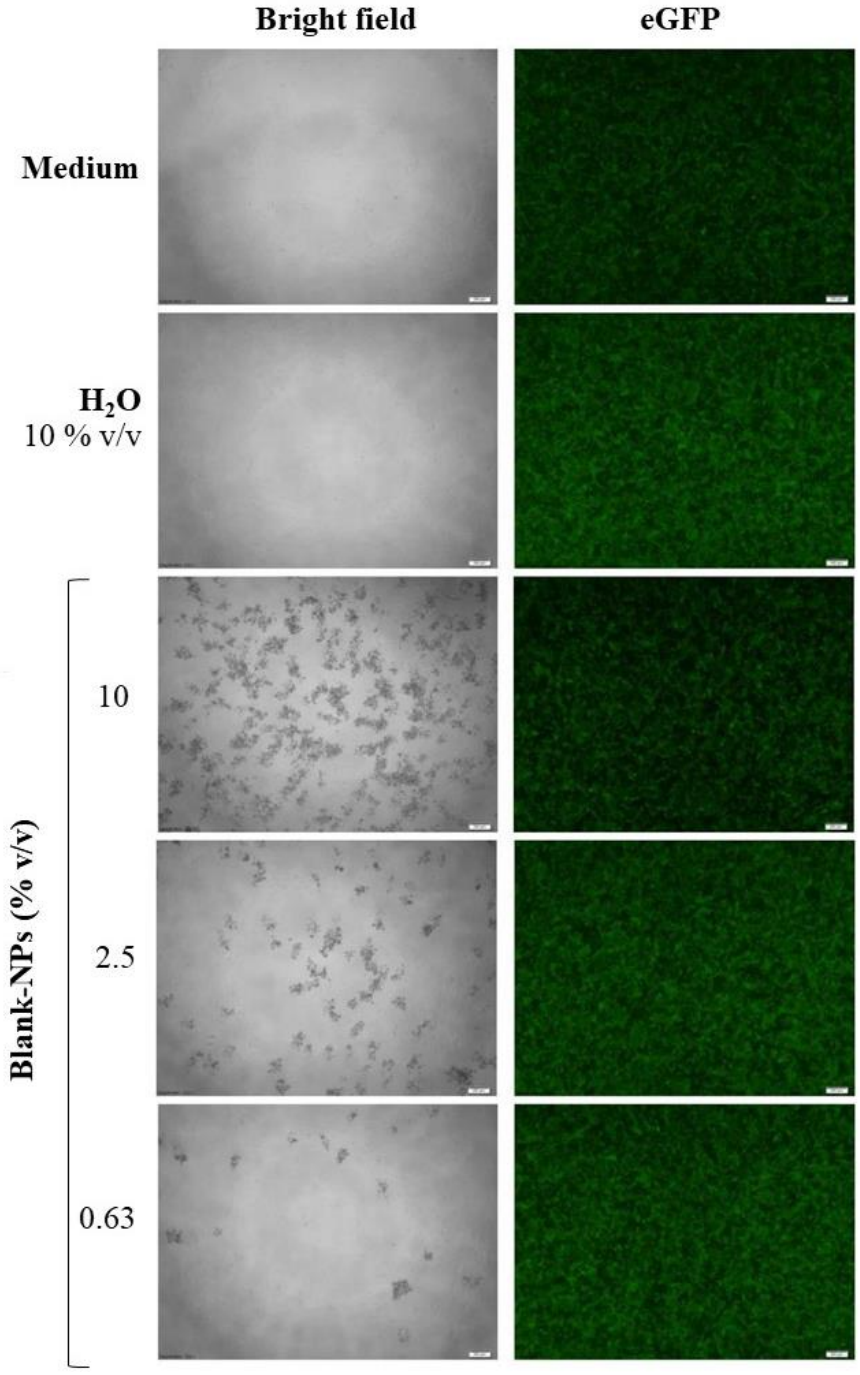

Fig. 21 *Cytotoxicity of the FVR-MCS-ALGP-NPs. eGFP-Vero cells were treated with H_2O or NPs at the indicated concentrations for 18 h. Control cells were the cells cultured in medium only. Cell viability was visualized by fluorescent microscopy and measured with a CCK-8 kit at an absorbance of 450 nm using a spectrophotometer.*

Furthermore, the non-cytotoxic concentrations of FVR (formulated and unformulated) were determined in eGFP-Vero cells by diluting the free FVR and FVR-MCS-ALG-NPs in H_2O or blank-NPs, respectively, to achieve the concentrations of 1.44, 2.88, 5.75, 11.5, 23, and 46 µg/ml followed by 18 h of incubation. The cytotoxicity of FVR was determined by the CCK-8 assay and the results showed that both samples at the maximum working concentration of 46 µg/ml did not cause substantial toxicity to host cells with a percent cell viability > 80% across all concentrations investigated (Fig. 20.b). Hence, this concentration was used for the antiviral assay in the PEDV model.

The anti-coronavirus effect of FPV was determined using a swine coronavirus-PEDV as a SARS-CoV-2 surrogate virus. eGFP-Vero cells were infected with the reporter virus, mCherry-PEDV followed by treatment with the FVR samples at different concentrations (1.44, 2.88, 5.75, 11.5, 23, and 46 µg/mL) for 18 h. The final concentration of H_2O or blank-NPs was normalized to 10% v/v. The controls were infected cells treated with H_2O or blank-NPs without FVR. The mock was uninfected cells treated with H_2O or blank-NPs without FVR. The cytopathic effects from the infection were detected as golden mCherry-syncytia under a high-content imaging system. The results showed that FVR-MCS-ALG-NPs caused a drastic reduction in virus replication in three independent experiments with a computed EC_{50} of 6.63 ± 2.42 µg/mL (Fig. 20.c). The posthoc test confirmed that the FVR-MCS-ALG-NPs had a significant inhibitory effect on viral replication even at its very lowest working

จุฬาลงกรณ์มหาวิทยาลัย
CHULALONGKORN UNIVERSITY

concentration compared to free FVR and the control cells ($p < 0.0001$), while free FVR had no significant reduction of PEDV replication across all concentrations investigated ($p > 0.9$). To further determine the antiviral activity of free FVR, we tested the samples in higher concentrations up to 230 µg/mL, which was not toxic to the eGFP-Vero cells (Fig. 20.d and Appendix I). We found out that the free FVR had a significant reduction in viral replication starting at a concentration of 115 µg/mL. These results clearly suggests that FVR-MCS-ALG-NPs exhibited a significant improvement in antiviral activity towards coronavirus by more than 30-folds compared to the free drug (EC_{50} 6.63 ± 2.42 vs >230 µg/mL). Previous study on FVR-loaded solid lipid nanoparticles (SLN) for nebulization resulted to an EC_{50} and IC_{50} of 29.9 µg/mL and 449.6 µg/mL, respectively towards coronavirus-infected vero cells [284]. In previous studies, NPs have successfully been used as carriers for antiviral drugs that greatly improved not only the physicochemical properties, but also the pharmacokinetics/dynamics of the drugs. Chen and Liang systematically reviewed the possible mechanisms for enhanced viral inhibition of NPs by interrupting crucial steps in the infectious process, including viral attachment and penetration, while subsequently reducing virulence and replication [95]. The positive effect of polymeric NPs on virucidal activity has been associated with their sustained and prolonged antiviral effect [285]. Moreover, polymeric NPs, particularly CS and ALG, have antiviral effects against various viruses. CS is effective for reducing the infectivity of SARS-CoV-2 in A549 and Vero E6 cells at 10–100 µg/mL [286]. The antiviral effect of CS was

จุฬาลงกรณ์มหาวิทยาลัย
CHULALONGKORN UNIVERSITY

reported by Loutfy and co-workers to be associated with inhibited viral binding, entry, and replication [287, 288]. Although the ALG antiviral mechanism is still uncertain [289], several studies have reported its virucidal effect in a wide range of viruses from double-stranded DNA viruses to positive-/negative-sense single-stranded RNA viruses. Pietropaolo and co-workers reported that the antiviral effect of anionic polymer could be attributed to the interaction between polymer and the viral envelopes, thus interfering with viral adsorption onto the host cells [290].

จุฬาลงกรณ์มหาวิทยาลัย
Chulalongkorn University

CHAPTER 5

SUMMARY, CONCLUSION, AND RECOMMENDATION

This research involves a pharmaceutical formulation approach in overcoming some drawbacks of FVR in terms of its physicochemical properties (eg., poor solubility) and poor permeability, that partially explains its limited antiviral activity towards SARS-CoV-2. Herein, we proposed a polymeric nanoparticulate carrier system to enhance the solubility and permeability of FVR. We also proposed a different administration route for FVR *via* intranasal delivery, which simulate the natural transmission route of the virus.

The use of natural carbohydrate polymers like CS and ALG as the material for the construction of nanocarriers could be a rational approach in producing an efficient and stable carrier. Moreover, their tunable size, surface characteristics, and mucoadhesive properties make them suitable for transmucosal delivery. The proposed delivery route for FVR could potentially reduce the viral load in the infected individuals and eventually mitigate the risk of viral transmission. In previous study, the FVR-loaded nano-emulsion for SARS-CoV-2 was hypothesized to effectively interfere with viral adsorption, invasion, and replication [291]. Another study demonstrated the use of solid-lipid nanoparticles (SLN) as a carrier for FVR inhalation, which resulted to a significant decrease in the EC_{50} of FVR. However, the physical characteristics of the FVR-SLN remain as a challenge due to their instability

and the risks of lipid degradation over time. In this study, we proposed an alternative and new delivery route for FVR via nasal administration using a biocompatible mucoadhesive CS-coated-ALG-NPs (FVR-MCS-ALG-NPs) that would target localized coronaviruses in the upper airways.

Here, we first demonstrate the optimization of the FVR-MCS-ALG-NPs by statistical analysis using RSM based on BBD of experiment in developing ideal NPs formulation for transmucosal delivery. The model employed had a high predictability for the critical parameters with the highest desirability of 93% with respect to the goal set for the size, surface charge, LC, and EE. In investigating the effects and interaction between the major factors and responses, we found that the CS mass ratio to ALG majorly contributes to the optimization of FVR-MCS-ALG-NPs. Increasing the concentration of CS in the system contributes to the formation of larger particles brought by the presence of excess CS molecules causes clumping and entanglement of the molecules. CS also contributes to the DL and EE of the optimized NPs attributed to the increase in amino groups that interact and cross-link with the COOH of ALG. Further, no chemical interaction was observed in the FVR-MCS-ALG-NPs by thermal analysis but the absence of the crystalline FVR in the XRD patterns of FVR-MCS-ALG-NPs was observed that is attributed the amorphous dispersion of FVR within the MCS-ALG-NPs during intermolecular interaction of polymers.

Also, we investigated the benefit of CS-coating onto the NPs regarding drug release, mucoadhesive, and transmucosal permeation by comparing it with the

uncoated-NPs (FVR-ALG-NPs) and the free FVR. Herein, we demonstrated sustained release of the FVR-MCS-ALG-NPs in both pH conditions (7.4 mucus environment and 5.5 nasal epithelium). Notably, the MCS-ALG-NPs had a higher release rate in the epithelium environment than in the mucus, owing to the pH-responsive drug release mechanism of CS than the uncoated-NPs. The amino groups of CS shrink at basic pH due to its deprotonation causing a slow release of FVR at pH 7.4. In contrast, an acidic pH that is below the isoelectric point (~7) of CS triggers protonation of the NH2+, followed by the swelling and erosion of the polymer matrix, and eventually the release of FVR.

Finding the correct balance between the critical factors in optimization, especially the concentration of the CS-coating, is important to maintain its ideal physical characteristics without compromising the mucoadhesive property of the NPs by electrostatic interaction with the mucus. The investigation of the mucoadhesive property of the NPs confirmed that the optimal amount of CS-coating on the FVR-ALG-NPs is still sufficient to elicit muco-interaction that is evident in the significant change in its size and surface charge of the NPs. The oligosaccharide chain of the mucin presents a negatively charged sialic acid terminal residue that enrobes its interaction with the CS layer, hence the change in the surface charge to more negative. This demonstrated that even though the FVR-MCS-ALG-NPs have a negative surface charge after CS-coating, the optimal concentration of CS can still obtain

mucoadhesion that is driven by electrostatic interaction with the positively charged amino groups of D-glucosamine molecule of CS with the sialic acid residue of mucin.

Moreover, we also demonstrated the sufficiency of the CS-coating to exhibit enhanced transmucosal permeation through PNM. Our result showed that the optimal concentration of CS on FVR-ALG-NPs still demonstrates 3- and 6-fold faster flux and superior deposition in the PNM when compared to uncoated-NPs and free FVR, respectively. In other studies, the favorable transmucosal permeation is associated with CS through its ability to disrupt tight epithelial junctions. However, this rationale generally supports the permeation of hydrophilic drugs, and some evidence proved that it is less efficient to open-tight junctions when used as a coating, than as the main material in constructing the NPs. Here, we postulated that the higher permeation and deposition of the FVR-MCS-ALG-NPs could be explained by a combination of factors specifically its small size and its proven mucoadhesive property that propels the particle to move through the mucus layer and facilitate its absorption into the nasal epithelium.

Lastly, we have proven the enhancement of the antiviral effect of the FVR-MCS-ALG-NPs by more than 35-fold when compared to free FVR towards the PEDV model that acts as a surrogate virus for SARS-CoV-2. A published concept of improving the antiviral activity of FVR by nano-emulsion for coronavirus was hypothesized to effectively interfere with viral adsorption, invasion, and replication. Another study demonstrated the use of SLN as a carrier for FVR, which resulted in a

significant decrease in the EC_{50} of FVR. Comparing the antiviral activity observed in this current study of using polymeric nanocarrier for FVR delivery, we have demonstrated superior enhancement of antiviral activity compared to previous reports. This can be explained by the collective features of the optimal formulation owing to its small size and high drug loading, its mucoadhesive and muco-penetrating property, and the enhanced permeation and deposition of FVR in the nasal mucosa. These collective properties of the FVR-MCS-ALG-NPs could have increased the intracellular drug concentration due to improved cellular uptake while subsequently boosting its antiviral activity. Typically, particles with a positive charge will bind to the negatively charged cell surface and promote internalization. But cellular internalization of NPs does not exclusively rely on the surface charge of the NPs and their electrostatic interaction with the cell membrane. Uptake of the nanoparticles by the cellular systems occurs with a process known as endocytosis and is influenced by the physicochemical characteristics of nanoparticles such as size, shape, and surface chemistry as well as the employed experimental conditions. In previous studies, the internalization of highly negatively charged polymeric NPs is associated with the electrostatic repulsive interaction with the cell surface, which promotes a hydrophobic interface. Moreover, the sufficient mucoadhesive property of the FVR-MCS-ALG-NPs could promote an absorption-enhancing mechanism and accumulation of mucus-producing RPMI-2650 nasal epithelial cells that might contribute to its superior uptake.

In conclusion, we demonstrated a proof-of-concept of using mucoadhesive NPs as an efficient FVR carrier that could potentially be developed for intranasal delivery of FVR against coronavirus and its transmucosal delivery and deposition in the nasal mucosa. However, a more comprehensive analysis on the intranasal delivery of the FVR-MCS-ALG-NPs is recommended due to the absence of mucociliary clearance and some physiological factors (e.g., posture and gravitational pull) in the experiments conducted herein that could affect the residence time of the FVR-MCS-ALG-NPs. Moreover, due to the weak fluorescence of FVR, 5-aminofluorescein (5-AF) was used and loaded in the MCS-ALG NPs for the qualitative cellular uptake studies. 5-AF was used owing to the amino functionality in its structure and its solubility in aqueous media that is almost similar to FVR. Also, its high fluorescence intensity and tolerable toxicity to the cells make them a preferred dye for cellular uptake studies. However, qualitative uptake of the NPs loaded with a fluorescent dye is not tantamount to the direct translation of the uptake of FVR into the cells. Quantifying the amount of FVR in the cells is necessary to better understand cellular internalization. This can be done by the ultrasonication of the treated cells followed by the extraction and quantification of FVR by organic solvents. Although no standardized and validated method is available for quantifying NPs internalized by the cells [64], correlation analysis on the qualitative and quantitative cellular uptake experiments is often suggested for better interpretation of data. Further, all though the concept of using PEDV model as a surrogate for SARS-CoV-2 in antiviral testing

have already been established, it is also recommended to test the formulation towards the actual SARS-CoV-2 to have an in-depth knowledge and guaranteed enhancement of its efficacy.

จุฬาลงกรณ์มหาวิทยาลัย
Chulalongkorn University

REFERENCES

จุฬาลงกรณ์มหาวิทยาลัย
Chulalongkorn University

1. Yesudhas, D., A. Srivastava, and M.M. Gromiha, *COVID-19 outbreak: history, mechanism, transmission, structural studies and therapeutics.* Infection, 2021. 49(2): p. 199-213.
2. Saber-Ayad, M., M.A. Saleh, and E. Abu-Gharbieh, *The Rationale for Potential Pharmacotherapy of COVID-19.* Pharmaceuticals (Basel), 2020. 13(5).
3. Joshi, S., et al., *Role of favipiravir in the treatment of COVID-19.* Int J Infect Dis, 2021. 102: p. 501-508.
4. He, H., et al., *Repurposing disulfiram for cancer therapy via targeted nanotechnology through enhanced tumor mass penetration and disassembly.* Acta Biomater, 2018. 68: p. 113-124.
5. Czech, T., R. Lalani, and M.O. Oyewumi, *Delivery Systems as Vital Tools in Drug Repurposing.* AAPS PharmSciTech, 2019. 20(3): p. 116.
6. Parvathaneni, V. and V. Gupta, *Utilizing drug repurposing against COVID-19 - Efficacy, limitations, and challenges.* Life Sci, 2020. 259: p. 118275.
7. Simsek-Yavuz, S. and F.I. Komsuoglu Celikyurt, *An update of anti-viral treatment of COVID-19.* Turk J Med Sci, 2021. 51(SI-1): p. 3372-3390.
8. Parasher, A., *COVID-19: Current understanding of its Pathophysiology, Clinical presentation and Treatment.* Postgrad Med J, 2021. 97(1147): p. 312-320.
9. Qomara, W.F., et al., *Effectiveness of Remdesivir, Lopinavir/Ritonavir, and Favipiravir for COVID-19 Treatment: A Systematic Review.* Int J Gen Med, 2021. 14: p. 8557-8571.
10. Deguchi, S., et al., *Ophthalmic Formulation Containing Nilvadipine Nanoparticles Prevents Retinal Dysfunction in Rats Injected with Streptozotocin.* Int J Mol Sci, 2017. 18(12).
11. Rostamkalaei, S.S., et al., *Topical gel of Metformin solid lipid nanoparticles: A hopeful promise as a dermal delivery system.* Colloids Surf B Biointerfaces, 2019. 175: p. 150-157.
12. Jaromin, A., et al., *Topical delivery of ebselen encapsulated in biopolymeric nanocapsules: drug repurposing enhanced antifungal activity.* Nanomedicine (Lond), 2018. 13(10): p. 1139-1155.

จุฬาลงกรณ์มหาวิทยาลัย
CHULALONGKORN UNIVERSITY

13. Nagai, N., et al., *A nanoparticle formulation of disulfiram prolongs corneal residence time of the drug and reduces intraocular pressure.* Exp Eye Res, 2015. 132: p. 115-23.
14. Grassin-Delyle, S., et al., *Intranasal drug delivery: an efficient and non-invasive route for systemic administration: focus on opioids.* Pharmacol Ther, 2012. 134(3): p. 366-79.
15. Battaglia, L., et al., *Lipid nanoparticles for intranasal administration: application to nose-to-brain delivery.* Expert Opin Drug Deliv, 2018. 15(4): p. 369-378.
16. Keller, L.A., O. Merkel, and A. Popp, *Intranasal drug delivery: opportunities and toxicologic challenges during drug development.* Drug Deliv Transl Res, 2021.
17. Chavda, V.P., et al., *Intranasal vaccines for SARS-CoV-2: From challenges to potential in COVID-19 management.* Drug Discov Today, 2021. 26(11): p. 2619-2636.
18. Porter, A.E., et al., *Uptake of C60 by human monocyte macrophages, its localization and implications for toxicity: studied by high resolution electron microscopy and electron tomography.* Acta Biomater, 2006. 2(4): p. 409-19.
19. Kreyling, W.G., M. Semmler-Behnke, and W. Moller, *Ultrafine particle-lung interactions: does size matter?* J Aerosol Med, 2006. 19(1): p. 74-83.
20. Popov, A., *Mucus-Penetrating Particles and the Role of Ocular Mucus as a Barrier to Micro- and Nanosuspensions.* J Ocul Pharmacol Ther, 2020. 36(6): p. 366-375.
21. Alexander, A., et al., *Approaches for breaking the barriers of drug permeation through transdermal drug delivery.* J Control Release, 2012. 164(1): p. 26-40.
22. Lockman, P.R., et al., *Nanoparticle technology for drug delivery across the blood-brain barrier.* Drug Dev Ind Pharm, 2002. 28(1): p. 1-13.
23. Na, L., et al., *Comparison of different absorption enhancers on the intranasal absorption of isosorbide dinitrate in rats.* Int J Pharm, 2010. 397(1-2): p. 59-66.
24. Nalini, T., et al., *Development and characterization of alginate / chitosan nanoparticulate system for hydrophobic drug encapsulation.* Journal of Drug Delivery Science and Technology, 2019. 52: p. 65-72.
25. Samyn, P., *A platform for functionalization of cellulose, chitin/chitosan, alginate with polydopamine: A review on fundamentals and technical applications.* Int J Biol Macromol, 2021. 178: p. 71-93.

จุฬาลงกรณ์มหาวิทยาลัย
CHULALONGKORN UNIVERSITY

26. Sosnowski, T.R., *Inhaled aerosols: Their role in COVID-19 transmission, including biophysical interactions in the lungs.* Current Opinion in Colloid & Interface Science, 2021. 54: p. 101451.
27. Chen, Y., et al., *Structure analysis of the receptor binding of 2019-nCoV.* Biochem Biophys Res Commun, 2020.
28. Gremese, E., et al., *Basic immunology may lead to translational therapeutic rationale: SARS-CoV-2 and rheumatic diseases.* Eur J Clin Invest, 2020. 50(9): p. e13342.
29. Han, H.J., et al., *COVID-19 and cancer: From basic mechanisms to vaccine development using nanotechnology.* International Immunopharmacology, 2021. 90: p. 107247.
30. Dos Santos, W.G., *Natural history of COVID-19 and current knowledge on treatment therapeutic options.* Biomed Pharmacother, 2020. 129: p. 110493.
31. Aslan, A., et al., *Acute respiratory distress syndrome in COVID-19: possible mechanisms and therapeutic management.* Pneumonia (Nathan), 2021. 13(1): p. 14.
32. Tang, Y., et al., *Cytokine Storm in COVID-19: The Current Evidence and Treatment Strategies.* Front Immunol, 2020. 11: p. 1708.
33. Younan, P., et al., *Ebola Virus Binding to Tim-1 on T Lymphocytes Induces a Cytokine Storm.* mBio, 2017. 8(5).
34. Tisoncik, J.R., et al., *Into the eye of the cytokine storm.* Microbiol Mol Biol Rev, 2012. 76(1): p. 16-32.
35. Zhang, Y., et al., *New understanding of the damage of SARS-CoV-2 infection outside the respiratory system.* Biomed Pharmacother, 2020. 127: p. 110195.
36. Savarino, A., et al., *New insights into the antiviral effects of chloroquine.* Lancet Infect Dis, 2006. 6(2): p. 67-9.
37. Keyaerts, E., et al., *In vitro inhibition of severe acute respiratory syndrome coronavirus by chloroquine.* Biochem Biophys Res Commun, 2004. 323(1): p. 264-8.
38. Wang, M., et al., *Remdesivir and chloroquine effectively inhibit the recently emerged novel coronavirus (2019-nCoV) in vitro.* Cell Res, 2020. 30(3): p. 269-271.
39. Huang, M., et al., *Treating COVID-19 with Chloroquine.* J Mol Cell Biol, 2020. 12(4): p. 322-325.

จุฬาลงกรณ์มหาวิทยาลัย
Chulalongkorn University

40. Liu, S., et al., *Chinese herbal medicine (weijing decoction) combined with pharmacotherapy for the treatment of acute exacerbations of chronic obstructive pulmonary disease.* Evid Based Complement Alternat Med, 2014. 2014: p. 257012.
41. Leung, P.C., *The efficacy of Chinese medicine for SARS: a review of Chinese publications after the crisis.* Am J Chin Med, 2007. 35(4): p. 575-81.
42. Ho, T.Y., et al., *Emodin blocks the SARS coronavirus spike protein and angiotensin-converting enzyme 2 interaction.* Antiviral Res, 2007. 74(2): p. 92-101.
43. Han, F., et al., *Current treatment strategies for COVID19 (Review).* Mol Med Rep, 2021. 24(6).
44. Ahmed, S.F., A.A. Quadeer, and M.R. McKay, *Preliminary Identification of Potential Vaccine Targets for the COVID-19 Coronavirus (SARS-CoV-2) Based on SARS-CoV Immunological Studies.* Viruses, 2020. 12(3).
45. Gao, Y., et al., *Structure of the RNA-dependent RNA polymerase from COVID-19 virus.* Science, 2020. 368(6492): p. 779-782.
46. Mentre, F., et al., *Dose regimen of favipiravir for Ebola virus disease.* Lancet Infect Dis, 2015. 15(2): p. 150-1.
47. Wang, Y., et al., *Comparative Effectiveness of Combined Favipiravir and Oseltamivir Therapy Versus Oseltamivir Monotherapy in Critically Ill Patients With Influenza Virus Infection.* J Infect Dis, 2020. 221(10): p. 1688-1698.
48. Du, Y.X. and X.P. Chen, *Favipiravir: Pharmacokinetics and Concerns About Clinical Trials for 2019-nCoV Infection.* Clin Pharmacol Ther, 2020. 108(2): p. 242-247.
49. Madelain, V., et al., *Ebola Virus Infection: Review of the Pharmacokinetic and Pharmacodynamic Properties of Drugs Considered for Testing in Human Efficacy Trials.* Clin Pharmacokinet, 2016. 55(8): p. 907-23.
50. Ivashchenko, A.A., et al., *AVIFAVIR for Treatment of Patients With Moderate Coronavirus Disease 2019 (COVID-19): Interim Results of a Phase II/III Multicenter Randomized Clinical Trial.* Clin Infect Dis, 2021. 73(3): p. 531-534.
51. Bocan, T.M., et al., *Synthesis of [(18)F]Favipiravir and Biodistribution in C3H/HeN Mice as Assessed by Positron Emission Tomography.* Sci Rep, 2019. 9(1): p. 1785.
52. Shannon, A., et al., *Favipiravir strikes the SARS-CoV-2 at its Achilles heel, the RNA polymerase.* bioRxiv, 2020.

จุฬาลงกรณ์มหาวิทยาลัย
CHULALONGKORN UNIVERSITY

53. Chen, C., et al., *Favipiravir Versus Arbidol for Clinical Recovery Rate in Moderate and Severe Adult COVID-19 Patients: A Prospective, Multicenter, Open-Label, Randomized Controlled Clinical Trial.* Front Pharmacol, 2021. 12: p. 683296.

54. Ives, J. *Preliminary report of favipiravir observational study in Japan released*. 2020 [cited 2021 December 2021]; Available from: https://www.news-medical.net/news/20200602/Preliminary-report-of-Favipiravir-Observational-Study-in-Japan-released.aspx.

55. Cojocaru, F.D., et al., *Nanomaterials Designed for Antiviral Drug Delivery Transport across Biological Barriers.* Pharmaceutics, 2020. 12(2).

56. Doane, T.L. and C. Burda, *The unique role of nanoparticles in nanomedicine: imaging, drug delivery and therapy.* Chem Soc Rev, 2012. 41(7): p. 2885-911.

57. Hasanzadeh, A., et al., *Nanotechnology against COVID-19: Immunization, diagnostic and therapeutic studies.* J Control Release, 2021. 336: p. 354-374.

58. Yayehrad, A.T., et al., *Could Nanotechnology Help to End the Fight Against COVID-19? Review of Current Findings, Challenges and Future Perspectives.* Int J Nanomedicine, 2021. 16: p. 5713-5743.

59. Xiao, M.F., et al., *Applications of nanomaterials in COVID-19 pandemic.* Rare Metals, 2021: p. 1-13.

60. Patel, G.V., et al., *Nanosuspension of efavirenz for improved oral bioavailability: formulation optimization, in vitro, in situ and in vivo evaluation.* Drug Dev Ind Pharm, 2014. 40(1): p. 80-91.

61. Sneha, R., B.N. Vedha Hari, and D. Ramya Devi, *Design of antiretroviral drug-polymeric nanoparticles laden buccal films for chronic HIV therapy in paediatrics.* Colloid and Interface Science Communications, 2018. 27: p. 49-59.

62. Li, Y., et al., *Inhibition of H1N1 influenza virus-induced apoptosis by functionalized selenium nanoparticles with amantadine through ROS-mediated AKT signaling pathways.* Int J Nanomedicine, 2018. 13: p. 2005-2016.

63. Li, Y., et al., *Inhibitory activity of selenium nanoparticles functionalized with oseltamivir on H1N1 influenza virus.* Int J Nanomedicine, 2017. 12: p. 5733-5743.

64. Hu, C.J., et al., *Antiviral efficacy of nanoparticulate vacuolar ATPase inhibitors against influenza virus infection.* Int J Nanomedicine, 2018. 13: p. 8579-8593.

65. Ferenci, P., *Peginterferon alfa-2a (40KD) (Pegasys) for the treatment of patients with chronic hepatitis C.* Int J Clin Pract, 2003. 57(7): p. 610-5.

จุฬาลงกรณ์มหาวิทยาลัย
CHULALONGKORN UNIVERSITY

66. Price, C.F., et al., *SPL7013 Gel (VivaGel(R)) retains potent HIV-1 and HSV-2 inhibitory activity following vaginal administration in humans.* PLoS One, 2011. 6(9): p. e24095.

67. Syedmoradi, L., et al., *Point of care testing: The impact of nanotechnology.* Biosens Bioelectron, 2017. 87: p. 373-387.

68. Kumar, V., et al., *Harnessing Plasmon-Induced Hot Carriers at the Interfaces With Ferroelectrics.* Front Chem, 2019. 7: p. 299.

69. Zhang, N., et al., *Current development of COVID-19 diagnostics, vaccines and therapeutics.* Microbes Infect, 2020. 22(6-7): p. 231-235.

70. Karakus, E., et al., *Colorimetric and electrochemical detection of SARS-CoV-2 spike antigen with a gold nanoparticle-based biosensor.* Anal Chim Acta, 2021. 1182: p. 338939.

71. Huang, C., et al., *Rapid Detection of IgM Antibodies against the SARS-CoV-2 Virus via Colloidal Gold Nanoparticle-Based Lateral-Flow Assay.* ACS Omega, 2020. 5(21): p. 12550-12556.

72. Repsilon®. *Repsilon® Virus killer membrane*. 2021 [cited 2021 December 6, 2021]; Available from: https://www.respilon.com/products/nanofiber-membranes/.

73. Yamashin-Filter. *Announcing the Launch of Our Latest Product: "Zexeed" YAMASHIN Filter Mask*. 2020 [cited 2021 December 6, 2021]; Available from: http://www.yamashin-filter.co.jp/eng/topics/topics202000911-001/main/0/link/Announcing_the_Launch_of_Our_Latest_Product_Zexeed_YAMASHIN_Filter_Mask.pdf.

74. NCBI+. *Here's How Nanotechnologies Tailor Face Masks for Coronavirus Era*. 2020 [cited 2021 December 6, 2021]; Available from: https://statnano.com/news/67662/Here%E2%80%99s-How-Nanotechnologies-Tailor-Face-Masks-for-Coronavirus-Era.

75. PrometheanParticles. *Promethean Particles puts its nano-copper to the test in the fight against viruses*. 2020 [cited 2021 December 6, 2021]; Available from: https://prometheanparticles.co.uk/promethean-particles-puts-its-nano-copper-to-the-test-in-the-fight-against-viruses/.

76. Balagna, C., et al., *Virucidal effect against coronavirus SARS-CoV-2 of a silver nanocluster/silica composite sputtered coating.* Open Ceramics, 2020. 1: p. 100006.

จุฬาลงกรณ์มหาวิทยาลัย
Chulalongkorn University

77. Lin, L.C., et al., *Viromimetic STING Agonist-Loaded Hollow Polymeric Nanoparticles for Safe and Effective Vaccination against Middle East Respiratory Syndrome Coronavirus.* Adv Funct Mater, 2019. 29(28): p. 1807616.

78. Raghuwanshi, D., et al., *Dendritic cell targeted chitosan nanoparticles for nasal DNA immunization against SARS CoV nucleocapsid protein.* Mol Pharm, 2012. 9(4): p. 946-56.

79. Chen, H.W., et al., *Synthetic virus-like particles prepared via protein corona formation enable effective vaccination in an avian model of coronavirus infection.* Biomaterials, 2016. 106: p. 111-8.

80. Jung, S.Y., et al., *Heterologous prime-boost vaccination with adenoviral vector and protein nanoparticles induces both Th1 and Th2 responses against Middle East respiratory syndrome coronavirus.* Vaccine, 2018. 36(24): p. 3468-3476.

81. Jackson, L.A., et al., *An mRNA Vaccine against SARS-CoV-2 - Preliminary Report.* N Engl J Med, 2020. 383(20): p. 1920-1931.

82. Baden, L.R., et al., *Efficacy and Safety of the mRNA-1273 SARS-CoV-2 Vaccine.* N Engl J Med, 2021. 384(5): p. 403-416.

83. Walsh, E.E., et al., *Safety and Immunogenicity of Two RNA-Based Covid-19 Vaccine Candidates.* N Engl J Med, 2020. 383(25): p. 2439-2450.

84. Polack, F.P., et al., *Safety and Efficacy of the BNT162b2 mRNA Covid-19 Vaccine.* N Engl J Med, 2020. 383(27): p. 2603-2615.

85. Hou, X., et al., *Lipid nanoparticles for mRNA delivery.* Nat Rev Mater, 2021: p. 1-17.

86. Tai, T.T., et al., *A Strategy to Treat COVID-19 Disease With Targeted Delivery of Inhalable Liposomal Hydroxychloroquine: A Preclinical Pharmacokinetic Study.* Clin Transl Sci, 2021. 14(1): p. 132-136.

87. Sadr, M.S., et al., *Production and characterization of biocompatible nano-carrier based on Fe3O4 for magnetically hydroxychloroquine drug delivery.* Polymers for Advanced Technologies, 2021. 32(2): p. 564-573.

88. Surnar, B., et al., *Clinically Approved Antiviral Drug in an Orally Administrable Nanoparticle for COVID-19.* ACS Pharmacol Transl Sci, 2020. 3(6): p. 1371-1380.

89. Sanna, V., et al., *Development of targeted nanoparticles loaded with antiviral drugs for SARS-CoV-2 inhibition.* European Journal of Medicinal Chemistry, 2022: p. 114121.

CHULALONGKORN UNIVERSITY

90. Ranjbar, S., Y. Fatahi, and F. Atyabi, *The quest for a better fight: How can nanomaterials address the current therapeutic and diagnostic obstacles in the fight against COVID-19?* J Drug Deliv Sci Technol, 2021: p. 102899.

91. Rai, M., et al., *Nanotechnology as a Shield against COVID-19: Current Advancement and Limitations.* Viruses, 2021. 13(7).

92. Chan, W.C.W., *Nano Research for COVID-19.* ACS Nano, 2020. 14(4): p. 3719-3720.

93. Sukhanova, A., et al., *Dependence of Nanoparticle Toxicity on Their Physical and Chemical Properties.* Nanoscale Res Lett, 2018. 13(1): p. 44.

94. Gurunathan, S., et al., *Antiviral Potential of Nanoparticles-Can Nanoparticles Fight Against Coronaviruses?* Nanomaterials (Basel), 2020. 10(9).

95. Chen, L. and J. Liang, *An overview of functional nanoparticles as novel emerging antiviral therapeutic agents.* Mater Sci Eng C Mater Biol Appl, 2020. 112: p. 110924.

96. Dey, P., et al., *Multivalent Flexible Nanogels Exhibit Broad-Spectrum Antiviral Activity by Blocking Virus Entry.* ACS Nano, 2018. 12(7): p. 6429-6442.

97. Halder, A., et al., *Highly monodispersed gold nanoparticles synthesis and inhibition of herpes simplex virus infections.* Mater Sci Eng C Mater Biol Appl, 2018. 89: p. 413-421.

98. Pedroso-Santana, S., et al., *Polymeric nanoencapsulation of alpha interferon increases drug bioavailability and induces a sustained antiviral response in vivo.* Mater Sci Eng C Mater Biol Appl, 2020. 116: p. 111260.

99. Dhoke, D.M., S.S. Basaiyye, and P.B. Khedekar, *Development and characterization of L-HSA conjugated PLGA nanoparticle for hepatocyte targeted delivery of antiviral drug.* Journal of Drug Delivery Science and Technology, 2018. 47: p. 77-94.

100. Ramana, L.N., et al., *Evaluation of chitosan nanoformulations as potent anti-HIV therapeutic systems.* Biochim Biophys Acta, 2014. 1840(1): p. 476-84.

101. Meng, J., et al., *Tenofovir Containing Thiolated Chitosan Core/Shell Nanofibers: In Vitro and in Vivo Evaluations.* Mol Pharm, 2016. 13(12): p. 4129-4140.

102. Cao, S., et al., *Hybrid nanocarriers incorporating mechanistically distinct drugs for lymphatic CD4(+) T cell activation and HIV-1 latency reversal.* Sci Adv, 2019. 5(3): p. eaav6322.

103. Joshy, K.S., et al., *Core–shell nanoparticles of carboxy methyl cellulose and compritol-PEG for antiretroviral drug delivery.* Cellulose, 2017. 24(11): p. 4759-4771.

จุฬาลงกรณ์มหาวิทยาลัย
CHULALONGKORN UNIVERSITY

104. Joshy, K.S., et al., *Poly (vinyl pyrrolidone)-lipid based hybrid nanoparticles for anti viral drug delivery.* Chem Phys Lipids, 2018. 210: p. 82-89.

105. Shang, Y., et al., *Prediction of nasal spray drug absorption influenced by mucociliary clearance.* PLoS One, 2021. 16(1): p. e0246007.

106. Lizal, F., et al., *The effect of oral and nasal breathing on the deposition of inhaled particles in upper and tracheobronchial airways.* J Aerosol Sci, 2020. 150: p. 105649.

107. Lobaina Mato, Y., *Nasal route for vaccine and drug delivery: Features and current opportunities.* Int J Pharm, 2019. 572: p. 118813.

108. Le Guellec, S., S. Ehrmann, and L. Vecellio, *In vitro - in vivo correlation of intranasal drug deposition.* Adv Drug Deliv Rev, 2021. 170: p. 340-352.

109. Li, Z., et al., *Characterization of nebulized liposomal amikacin (Arikace) as a function of droplet size.* J Aerosol Med Pulm Drug Deliv, 2008. 21(3): p. 245-54.

110. Laube, B.L., *Devices for aerosol delivery to treat sinusitis.* J Aerosol Med, 2007. 20 Suppl 1: p. S5-17; discussion S17-8.

111. Pires, A., et al., *Intranasal drug delivery: how, why and what for?* J Pharm Pharm Sci, 2009. 12(3): p. 288-311.

112. Alam, S., et al., *Development and evaluation of thymoquinone-encapsulated chitosan nanoparticles for nose-to-brain targeting: a pharmacoscintigraphic study.* Int J Nanomedicine, 2012. 7: p. 5705-18.

113. Newman, S.P., et al., *The distribution of an intranasal insulin formulation in healthy volunteers: effect of different administration techniques.* J Pharm Pharmacol, 1994. 46(8): p. 657-60.

114. Kundoor, V. and R.N. Dalby, *Effect of formulation- and administration-related variables on deposition pattern of nasal spray pumps evaluated using a nasal cast.* Pharm Res, 2011. 28(8): p. 1895-904.

115. Foo, M.Y., et al., *The influence of spray properties on intranasal deposition.* J Aerosol Med, 2007. 20(4): p. 495-508.

116. Xu, J., J. Tao, and J. Wang, *Design and Application in Delivery System of Intranasal Antidepressants.* Front Bioeng Biotechnol, 2020. 8: p. 626882.

117. Ostrowski, L.E. and W.D. Bennett, *CILIA AND MUCOCILIARY CLEARANCE*, in *Encyclopedia of Respiratory Medicine*, G.J. Laurent and S.D. Shapiro, Editors. 2006, Academic Press: Oxford. p. 466-470.

จุฬาลงกรณ์มหาวิทยาลัย
CHULALONGKORN UNIVERSITY

118. Wittig, T., *[Mucociliary clearance in COVID-19 - an underestimated danger area in early phase of disease?].* MMW Fortschr Med, 2021. 163(Suppl 5): p. 21-27.

119. Duvvuri, S., S. Majumdar, and A.K. Mitra, *Drug delivery to the retina: challenges and opportunities.* Expert Opin Biol Ther, 2003. 3(1): p. 45-56.

120. Illum, L., *Nasal drug delivery--possibilities, problems and solutions.* J Control Release, 2003. 87(1-3): p. 187-98.

121. Illum, L., *Nasal drug delivery: new developments and strategies.* Drug Discov Today, 2002. 7(23): p. 1184-9.

122. Proschak, E., et al., *Opportunities and Challenges for Fatty Acid Mimetics in Drug Discovery.* J Med Chem, 2017. 60(13): p. 5235-5266.

123. Li, Y., et al., *Metoclopramide nasal spray in vitro evaluation and in vivo pharmacokinetic studies in dogs.* Pharm Dev Technol, 2018. 23(3): p. 275-281.

124. McMartin, C., et al., *Analysis of structural requirements for the absorption of drugs and macromolecules from the nasal cavity.* J Pharm Sci, 1987. 76(7): p. 535-40.

125. Arora, P., S. Sharma, and S. Garg, *Permeability issues in nasal drug delivery.* Drug Discov Today, 2002. 7(18): p. 967-75.

126. Costantino, H.R., et al., *Intranasal delivery: physicochemical and therapeutic aspects.* Int J Pharm, 2007. 337(1-2): p. 1-24.

127. Cass, L.M., C. Efthymiopoulos, and A. Bye, *Pharmacokinetics of zanamivir after intravenous, oral, inhaled or intranasal administration to healthy volunteers.* Clin Pharmacokinet, 1999. 36 Suppl 1: p. 1-11.

128. Duquesnoy, C., et al., *Comparative clinical pharmacokinetics of single doses of sumatriptan following subcutaneous, oral, rectal and intranasal administration.* Eur J Pharm Sci, 1998. 6(2): p. 99-104.

129. Haschke, M., et al., *Pharmacokinetics and pharmacodynamics of nasally delivered midazolam.* Br J Clin Pharmacol, 2010. 69(6): p. 607-16.

130. Davis, S.S. and L. Illum, *Absorption enhancers for nasal drug delivery.* Clin Pharmacokinet, 2003. 42(13): p. 1107-28.

131. Karasulu, E., et al., *Permeation studies and histological examination of sheep nasal mucosa following administration of different nasal formulations with or without absorption enhancers.* Drug Deliv, 2008. 15(4): p. 219-25.

132. Hou, J., *Chapter 6 - Paracellular Water Channel*, in *The Paracellular Channel*, J. Hou, Editor. 2019, Academic Press. p. 83-92.

จุฬาลงกรณ์มหาวิทยาลัย
CHULALONGKORN UNIVERSITY

133. Illum, L., *Nanoparticulate systems for nasal delivery of drugs: a real improvement over simple systems?* J Pharm Sci, 2007. 96(3): p. 473-83.

134. Behrens, I., et al., *Comparative uptake studies of bioadhesive and non-bioadhesive nanoparticles in human intestinal cell lines and rats: the effect of mucus on particle adsorption and transport.* Pharm Res, 2002. 19(8): p. 1185-93.

135. Artursson, P., et al., *Effect of chitosan on the permeability of monolayers of intestinal epithelial cells (Caco-2).* Pharm Res, 1994. 11(9): p. 1358-61.

136. Smith, J., E. Wood, and M. Dornish, *Effect of chitosan on epithelial cell tight junctions.* Pharm Res, 2004. 21(1): p. 43-9.

137. Lai, S.K., Y.Y. Wang, and J. Hanes, *Mucus-penetrating nanoparticles for drug and gene delivery to mucosal tissues.* Adv Drug Deliv Rev, 2009. 61(2): p. 158-71.

138. Khutoryanskiy, V.V., *Advances in mucoadhesion and mucoadhesive polymers.* Macromol Biosci, 2011. 11(6): p. 748-64.

139. Hasnain, M.S. and A.K. Nayak, *Chapter 9 - Chitosan as mucoadhesive polymer in drug delivery*, in *Chitosan in Drug Delivery*, M.S. Hasnain, S. Beg, and A.K. Nayak, Editors. 2022, Academic Press. p. 225-246.

140. Bansil, R. and B.S. Turner, *Mucin structure, aggregation, physiological functions and biomedical applications.* Current Opinion in Colloid & Interface Science, 2006. 11(2): p. 164-170.

141. Leal, J., H.D.C. Smyth, and D. Ghosh, *Physicochemical properties of mucus and their impact on transmucosal drug delivery.* Int J Pharm, 2017. 532(1): p. 555-572.

142. Boegh, M. and H.M. Nielsen, *Mucus as a barrier to drug delivery - understanding and mimicking the barrier properties.* Basic Clin Pharmacol Toxicol, 2015. 116(3): p. 179-86.

143. Giuliani, A., et al., *In vivo nose-to-brain delivery of the hydrophilic antiviral ribavirin by microparticle agglomerates.* Drug Deliv, 2018. 25(1): p. 376-387.

144. Alsarra, I.A., A.Y. Hamed, and F.K. Alanazi, *Acyclovir liposomes for intranasal systemic delivery: development and pharmacokinetics evaluation.* Drug Deliv, 2008. 15(5): p. 313-21.

145. Shao, Z., et al., *The Physicochemical Properties, Plasma Enzymatic Hydrolysis, and Nasal Absorption of Acyclovir and Its 2'-Ester Prodrugs.* Pharmaceutical Research, 1994. 11(2): p. 237-242.

จุฬาลงกรณ์มหาวิทยาลัย
CHULALONGKORN UNIVERSITY

146. Mahajan, H.S., et al., *Nanoemulsion-based intranasal drug delivery system of saquinavir mesylate for brain targeting.* Drug Deliv, 2014. 21(2): p. 148-54.

147. Ved, P.M. and K. Kim, *Poly(ethylene oxide/propylene oxide) copolymer thermo-reversible gelling system for the enhancement of intranasal zidovudine delivery to the brain.* Int J Pharm, 2011. 411(1-2): p. 1-9.

148. Colombo, G., et al., *Brain distribution of ribavirin after intranasal administration.* Antiviral Res, 2011. 92(3): p. 408-14.

149. Smart, J.D., *The basics and underlying mechanisms of mucoadhesion.* Advanced Drug Delivery Reviews, 2005. 57(11): p. 1556-1568.

150. Ben-Zion, O. and A. Nussinovitch, *Physical properties of hydrocolloid wet glues.* Food Hydrocolloids, 1997. 11(4): p. 429-442.

151. Ponnusamy, C., et al., *Development and Evaluation of Polyvinylpyrrolidone K90 and Poloxamer 407 Self-Assembled Nanomicelles: Enhanced Topical Ocular Delivery of Artemisinin.* Polymers (Basel), 2021. 13(18).

152. Cazorla-Luna, R., et al., *Naturally Occurring Polyelectrolytes and Their Use for the Development of Complex-Based Mucoadhesive Drug Delivery Systems: An Overview.* Polymers (Basel), 2021. 13(14).

153. Edsman, K. and H. Hagerstrom, *Pharmaceutical applications of mucoadhesion for the non-oral routes.* J Pharm Pharmacol, 2005. 57(1): p. 3-22.

154. Smart, J.D., *The basics and underlying mechanisms of mucoadhesion.* Adv Drug Deliv Rev, 2005. 57(11): p. 1556-68.

155. Peppas, N.A. and J.J. Sahlin, *Hydrogels as mucoadhesive and bioadhesive materials: a review.* Biomaterials, 1996. 17(16): p. 1553-1561.

156. Shinkar, D.M., A.S. Dhake, and C.M. Setty, *Drug delivery from the oral cavity: a focus on mucoadhesive buccal drug delivery systems.* PDA J Pharm Sci Technol, 2012. 66(5): p. 466-500.

157. Peppas, N.A. and Y. Huang, *Nanoscale technology of mucoadhesive interactions.* Adv Drug Deliv Rev, 2004. 56(11): p. 1675-87.

158. Voyutskii, S.S., *Autoadhesion and Adhesion of High Polymers*. 1963, New York: Wiley.

159. Qaqish, R. and M. Amiji, *Synthesis of a fluorescent chitosan derivative and its application for the study of chitosan–mucin interactions.* Carbohydrate Polymers, 1999. 38(2): p. 99-107.

จุฬาลงกรณ์มหาวิทยาลัย
Chulalongkorn University

160. Dinu, V., et al., *Mucin immobilization in calcium alginate: A possible mucus mimetic tool for evaluating mucoadhesion and retention of flavour.* International Journal of Biological Macromolecules, 2019. 138: p. 831-836.

161. Hadjittofis, E., et al., *Chapter 8 - Interfacial Phenomena*, in *Developing Solid Oral Dosage Forms (Second Edition)*, Y. Qiu, et al., Editors. 2017, Academic Press: Boston. p. 225-252.

162. TM, M.W., W.M. Lau, and V.V. Khutoryanskiy, *Chitosan and Its Derivatives for Application in Mucoadhesive Drug Delivery Systems.* Polymers (Basel), 2018. 10(3).

163. Subramanian, P., *Mucoadhesive Delivery System: A Smart Way to Improve Bioavailability of Nutraceuticals.* Foods, 2021. 10(6).

164. Yakubov, G.E., S. Singleton, and A.-M. Williamson, *Methods for Assessing Mucoadhesion: The Experience of an Integrative Approach*, in *Mucoadhesive Materials and Drug Delivery Systems*. 2014. p. 197-232.

165. Agüero, L., et al., *Alginate microparticles as oral colon drug delivery device: A review.* Carbohydrate Polymers, 2017. 168: p. 32-43.

166. Mohammed, A., et al., *Multistage extraction and purification of waste Sargassum natans to produce sodium alginate: an optimization approach.* Carbohydrate polymers, 2018. 198: p. 109-118.

167. Pawar, S.N. and K.J. Edgar, *Alginate derivatization: a review of chemistry, properties and applications.* Biomaterials, 2012. 33(11): p. 3279-3305.

168. Goh, C.H., P.W.S. Heng, and L.W. Chan, *Alginates as a useful natural polymer for microencapsulation and therapeutic applications.* Carbohydrate Polymers, 2012. 88(1): p. 1-12.

169. Draget, K.I., O. Smidsrød, and G. Skjåk-Bræk, *Alginates from algae.* Polysaccharides and polyamides in the food industry: properties, production, and patents, 2005: p. 1-30.

170. Yang, J.-S., Y.-J. Xie, and W. He, *Research progress on chemical modification of alginate: A review.* Carbohydrate polymers, 2011. 84(1): p. 33-39.

171. Li, J., J. He, and Y. Huang, *Role of alginate in antibacterial finishing of textiles.* International journal of biological macromolecules, 2017. 94: p. 466-473.

172. Dalheim, M.Ø., et al., *Efficient functionalization of alginate biomaterials.* Biomaterials, 2016. 80: p. 146-156.

จุฬาลงกรณ์มหาวิทยาลัย
CHULALONGKORN UNIVERSITY

173. Phillips, G., P. Williams, and D. Wedlock, *Gums and stabilizers for the food industry 5: Applications of alginates*. 1990, New York: IRL Press at Oxford University Press.

174. Tønnesen, H.H. and J. Karlsen, *Alginate in drug delivery systems.* Drug development and industrial pharmacy, 2002. 28(6): p. 621-630.

175. De, S. and D. Robinson, *Polymer relationships during preparation of chitosan–alginate and poly-l-lysine–alginate nanospheres.* Journal of Controlled Release, 2003. 89(1): p. 101-112.

176. Lertsutthiwong, P., et al., *Preparation of alginate nanocapsules containing turmeric oil.* Carbohydrate Polymers, 2008. 74(2): p. 209-214.

177. Mallikarjuna Setty, C., S.S. Sahoo, and B. Sa, *Alginate-coated alginate-polyethyleneimine beads for prolonged release of furosemide in simulated intestinal fluid.* Drug development and industrial pharmacy, 2005. 31(4-5): p. 435-446.

178. Lertsutthiwong, P., P. Rojsitthisak, and U. Nimmannit, *Preparation of turmeric oil-loaded chitosan-alginate biopolymeric nanocapsules.* Materials Science and Engineering: C, 2009. 29(3): p. 856-860.

179. Ritthidej, G.C., *Chapter 3 - Nasal Delivery of Peptides and Proteins with Chitosan and Related Mucoadhesive Polymers*, in *Peptide and Protein Delivery*, C. Van Der Walle, Editor. 2011, Academic Press: Boston. p. 47-68.

180. Bernkop-Schnurch, A., C.E. Kast, and M.F. Richter, *Improvement in the mucoadhesive properties of alginate by the covalent attachment of cysteine.* J Control Release, 2001. 71(3): p. 277-85.

181. Pawar, H.A., K.G. Lalitha, and K. Ruckmani, *Alginate beads of Captopril using galactomannan containing Senna tora gum, guar gum and locust bean gum.* Int J Biol Macromol, 2015. 76: p. 119-31.

182. Kesavan, K., G. Nath, and J.K. Pandit, *Sodium alginate based mucoadhesive system for gatifloxacin and its in vitro antibacterial activity.* Sci Pharm, 2010. 78(4): p. 941-57.

183. Shtenberg, Y., et al., *Mucoadhesive alginate pastes with embedded liposomes for local oral drug delivery.* Int J Biol Macromol, 2018. 111: p. 62-69.

184. Patil, S.B. and K.K. Sawant, *Development, optimization and in vitro evaluation of alginate mucoadhesive microspheres of carvedilol for nasal delivery.* J Microencapsul, 2009. 26(5): p. 432-43.

จุฬาลงกรณ์มหาวิทยาลัย
Chulalongkorn University

185. Rajinikanth, P.S., C. Sankar, and B. Mishra, *Sodium alginate microspheres of metoprolol tartrate for intranasal systemic delivery: development and evaluation.* Drug Deliv, 2003. 10(1): p. 21-8.

186. Dukovski, B.J., et al., *Lipid/alginate nanoparticle-loaded in situ gelling system tailored for dexamethasone nasal delivery.* Int J Pharm, 2017. 533(2): p. 480-487.

187. Lin, H.R., K.C. Sung, and W.J. Vong, *In situ gelling of alginate/pluronic solutions for ophthalmic delivery of pilocarpine.* Biomacromolecules, 2004. 5(6): p. 2358-65.

188. Chang, M.C., et al., *Liposomal dexamethasone-moxifloxacin nanoparticle combinations with collagen/gelatin/alginate hydrogel for corneal infection treatment and wound healing.* Biomed Mater, 2020. 15(5): p. 055022.

189. Hussein, N., et al., *Spray-dried alginate microparticles for potential intranasal delivery of ropinirole hydrochloride: development, characterization and histopathological evaluation.* Pharm Dev Technol, 2020. 25(3): p. 290-299.

190. Trapani, A., et al., *Oxidized Alginate Dopamine Conjugate: In Vitro Characterization for Nose-to-Brain Delivery Application.* Materials (Basel), 2021. 14(13).

191. Sogias, I.A., A.C. Williams, and V.V. Khutoryanskiy, *Why is Chitosan Mucoadhesive?* Biomacromolecules, 2008. 9(7): p. 1837-1842.

192. Illum, L., N.F. Farraj, and S.S. Davis, *Chitosan as a Novel Nasal Delivery System for Peptide Drugs.* Pharmaceutical Research, 1994. 11(8): p. 1186-1189.

193. Cerchiara, T., et al., *Chitosan salts as nasal sustained delivery systems for peptidic drugs.* J Pharm Pharmacol, 2003. 55(12): p. 1623-7.

194. Varshosaz, J., H. Sadrai, and R. Alinagari, *Nasal delivery of insulin using chitosan microspheres.* J Microencapsul, 2004. 21(7): p. 761-74.

195. Jin, H., et al., *Nasal Delivery of Hesperidin/Chitosan Nanoparticles Suppresses Cytokine Storm Syndrome in a Mouse Model of Acute Lung Injury.* Front Pharmacol, 2020. 11: p. 592238.

196. Gholizadeh, H., et al., *Smart thermosensitive chitosan hydrogel for nasal delivery of ibuprofen to treat neurological disorders.* Expert Opin Drug Deliv, 2019. 16(4): p. 453-466.

197. Fachel, F.N.S., et al., *Box-Behnken design optimization of mucoadhesive chitosan-coated nanoemulsions for rosmarinic acid nasal delivery-In vitro studies.* Carbohydr Polym, 2018. 199: p. 572-582.

จุฬาลงกรณ์มหาวิทยาลัย
CHULALONGKORN UNIVERSITY

198. Chatzitaki, A.T., et al., *Chitosan-coated PLGA nanoparticles for the nasal delivery of ropinirole hydrochloride: In vitro and ex vivo evaluation of efficacy and safety.* Int J Pharm, 2020. 589: p. 119776.

199. Qi, X.J., et al., *Anti-depressant effect of curcumin-loaded guanidine-chitosan thermo-sensitive hydrogel by nasal delivery.* Pharm Dev Technol, 2020. 25(3): p. 316-325.

200. Wang, S., et al., *Astragalus Polysaccharides/Chitosan Microspheres for Nasal Delivery: Preparation, Optimization, Characterization, and Pharmacodynamics.* Front Pharmacol, 2020. 11: p. 230.

201. Li, Y., et al., *Chitosan-based thermosensitive hydrogel for nasal delivery of exenatide: Effect of magnesium chloride.* Int J Pharm, 2018. 553(1-2): p. 375-385.

202. De Gaetano, F., et al., *Development of Chitosan/Cyclodextrin Nanospheres for Levofloxacin Ocular Delivery.* Pharmaceutics, 2021. 13(8).

203. Bao, Z., et al., *Glycol chitosan/oxidized hyaluronic acid hydrogel film for topical ocular delivery of dexamethasone and levofloxacin.* Int J Biol Macromol, 2021. 167: p. 659-666.

204. Potas, J., et al., *Multilayer Films Based on Chitosan/Pectin Polyelectrolyte Complexes as Novel Platforms for Buccal Administration of Clotrimazole.* Pharmaceutics, 2021. 13(10).

205. Lim, L.M. and K. Hadinoto, *High-Payload Buccal Delivery System of Amorphous Curcumin-Chitosan Nanoparticle Complex in Hydroxypropyl Methylcellulose and Starch Films.* Int J Mol Sci, 2021. 22(17).

206. Zarrintaj, P., et al., *Poloxamer: A versatile tri-block copolymer for biomedical applications.* Acta Biomater, 2020. 110: p. 37-67.

207. Mishra, P.R., et al., *Production and characterization of Hesperetin nanosuspensions for dermal delivery.* Int J Pharm, 2009. 371(1-2): p. 182-9.

208. Wei, D., L. Ge, and R. Guo, *Effect of hydrophilically modified ibuprofen on thermoresponsive gelation of pluronic copolymer.* Colloids and Surfaces A: Physicochemical and Engineering Aspects, 2018. 553: p. 1-10.

209. Xu, H.-L., et al., *Dual Regulations of Thermosensitive Heparin–Poloxamer Hydrogel Using **ε**-Polylysine: Bioadhesivity and Controlled KGF Release for Enhancing Wound Healing of Endometrial Injury.* ACS Applied Materials & Interfaces, 2017. 9(35): p. 29580-29594.

CHULALONGKORN UNIVERSITY

210. Vasa, D.M., et al., *Evaluation of Ribavirin-Poloxamer Microparticles for Improved Intranasal Absorption.* Pharmaceutics, 2021. 13(8).

211. Modi, D., et al., *Formulation development, optimization, and in vitro assessment of thermoresponsive ophthalmic pluronic F127-chitosan in situ tacrolimus gel.* J Biomater Sci Polym Ed, 2021. 32(13): p. 1678-1702.

212. Yurtdaş-Kırımlıoğlu, G., *A promising approach to design thermosensitive in situ gel based on solid dispersions of desloratadine with Kolliphor® 188 and Pluronic® F127.* Journal of Thermal Analysis and Calorimetry, 2021.

213. Gadhave, D., et al., *Nose-to-brain delivery of amisulpride-loaded lipid-based poloxamer-gellan gum nanoemulgel: In vitro and in vivo pharmacological studies.* Int J Pharm, 2021. 607: p. 121050.

214. Elahehnaz, P., M. Saba, and A. Shohreh, *Pharmacokinetics and bioavailability of midazolam in rats following*

single dose administration of intravenous solution, intranasal

dispersion, and in situ nasal gel. Journal of Applied Pharmaceutical Science 2021. 11(11): p. 070-075.

215. Niyompanich, J., et al., *Development of thermoresponsive poloxamer in situ gel loaded with gentamicin sulfate for cavity wounds.* Journal of Polymer Research, 2021. 28(4): p. 128.

216. Perminaite, K., et al., *Formulation of Ocular In Situ Gels with Lithuanian Royal Jelly and Their Biopharmaceutical Evaluation In Vitro.* Molecules, 2021. 26(12).

217. Diaz-Salmeron, R., et al., *Mucoadhesive Poloxamer-Based Hydrogels for the Release of HP-beta-CD-Complexed Dexamethasone in the Treatment of Buccal Diseases.* Pharmaceutics, 2021. 13(1).

218. de Araujo, P.R., et al., *In vivo study of hypericin-loaded poloxamer-based mucoadhesive in situ gelling liquid crystalline precursor system in a mice model of vulvovaginal candidiasis.* Med Mycol, 2021. 59(8): p. 821-827.

219. Sorasitthiyanukarn, F.N., et al., *Chitosan oligosaccharide/alginate nanoparticles as an effective carrier for astaxanthin with improving stability, in vitro oral bioaccessibility, and bioavailability.* Food Hydrocolloids, 2022. 124: p. 107246.

220. Clementino, A.R., et al., *Structure and Fate of Nanoparticles Designed for the Nasal Delivery of Poorly Soluble Drugs.* Mol Pharm, 2021. 18(8): p. 3132-3146.

จุฬาลงกรณ์มหาวิทยาลัย
CHULALONGKORN UNIVERSITY

221. Yostawonkul, J., et al., *Surface modification of nanostructure lipid carrier (NLC) by oleoyl-quaternized-chitosan as a mucoadhesive nanocarrier.* Colloids Surf B Biointerfaces, 2017. 149: p. 301-311.

222. Rossi, S., et al., *Characterization of chitosan hydrochloride--mucin rheological interaction: influence of polymer concentration and polymer:mucin weight ratio.* Eur J Pharm Sci, 2001. 12(4): p. 479-85.

223. Pawar, D., et al., *Evaluation of mucoadhesive PLGA microparticles for nasal immunization.* AAPS J, 2010. 12(2): p. 130-7.

224. Jengarn, J., et al., *Genetic manipulation of porcine epidemic diarrhoea virus recovered from a full-length infectious cDNA clone.* J Gen Virol, 2015. 96(8): p. 2206-2218.

225. Bezerra, M.A., et al., *Response surface methodology (RSM) as a tool for optimization in analytical chemistry.* Talanta, 2008. 76(5): p. 965-77.

226. Abd-Allah, H., R.T.A. Abdel-Aziz, and M. Nasr, *Chitosan nanoparticles making their way to clinical practice: A feasibility study on their topical use for acne treatment.* Int J Biol Macromol, 2020. 156: p. 262-270.

227. Abul Kalam, M., et al., *Optimizing indomethacin-loaded chitosan nanoparticle size, encapsulation, and release using Box-Behnken experimental design.* Int J Biol Macromol, 2016. 87: p. 329-40.

228. Dong, Y., et al., *Scalable ionic gelation synthesis of chitosan nanoparticles for drug delivery in static mixers.* Carbohydr Polym, 2013. 94(2): p. 940-5.

229. Fan, W., et al., *Formation mechanism of monodisperse, low molecular weight chitosan nanoparticles by ionic gelation technique.* Colloids Surf B Biointerfaces, 2012. 90: p. 21-7.

230. Perinelli, D.R., et al., *Chitosan Loaded into a Hydrogel Delivery System as a Strategy to Treat Vaginal Co-Infection.* Pharmaceutics, 2018. 10(1).

231. Mokhtari, S., S.M. Jafari, and E. Assadpour, *Development of a nutraceutical nano-delivery system through emulsification/internal gelation of alginate.* Food Chem, 2017. 229: p. 286-295.

232. Choukaife, H., A.A. Doolaanea, and M. Alfatama, *Alginate Nanoformulation: Influence of Process and Selected Variables.* Pharmaceuticals (Basel), 2020. 13(11).

จุฬาลงกรณ์มหาวิทยาลัย
CHULALONGKORN UNIVERSITY

233. Elgegren, M., et al., *Ultrasound-Assisted Encapsulation of Sacha Inchi (Plukenetia volubilis Linneo.) Oil in Alginate-Chitosan Nanoparticles.* Polymers (Basel), 2019. 11(8).

234. Kim, S., et al., *Chitosan-lignosulfonates sono-chemically prepared nanoparticles: characterisation and potential applications.* Colloids Surf B Biointerfaces, 2013. 103: p. 1-8.

235. Quinones, J.P., H. Peniche, and C. Peniche, *Chitosan Based Self-Assembled Nanoparticles in Drug Delivery.* Polymers (Basel), 2018. 10(3).

236. Skoglund, S., et al., *Effect of laundry surfactants on surface charge and colloidal stability of silver nanoparticles.* Langmuir, 2013. 29(28): p. 8882-91.

237. Rahaiee, S., et al., *Improvement of crocin stability by biodegradeble nanoparticles of chitosan-alginate.* Int J Biol Macromol, 2015. 79: p. 423-32.

238. Gazori, T., et al., *Evaluation of Alginate/Chitosan nanoparticles as antisense delivery vector: Formulation, optimization and in vitro characterization.* Carbohydrate Polymers, 2009. 77(3): p. 599-606.

239. Abosabaa, S.A., A.N. ElMeshad, and M.G. Arafa, *Chitosan Nanocarrier Entrapping Hydrophilic Drugs as Advanced Polymeric System for Dual Pharmaceutical and Cosmeceutical Application: A Comprehensive Analysis Using Box-Behnken Design.* Polymers (Basel), 2021. 13(5).

240. Muzzarelli, R.A., *Chitins and chitosans as immunoadjuvants and non-allergenic drug carriers.* Mar Drugs, 2010. 8(2): p. 292-312.

241. Alishahi, A., et al., *Shelf life and delivery enhancement of vitamin C using chitosan nanoparticles.* Food Chemistry, 2011. 126(3): p. 935-940.

242. Alishahi, A., *Antibacterial Effect of Chitosan Nanoparticle Loaded with Nisin for the Prolonged Effect.* Journal of Food Safety, 2014. 34(2): p. 111-118.

243. Khlibsuwan, R., W. Khunkitti, and T. Pongjanyakul, *Alginate-poloxamer beads for clotrimazole delivery: Molecular interactions, mechanical properties, and anticandidal activity.* Int J Biol Macromol, 2020. 148: p. 1061-1071.

244. Nguyen-Kim, V., et al., *Solubilization of active ingredients of different polarity in Pluronic(R) micellar solutions - Correlations between solubilizate polarity and solubilization site.* J Colloid Interface Sci, 2016. 477: p. 94-102.

245. Degen, P., et al., *Surfactant-mediated formation of alginate layers at the water-air interface.* Surface and Interface Analysis, 2019. 51(11): p. 1051-1058.

จุฬาลงกรณ์มหาวิทยาลัย
CHULALONGKORN UNIVERSITY

246. Tummino, M.L., et al., *The Innovation Comes from the Sea: Chitosan and Alginate Hybrid Gels and Films as Sustainable Materials for Wastewater Remediation.* Int J Mol Sci, 2020. 21(2).

247. Ablouh, E.-h., et al., *Chitosan microspheres/sodium alginate hybrid beads: an efficient green adsorbent for heavy metals removal from aqueous solutions.* Sustainable Environment Research, 2019. 29(1): p. 5.

248. Shamshina, J.L., et al., *Chitin-calcium alginate composite fibers for wound care dressings spun from ionic liquid solution.* J Mater Chem B, 2014. 2(25): p. 3924-3936.

249. Mirabedini, A., *Preparation and Characterisation of Novel Hybrid Hydrogel Fibres*, in *Developing Novel Spinning Methods to Fabricate Continuous Multifunctional Fibres for Bioapplications*, A. Mirabedini, Editor. 2018, Springer International Publishing: Cham. p. 57-77.

250. Wang, X., et al., *Novel Formulations of the Antiviral Drug Favipiravir: Improving Permeability and Tabletability.* Crystal Growth & Design, 2021. 21(7): p. 3807-3817.

251. Goloveshkin, A.S., A.A. Korlyukov, and A.V. Vologzhanina, *Novel Polymorph of Favipiravir-An Antiviral Medication.* Pharmaceutics, 2021. 13(2).

252. Sikorski, P., et al., *Evidence for Egg-Box-Compatible Interactions in Calcium–Alginate Gels from Fiber X-ray Diffraction.* Biomacromolecules, 2007. 8(7): p. 2098-2103.

253. Li, L., et al., *Reexamining the egg-box model in calcium-alginate gels with X-ray diffraction.* Biomacromolecules, 2007. 8(2): p. 464-8.

254. Liang, J., et al., *Encapsulation of epigallocatechin gallate in zein/chitosan nanoparticles for controlled applications in food systems.* Food Chem, 2017. 231: p. 19-24.

255. Majumdar, S., T. Mandal, and D. Dasgupta Mandal, *Comparative performance evaluation of chitosan based polymeric microspheres and nanoparticles as delivery system for bacterial beta-carotene derived from Planococcus sp. TRC1.* Int J Biol Macromol, 2022. 195: p. 384-397.

256. Hazra, M., et al., *Designing polymeric microparticulate drug delivery system for hydrophobic drug quercetin.* Saudi Pharm J, 2015. 23(4): p. 429-36.

จุฬาลงกรณ์มหาวิทยาลัย
CHULALONGKORN UNIVERSITY

257. Popat, A., et al., *A pH-responsive drug delivery system based on chitosan coated mesoporous silica nanoparticles.* Journal of Materials Chemistry, 2012. 22(22): p. 11173-11178.

258. Thai, H., et al., *Characterization of chitosan/alginate/lovastatin nanoparticles and investigation of their toxic effects in vitro and in vivo.* Sci Rep, 2020. 10(1): p. 909.

259. Arifin, D.Y., L.Y. Lee, and C.-H. Wang, *Mathematical modeling and simulation of drug release from microspheres: Implications to drug delivery systems.* Advanced Drug Delivery Reviews, 2006. 58(12): p. 1274-1325.

260. Papadopoulou, V., et al., *On the use of the Weibull function for the discernment of drug release mechanisms.* Int J Pharm, 2006. 309(1-2): p. 44-50.

261. Kobryń, J., et al., *Influence of Hydrophilic Polymers on the Factor in Weibull Equation Applied to the Release Kinetics of a Biologically Active Complex of Aesculus hippocastanum.* International Journal of Polymer Science, 2017. 2017: p. 3486384.

262. Siepmann, J. and F. Siepmann, *Mathematical modeling of drug delivery.* Int J Pharm, 2008. 364(2): p. 328-43.

263. Lin, S.B., et al., *Segmental orientation studies of polyether polyurethane block copolymers with different hard segment lengths and distributions.* Colloid and Polymer Science, 1985. 263(2): p. 128-140.

264. Li, P., et al., *Chitosan-alginate nanoparticles as a novel drug delivery system for nifedipine.* International journal of biomedical science : IJBS, 2008. 4(3): p. 221-228.

265. Khan, A., et al., *Temozolomide loaded nano lipid based chitosan hydrogel for nose to brain delivery: Characterization, nasal absorption, histopathology and cell line study.* Int J Biol Macromol, 2018. 116: p. 1260-1267.

266. Colombo, M., et al., *Kaempferol-loaded mucoadhesive nanoemulsion for intranasal administration reduces glioma growth in vitro.* Int J Pharm, 2018. 543(1-2): p. 214-223.

267. Bruinsmann, F.A., et al., *Chitosan-Coated Nanoparticles: Effect of Chitosan Molecular Weight on Nasal Transmucosal Delivery.* Pharmaceutics, 2019. 11(2).

268. Casettari, L. and L. Illum, *Chitosan in nasal delivery systems for therapeutic drugs.* J Control Release, 2014. 190: p. 189-200.

269. Turker, S., E. Onur, and Y. Ozer, *Nasal route and drug delivery systems.* Pharm World Sci, 2004. 26(3): p. 137-42.

จุฬาลงกรณ์มหาวิทยาลัย
Chulalongkorn University

270. Samson, G., et al., *Ex vivo study of bevacizumab transport through porcine nasal mucosa.* Eur J Pharm Biopharm, 2012. 80(2): p. 465-9.

271. Almalik, A., et al., *Effect of cryoprotection on particle size stability and preservation of chitosan nanoparticles with and without hyaluronate or alginate coating.* Saudi Pharm J, 2017. 25(6): p. 861-867.

272. Jeong, H., et al., *In vitro blood cell viability profiling of polymers used in molecular assembly.* Sci Rep, 2017. 7(1): p. 9481.

273. Sibinovska, N., S. Zakelj, and K. Kristan, *Suitability of RPMI 2650 cell models for nasal drug permeability prediction.* Eur J Pharm Biopharm, 2019. 145: p. 85-95.

274. Pozzoli, M., et al., *Application of RPMI 2650 nasal cell model to a 3D printed apparatus for the testing of drug deposition and permeation of nasal products.* Eur J Pharm Biopharm, 2016. 107: p. 223-33.

275. ISO, *ISO 10993-5:2009 Biological Evaluation of Medical Devices Part 5: Tests for in Vitro Cytotoxicity*. 2009.

276. Foroozandeh, P. and A.A. Aziz, *Insight into Cellular Uptake and Intracellular Trafficking of Nanoparticles.* Nanoscale Res Lett, 2018. 13(1): p. 339.

277. Curtis, E.M., et al., *Modeling nanoparticle wrapping or translocation in bilayer membranes.* Nanoscale, 2015. 7(34): p. 14505-14.

278. Antas, M., A. Szczotka-Bochniarz, and G. Wozniakowski, *Effective inactivation of porcine epidemic diarrhea virus on contaminated surgery masks by low-concentrated sodium hypochlorite dispersion.* Pol J Vet Sci, 2020. 23(4): p. 647-650.

279. Singh, G., et al., *A Minimally Replicative Vaccine Protects Vaccinated Piglets Against Challenge With the Porcine Epidemic Diarrhea Virus.* Front Vet Sci, 2019. 6: p. 347.

280. Sadique, M.A., et al., *High-performance antiviral nano-systems as a shield to inhibit viral infections: SARS-CoV-2 as a model case study.* J Mater Chem B, 2021. 9(23): p. 4620-4642.

281. Singh, G., et al., *Monitoring SARS-CoV-2 decontamination by dry heat and ultraviolet treatment with a swine coronavirus as a surrogate.* Infect Prev Pract, 2021. 3(1): p. 100103.

282. Aggarwal, P., et al., *Nanoparticle interaction with plasma proteins as it relates to particle biodistribution, biocompatibility and therapeutic efficacy.* Adv Drug Deliv Rev, 2009. 61(6): p. 428-37.

จุฬาลงกรณ์มหาวิทยาลัย
CHULALONGKORN UNIVERSITY

283. Gessner, A., et al., *Influence of surface charge density on protein adsorption on polymeric nanoparticles: analysis by two-dimensional electrophoresis.* European Journal of Pharmaceutics and Biopharmaceutics, 2002. 54(2): p. 165-170.

284. Tulbah, A.S. and W.H. Lee, *Physicochemical Characteristics and In Vitro Toxicity/Anti-SARS-CoV-2 Activity of Favipiravir Solid Lipid Nanoparticles (SLNs).* Pharmaceuticals (Basel), 2021. 14(10).

285. Jyothi, K.R., et al., *Liver-targeted cyclosporine A-encapsulated poly (lactic-co-glycolic) acid nanoparticles inhibit hepatitis C virus replication.* Int J Nanomedicine, 2015. 10: p. 903-21.

286. Pyrc, K., et al., *SARS-CoV-2 inhibition using a mucoadhesive, amphiphilic chitosan that may serve as an anti-viral nasal spray.* Sci Rep, 2021. 11(1): p. 20012.

287. Loutfy, S.A., et al., *Antiviral Activity of Chitosan Nanoparticles Encapsulating Curcumin Against Hepatitis C Virus Genotype 4a in Human Hepatoma Cell Lines.* Int J Nanomedicine, 2020. 15: p. 2699-2715.

288. Sano, Y., *Antiviral activity of alginate against infection by tobacco mosaic virus.* Carbohydrate Polymers, 1999. 38: p. 183-186.

289. Serrano-Aroca, A., M. Ferrandis-Montesinos, and R. Wang, *Antiviral Properties of Alginate-Based Biomaterials: Promising Antiviral Agents against SARS-CoV-2.* ACS Appl Bio Mater, 2021. 4(8): p. 5897-5907.

290. Pietropaolo, V., et al., *Effect of natural and semisynthetic polymers on rabies virus infection in CER cells.* Research in Virology, 1993. 144: p. 151-158.

291. Abd Elkodous, M., et al., *Nanomaterial-based drug delivery systems as promising carriers for patients with COVID-19.* RSC Adv, 2021. 11(43): p. 26463-26480.

จุฬาลงกรณ์มหาวิทยาลัย
CHULALONGKORN UNIVERSITY

Appendix A

Calibration curve of standard FVR

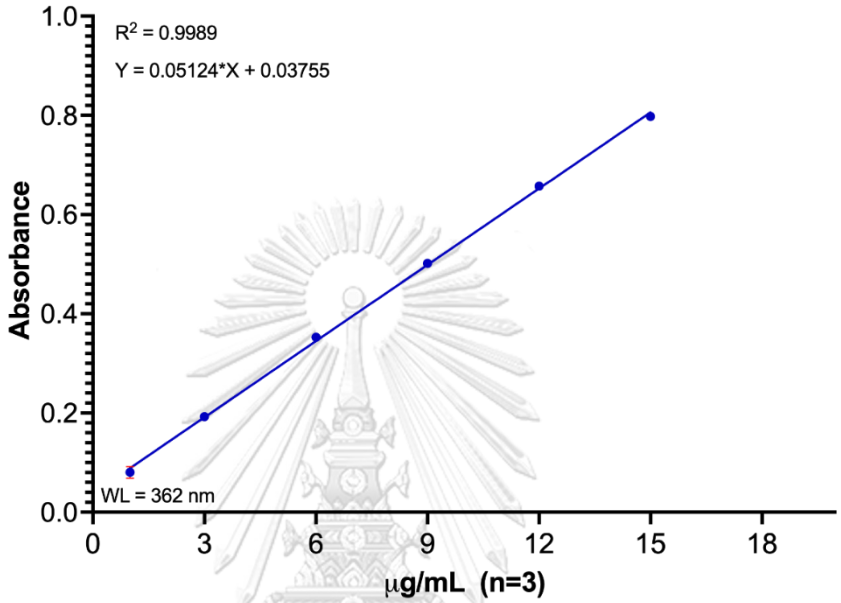

จุฬาลงกรณ์มหาวิทยาลัย
Chulalongkorn University

Appendix B

Calibration curve of standard mucin

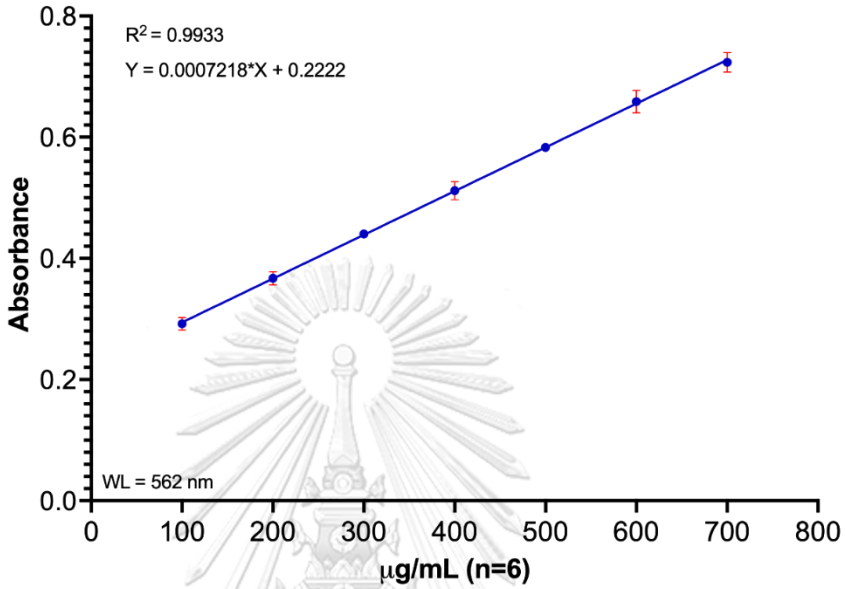

จุฬาลงกรณ์มหาวิทยาลัย
Chulalongkorn University

Appendix C

Release kinetics of free FVR solution

Model	Media	Parameter	$R^2_{adjusted}$	AIC	MSC
Zero-order	SNF	K_0 = 6.96	-1.49	142.81	-1.72
($F = k_0 \cdot t$)	pH 7.4	K_0 = 7.14	-1.25	143.41	-1.52
First-order	SNF	k_1 = 0.48	0.76	109.77	0.64
($F = 100 \cdot e^{-k1t}$)	pH 7.4	k_1= 0.52	0.87	103.46	1.34
Higuchi	SNF	K_H = 28.55	0.41	122.52	-0.27
($F = k_H \cdot t^{0.5}$)	pH 7.4	K_H= 29.29	0.48	122.72	-0.04
Korsmeyer-Peppas	SNF	k_{KP} =54.32, n= 0.237	0.97	83.16	2.54
($F = k_{KP} \cdot t^n$)	pH 7.4	k_{KP} = 53.80, n= 0.22	0.94	94.28	1.90
Hixson-Crowell	SNF	k_{HC} = 0.07	0.39	123.03	-0.31
($F = 100 \cdot [1 - (1 - k_{HC} \cdot t)^3]$)	pH 7.4	k_{HC} = 0.07	0.50	122.21	-0.01
[a]Weibull	SNF	α = 1.551, β = 0.369, T_i = 0.187	0.9894	65.1715	3.8132
($F = 100 \cdot [1 - e^{-(t-T1)\beta/\alpha}]$)	pH 7.4	α = 1.23, β= 0.46, T_i = 0.14	0.99	62.76	4.24

[a]Best fit release kinetic model for free FVR. *F*: fraction (%) of drug released in time *t;* k_0: zero-order release constant; k_1: first-order release constant; k_H: Higuchi release constant; k_{KP}: release constant incorporating structural and geometric characteristics of the drug-dosage form; *n*: diffusional exponent indicating the drug release mechanism; α: scale parameter defining the time scale of the process; β: shape parameter characterizing the curve as exponential (β = 1; case 1), sigmoid, S-shaped, with upward curvature followed by a turning point (β > 1; case 2), or parabolic, with a higher initial slope and then consistent with an exponential (β < 1; case 3); T_i: location parameter representing the lag time before the onset of the dissolution or release process, which in most cases will be near zero; k_{HC} is the Hixon-Crowell release constant.

จุฬาลงกรณ์มหาวิทยาลัย
Chulalongkorn University

Appendix D.

Release kinetic of FVR from MCS-ALG-NPs

Model	Media	Parameter	$R^2_{adjusted}$	AIC	MSC
Zero-order	SNF	K_0 = 6.32	-1.68	141.84	-1.78
($F = k_0 \cdot t$)	pH 7.4	K_0 = 4.72	-1.05	133.17	-1.30
First-order	SNF	k_1 = 0.37	0.64	113.87	0.21
($F = 100 \cdot e^{-k1t}$)	pH 7.4	k_1= 0.14	0.35	117.09	-0.15
Higuchi	SNF	K_H = 26.24	0.30	123.04	-0.44
($F = k_H \cdot t^{0.5}$)	pH 7.4	K_H = 19.55	0.48	113.84	0.08
Korsmeyer-Peppas	SNF	k_{KP} = 51.34, n= 0.19	0.92	93.30	1.68
($F = k_{KP} \cdot t^n$)	pH 7.4	k_{KP} = 47.81, n= 0.27			
Hixson-Crowell	SNF	k_{HC} = 0.06	0.29	123.21	-0.45
($F = 100 \cdot [1 - (1 - k_{HC} \cdot t)^3]$)	pH 7.4	k_{HC} = 0.04	0.1822	120.33	-0.39
[a]Weibull	SNF	α = 1.23, β = 0.31, T_i = 0.22	0.98	72.05	3.20
($F = 100 \cdot [1 - e^{-(t-T1)\beta/\alpha}]$)	pH 7.4	α = 1.89, β = 0.24, T_i = 0.33	0.95	82.56	2.31

[a]Best fit release kinetic model for free FVR. *F*: fraction (%) of drug released in time *t;* k_0: zero-order release constant; k_1: first-order release constant; k_H: Higuchi release constant; k_{KP}: release constant incorporating structural and geometric characteristics of the drug-dosage form; *n*: diffusional exponent indicating the drug release mechanism; α: scale parameter defining the time scale of the process; β: shape parameter characterizing the curve as exponential (β = 1; case 1), sigmoid, S-shaped, with upward curvature followed by a turning point (β > 1; case 2), or parabolic, with a higher initial slope and then consistent with an exponential (β < 1; case 3); T_i: location parameter representing the lag time before the onset of the dissolution or release process, which in most cases will be near zero; k_{HC} is the Hixon-Crowell release constant.

จุฬาลงกรณ์มหาวิทยาลัย
Chulalongkorn University

Appendix E.

Release kinetic of FVR from ALG-NPs

Model	Media	Parameter	$R^2_{adjusted}$	AIC	MSC
Zero order	SNF	K_0 = 5.34	-1.26	135.74	-1.51
($F = k_0 \cdot t$)	pH 7.4	K_0 = 6.36	-1.34	140.87	-1.56
First order	SNF	k_1 = 0.19	0.42	116.60	-0.14
($F = 100 \cdot e^{-k1t}$)	pH 7.4	k_1= 0.33	0.72	110.66	0.60
Higuchi	SNF	K_H = 21.95	0.46	115.78	-0.08
($F = k_H \cdot t^{0.5}$)	pH 7.4	K_H = 26.24	0.44	120.72	-0.12
Korsmeyer-Peppas	SNF	k_{KP} = 40.62, n= 0.22	0.91	90.40	1.73
($F = k_{KP} \cdot t^n$)	pH 7.4	k_{KP} = 48.82, n= 0.22	0.92	93.94	1.79
Hixson-Crowell	SNF	k_{HC} = 0.05	0.2492	120.24	-0.40
($F = 100 \cdot [1 - (1 - k_{HC} \cdot t)^3]$)	pH 7.4	k_{HC} = 0.06	0.4672	119.94	-0.06
[a] Weibull	SNF	α = 1.67, β = 0.28, T_i = 0.24	0.97	72.47	3.01
($F = 100 \cdot [1 - e^{-(t-T1)\beta/\alpha}]$)	pH 7.4	α = 1.36, β = 0.36, T_i = 0.20	0.98	72.62	3.32

[a]Best fit release kinetic model for free FVR. *F*: fraction (%) of drug released in time *t;* k_0: zero-order release constant; k_1: first-order release constant; k_H: Higuchi release constant; k_{KP}: release constant incorporating structural and geometric characteristics of the drug-dosage form; *n*: diffusional exponent indicating the drug release mechanism; α: scale parameter defining the time scale of the process; β: shape parameter characterizing the curve as exponential (β = 1; case 1), sigmoid, S-shaped, with upward curvature followed by a turning point (β > 1; case 2), or parabolic, with a higher initial slope and then consistent with an exponential (β < 1; case 3); T_i: location parameter representing the lag time before the onset of the dissolution or release process, which in most cases will be near zero; k_{HC} is the Hixon-Crowell release constant.

จุฬาลงกรณ์มหาวิทยาลัย
Chulalongkorn University

Appendix F

Quantitative data of the antiviral effect of FVR (formulated and unformulated) from 3 independent experiments

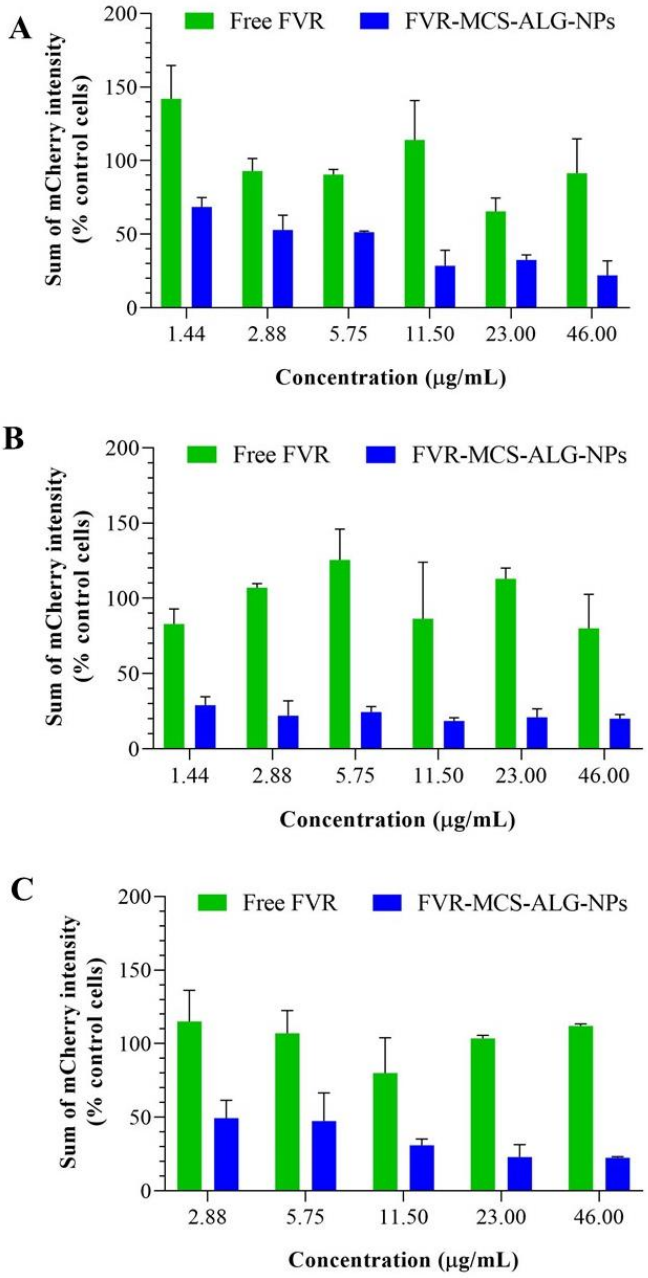

The mCherry fluorescent intensity of the infected cells treated with FVR from experiment 1 **(A)** (from Fig. 21), experiment 2 **(B)** (Appendix G) and experiment 3 **(C)** (Appendix H) were measured by the high-content imaging system. Data shown are the mean ± SD of the relative sum of mCherry fluorescent intensity (% control).

Appendix G

Antiviral effect of FVR (formulated and unformulated) from trial 2

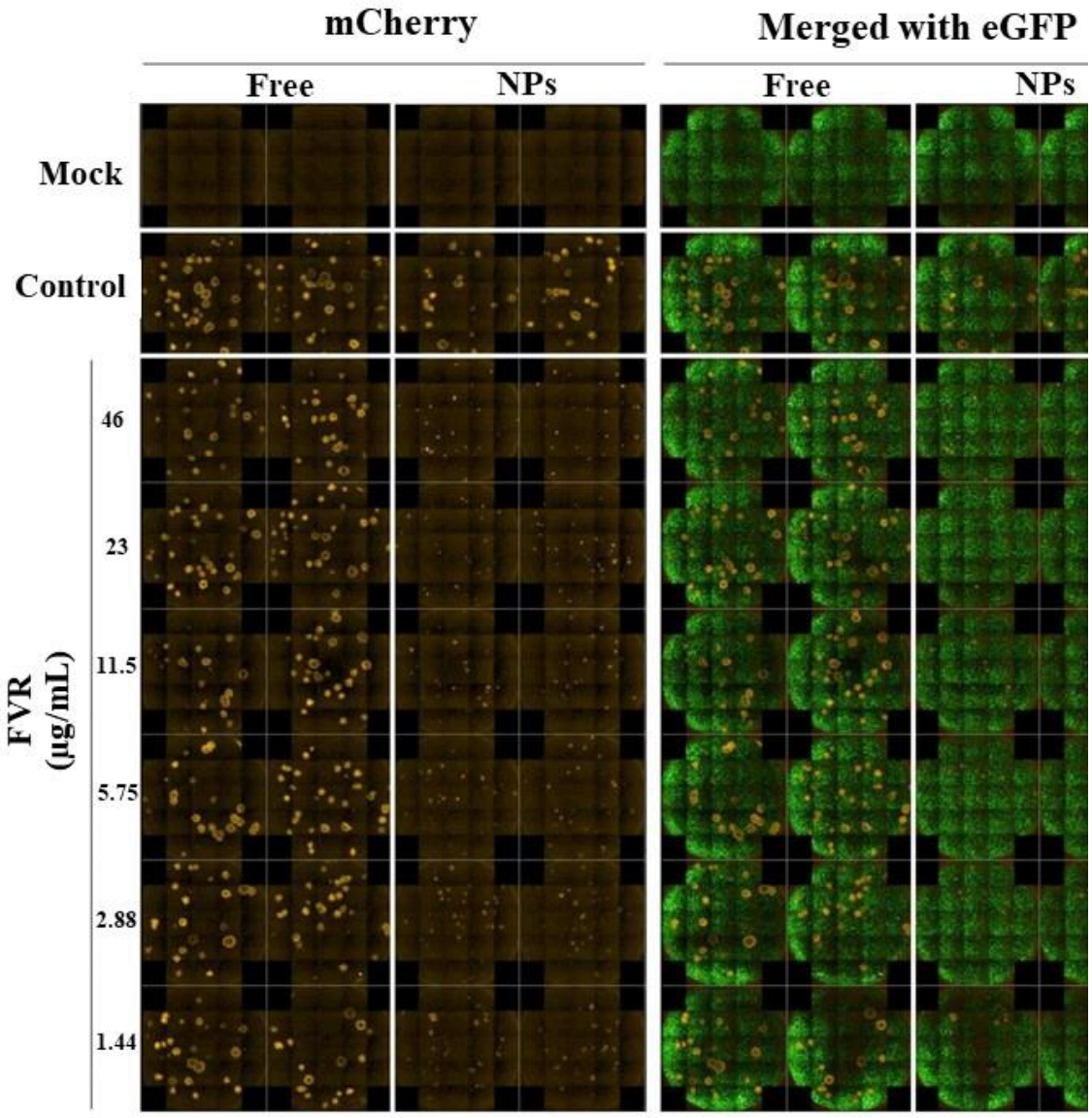

The stitched image of mCherry and eGFP signals from the cells were acquired by a high-content imaging system at 21 images/well. Each condition was tested in duplicate.

Appendix H

Antiviral effect of FVR (formulated and unformulated) from trial 3

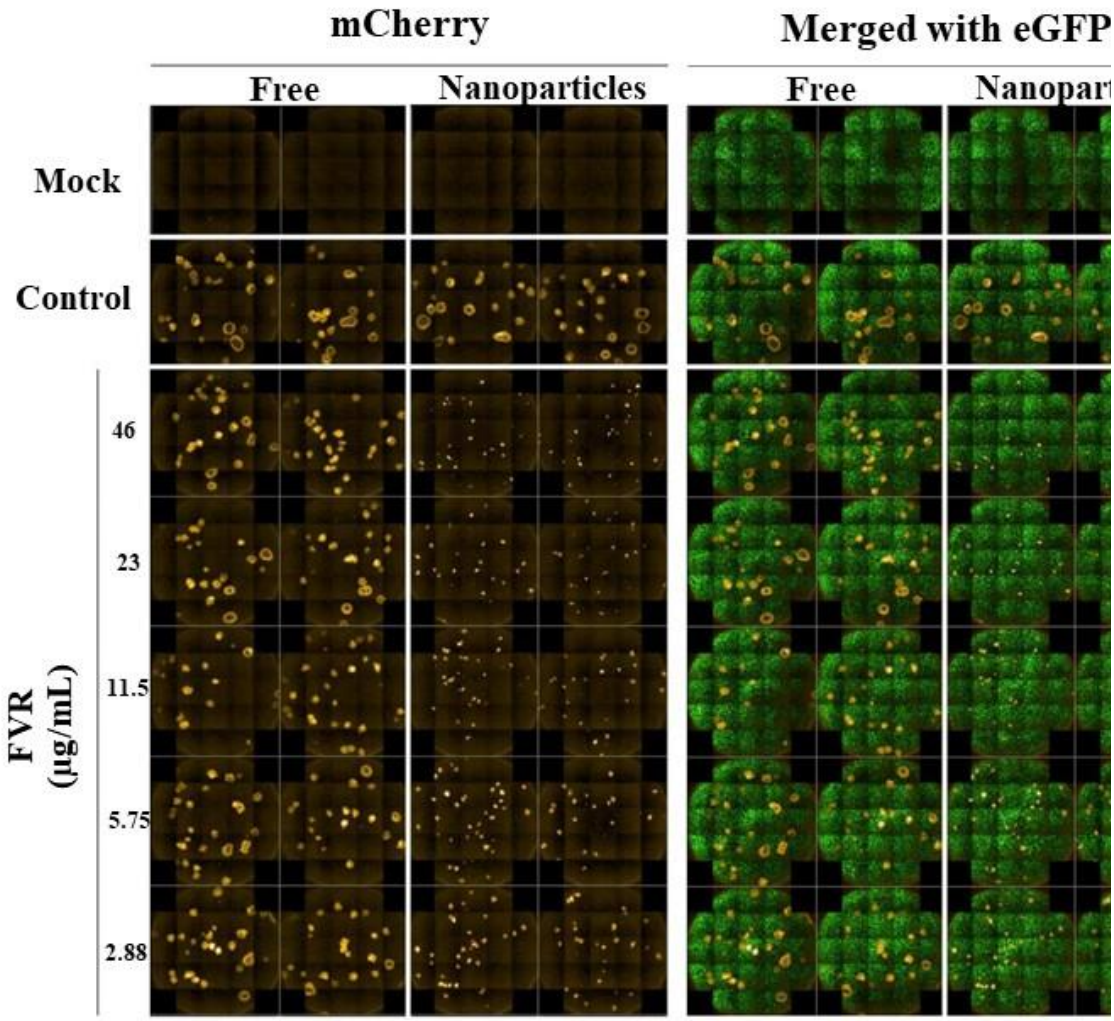

The stitched image of mCherry and eGFP signals from the cells were acquired by a high-content imaging system at 21 images/well. Each condition was tested in duplicate.

Appendix I

Antiviral effect of free FVR at high concentrations

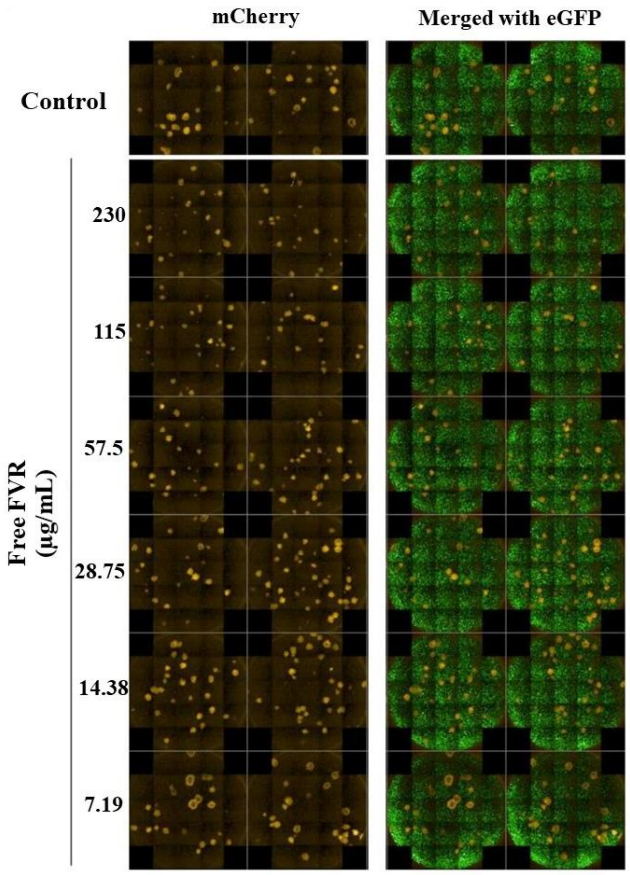

จุฬาลงกรณ์มหาวิทยาลัย
Chulalongkorn University

The stitched images of the mCherry and eGFP signals from the cells were acquired by a high-content imaging system.

VITA

NAME	Khent Primo Alcantara
DATE OF BIRTH	June 7 1992
PLACE OF BIRTH	Tanay, Rizal Philippines
INSTITUTIONS ATTENDED	Pontifical and Royal University of Santo Tomas, Manila Philippines
HOME ADDRESS	95 Pastor G. Santos Street Barangay Wawa Tanay Rizal 1980, Philippines
PUBLICATION	1. Truong, T. H., Alcantara, K. P., Bulatao, B. P. I., Sorasitthiyanukarn, F. N., Muangnoi, C., Nalinratana, N., ... & Rojsitthisak, P. (2022). Chitosan-coated nanostructured lipid carriers for transdermal delivery of tetrahydrocurcumin for breast cancer therapy. Carbohydrate Polymers, 288, 119401. 2. San, H. H. M., Alcantara, K. P., Bulatao, B. P. I., Chaichompoo, W., Nalinratana, N., Suksamrarn, A., ... & Rojsitthisak, P. (2022). Development of Turmeric Oil—Loaded Chitosan/Alginate Nanocapsules for Cytotoxicity Enhancement against Breast Cancer. Polymers, 14(9), 1835. 3. Luckanagul, J. A., Alcantara, K. P., Bulatao, B. P. I., Wong, T. W., Rojsitthisak, P., & Rojsitthisak, P. (2021). Thermo-Responsive Polymers and Their Application as Smart Biomaterials. In Smart Nanomaterials in Biomedical Applications (pp. 291-343). Springer, Cham. 4. Alcantara, Khent P., Mohd Hanif Zulfakar, and Agnes L. Castillo. "Development, characterization and pharmacokinetics of mupirocin-loaded nanostructured lipid carriers (NLCs) for intravascular administration." International journal of Pharmaceutics 571 (2019): 118705.

จุฬาลงกรณ์มหาวิทยาลัย
Chulalongkorn University